Master's thesis

NTNU
Norwegian University of Science and Technology
Faculty of Natural Sciences
Department of Chemistry

Gabrielle Emma Kleber

Spatial Variability of Black Carbon Deposited on Snow in Ny-Ålesund, Svalbard: Impact of Anthropogenic Activities

Master's thesis in Environmental Toxicology and Chemistry
Supervisor: Øyvind Mikkelsen
May 2019

NTNU
Norwegian University of Science and Technology

Gabrielle Emma Kleber

Spatial Variability of Black Carbon Deposited on Snow in Ny-Ålesund, Svalbard: Impact of Anthropogenic Activities

Master's thesis in Environmental Toxicology and Chemistry
Supervisor: Øyvind Mikkelsen
May 2019

Norwegian University of Science and Technology
Faculty of Natural Sciences
Department of Chemistry

NTNU
Norwegian University of
Science and Technology

Abstract

Black Carbon (BC) is a carbonaceous particle emitted globally during the incomplete combustion of biomass and carbon-based fuels. It is considered one of the strongest climate-forcing agents due to its high capacity to absorb solar radiation and heat the atmosphere. When deposited over highly reflective surfaces such as snow and ice, BC particles reduce surface albedo and accelerate the rate of melt. The region around Ny-Ålesund, Svalbard is considered a pristine Arctic site and is used to study background levels of contaminants such as BC in the European Arctic. The spatial distribution of BC on glaciers was used as a proxy to investigate potential environmental impacts of anthropogenic activity in the Ny-Ålesund settlement. Surface snow samples were collected from glaciers at varying altitudes and distances from Ny-Ålesund during spring 2018 and analyzed for BC content by Thermal Optical Analysis. Measurements were compared to a similar dataset gathered during spring 2017, when extensive building activities were underway in Ny-Ålesund. Measured BC levels of 2018 snow samples ranged from 0 ng per gram of snow to 9.8 ng/g, with a mean concentration of 1.9 ng/g. BC levels from 2017 ranged from 0 to 68 ng/g with a mean concentration of 14 ng/g. A comparison of the datasets confirmed that when strong anthropogenic activities are present in Ny-Ålesund, there is a measurable impact on the contaminant levels in snow in the surrounding region. Areas within a 15 km radius of the settlement are most impacted and exhibited 2.3 times higher BC levels than locations further away in 2017 and 1.3 times higher in 2018. Altitude of sampling locations was also a major contributing factor, leading to 1.5 times higher BC levels for sites lower than 450 m.a.s.l. in 2017 and 4.6 times higher levels in 2018. It is therefore recommended that sampling campaigns are completed further than 15 km from Ny-Ålesund and at altitudes greater than 450 m for future studies aiming to measure long range transport of contaminants to Svalbard.

ACKNOWLEDGEMENTS

I would first like to thank my thesis supervisors, Dr. Jean-Charles Gallet of the Norwegian Polar Institute and Professor Øyvind Mikkelsen of the Department of Chemistry at the Norwegian University of Science and Technology. Dr. Gallet's continued guidance and expertise were fundamental throughout the development, execution and analysis of the project. He has been incredibly generous with his time, providing me with unwavering support since our initial contact, despite his own endeavors taking him from Antarctica to the Arctic. I have learned an enormous amount from him and will continue to draw on his knowledge and experience as I pursue a career in Arctic research. Professor Mikkelsen has been imperative in the analysis and write-up of the thesis, providing valuable insights to consider from his extensive experience and taking time to conduct several rounds of editing. Both gentlemen have been essential in the success of the project.

I would also like to thank the team at the Institute for the Dynamics of Environmental Processes-CNR at the Ca'Foscari University of Venice for welcoming and supporting me during the chemical analysis portion of the project. Subject matter experts Andrea Spolaor and Elena Barbaro were tremendously helpful in introducing me to the instrumentation and in interpreting results. I am also grateful for their time and expertise in developing and editing my written work.

This project would not have been possible without the team of researchers that assisted in the sampling campaigns in Ny-Ålesund. Dr. Gallet, Dr. Spolaor, Dr. Barbaro, Professor David Cappelletti of the Department of Chemistry, Biology and Biotechnology at the University of Perugia and Dr. Catherine Larose of the Environmental Microbial Genomics group at the University of Lyon were crucial in the success of the field work. Their expertise and experience made for a comprehensive sampling strategy and provided me with a valuable introduction to field work in the Arctic. The logistical support of Jon Leithe's team at the Sverdrup Research Station made the whole sampling campaign possible.

Finally, I must express my gratitude to the many people supporting me along the way. This includes my parents, Richard and Janet and my brother, Christian. Last but certainly not least I would like to thank my classmates and friends Rosalie McKay, Connor McKnight and Leo Magerl for their continued support, encouragement, editing, sanity checks and coffee breaks throughout the course of the project. They have helped to make the experience not only possible, but thoroughly enjoyable.

Thank you!

Table of Contents

List of Figures

List of Tables

List of Acronyms and Nomenclature

Acronyms

AMAP	Arctic Monitoring and Assessment Programme
BC	Black carbon
BR	Austre Brøggerbreen glacier
CE	Collision energy
CXP	Collision cell exit potential
EB	Edithbreen glacier
EC	Elemental carbon
EF	Enrichment factor
EUSAAR	European Supersites for Atmospheric Aerosol Research
FID	Flame ionization detector
GVB	Gruvebadet sampling site
HC	Hydrocarbon
HDF	Holtedahlfonna glacier
HPLC	High-performance liquid chromatography
HYSPLIT	Hybrid Single-Particle Lagrangian Integrated Trajectory model
ICP-SFMS	Inductively coupled plasma sector field mass spectrometer
IPCC	Intergovernmental Panel on Climate Change
KV	Kongsvegen glacier
LOD	Limit of detection
MAC	Mass absorption coefficient
MACS	Mass absorption cross-section
MDL	Method detection limit

ML	Midtre Lovènbreen glacier
MRM	Multiple reaction monitoring
MS	Mass spectrometry
MS/MS	Triple quadrupole mass spectrometer
NOAA	National Oceanic and Atmospheric Administration
NPI	Norwegian Polar Institute
OC	Organic carbon
POC	Pyrolytic organic carbon
PSAP	Particle soot absorber photometer
Q1, Q2, Q3	Quadrupoles 1 – 3
UPW	Ultrapure water
RF	Response factor
SWE	Snow water equivalent
TOA	Thermal optical analysis

Nomenclature

A_{filt}	Total area of filter through which meltwater passed, cm^2
$[EC]$	Elemental carbon concentration, $\mu g/L$ or ng/g
$[EC]_i$	Elemental carbon concentration of segment *i* of snowpack, ng/g
F_{EC}, F_{OC}	Total seasonal flux of EC and OC, ng/cm^2
L_{EC}, L_{OC}	Loading of EC and OC on filters from thermal optical analysis, $\mu g/cm^2$
$L_{EC,i}$, $L_{OC,i}$	Loading of EC and OC in segment *i* of snowpack, ng/cm^2
m_{EC}, m_{OC}	Mass of EC and OC particles retained during filtration of meltwater, μg
m/z	Mass to charge ratio, Da/e
n	Number of samples
$[OC]$	Organic carbon concentration, $\mu g/L$ or ng/g
$[OC]_i$	Organic carbon concentration of segment *i* of snowpack, ng/g
ρ_i	Measured density of segment *i* of snowpack, g/cm^3 or kg/m^3
SWE_i	Snow water equivalent of segment *i* of snowpack, g/cm^2
σ_{LB}	Standard deviation of laboratory blanks
V_{MW}	Total volume of filtered meltwater, L
z_i	Thickness of segment *i* of snowpack, cm

1. Introduction

The Arctic is often used as an indicator of climate trends, as its vulnerable ecosystems provide earlier or amplified responses to the changes induced by global warming. The Intergovernmental Panel on Climate Change (IPCC) has identified changes in the cryosphere, such as the reduction in annual mean Arctic sea ice and the shrinking of glaciers worldwide, as likely evidence for the impacts of anthropogenic warming (Cramer et al., 2014). While reduction of carbon dioxide emissions remains the key focus in long term efforts to restrain or mitigate climate change, it is estimated that it will take longer than 1000 years for 60-85% of anthropogenic CO_2 to be removed from the atmosphere (Ciais et al., 2013). Thus, even in scenarios of immediate reductions in emissions, the Arctic environment will continue to respond to warming trends and increased atmospheric CO_2 concentrations well beyond the 21st century.

In order to delay the thawing of Arctic sea ice and glaciers in the short term, an additional focus should be made on climate forcing agents with much shorter atmospheric residence times, such as Black Carbon (BC). BC is emitted globally during the incomplete combustion of biomass and carbon-based fuels and remains in the atmosphere for only days or weeks before being removed by precipitation or contact with surfaces. These dark carbonaceous particles efficiently absorb light and exert an atmospheric warming effect that has led to their classification as the second most important climate warming agent after CO_2 (Bond et al., 2013). This warming effect is also observed when BC is deposited over highly reflective surfaces such as snow and ice, inducing accelerated melt of the cryosphere. Reducing emissions of short-lived aerosols such as BC can yield observable climactic impacts in shorter timespans and could be effective in delaying the start of the yearly Arctic melt season.

1.1. Properties of Black Carbon

Black carbon is a product of the incomplete combustion of fossil and biogenic fuels (Bond et al., 2013). When insufficient oxygen is available for complete combustion, small, dark carbonaceous particles are formed in the flames and are emitted directly to the atmosphere. During and after emission, BC particles mix with other aerosols to create complex agglomerates comprised of a

pure carbon core coated with other aerosols. BC particles have a unique set of physical and chemical properties, which are highly influenced by their coating structure and contribute to their climate forcing capacity.

The most notable property of BC is that it is a strong light absorber. The amount of light absorbed per mass of BC at a particular wavelength is described as the mass absorption cross-section (MACS) and is used to calculate the radiative forcing caused by particles. Various MACS values for uncoated BC particles have been reported from 7.5 ± 1.2 m^2/g at a wavelength of 550 nm (Bond and Bergstrom, 2006) to 10.0 m^2/g at 637 nm (Zanatta et al., 2016), but all agree to a comparatively high degree of absorption capacity. No other substance that is present in the atmosphere in significant concentrations has as strong of a light absorbing capacity per unit mass. This is of particular interest for studies in climate and radiative forcing in the atmosphere, as well as studies in albedo, or reflectivity, of highly reflective surfaces such as snow and ice.

Black carbon is a refractory material with a vaporization temperature of about 4000K, and thus remains stable at very high temperatures. This property is key in differentiating BC and organic carbon content in laboratory analysis of snow samples. Pure BC particles are hydrophobic and thus insoluble in water, as well as insoluble in common organic solvents such as methanol and acetone. This makes them initially resistant to atmospheric removal through wet deposition. However, their aggregate morphology and tendency to coagulate with other particles in the atmosphere gives them some hydrophilic characteristics that encourages cloud nucleation and shortens their atmospheric lifespan.

1.2 Impacts of Black Carbon

The impacts of BC are measurable in its forms as both an aerosol pollutant as well as a particulate contaminant on the surface of the Earth. In the atmosphere, the presence of BC leads to climatic implications through its ability to scatter and absorb incoming solar radiation. In addition, BC aerosols contribute to poor air quality, particularly in urban areas, which can affect human health through respiratory and cardiovascular issues (Highwood & Kinnersley, 2006). Once deposited

onto the Earth's surface, BC can alter the heat and energy budget of the cryosphere and lower troposphere, as well as impair the health of vegetational ecosystems.

1.2.1. Atmospheric Warming

Atmospheric black carbon can make disturbances to the Earth's energy balance due to its strong light absorption capacity. Studies vary in estimates of the effect of BC on climate, however the globally averaged industrial-era forcing of BC is estimated at +1.1 W/m^2 (90% uncertainty bounds of +0.17 to +2.1) (Bond et al., 2013). This is significant when compared to other major climate forcing agents such as greenhouse gases CO_2 and methane (+1.66 and +0.48 W/m^2, respectively) (Forster et al., 2007). These values have identified BC as the second most significant agent to climate warming.

While suspended in the atmosphere, BC particles absorb solar radiation which can reduce planetary albedo, alter the temperature structure of the atmosphere and influence cloud processes (Bond et al., 2013). Planetary albedo is reduced because sunlight is absorbed or scattered by BC in the atmosphere before reaching reflective surfaces such as deserts, snow or clouds that would reflect it back to space. Known as direct radiative forcing, this causes a net increase in energy contained in the atmosphere and is considered one of the most significant climate forcing processes of BC.

Complex processes dictate the interaction of BC with clouds and can cause an indirect warming or cooling effect in the atmosphere. Cloud distribution can be altered by changes in the atmospheric temperature structure caused by BC warming effects. BC aerosol particles can act as nuclei within a cloud, thus affecting cloud formation. Increased droplet numbers within clouds caused by the nucleation effects of BC can increase cloud albedo and cause a cooling effect. On the other hand, this can encourage precipitation and ultimately lessen cloud cover.

Aerosol interactions with clouds and the resulting climatic impacts are highly uncertain and can vary by season or time of day. Reduced cloud cover can have a net warming effect by allowing more light to penetrate the atmosphere during the day or throughout the Arctic summer. However, cloud cover acts as an insulator by preventing longwave radiation emitted by the surface of the

Earth from escaping the troposphere. Thus, reduced cloud cover could induce a net cooling effect, particularly at night or during the polar night when there is little incoming solar radiation.

When evaluating the climatic impacts of BC, it is also necessary to consider its interactions with other aerosol components. Primary BC particles tend to range from 20-50 nm in diameter and are nearly spherical in shape (Smallwood et al., 2003). During or very shortly after emission, BC particles are cooled rapidly and become encapsulated with non-BC aerosol species through coagulation and condensation of organic vapors, forming the larger aggregate particles that are observed in the environment (Liousse et al., 1993). Adsorption of or internal mixing with organic matter and other species such as sulfates and nitrates increases as the particle ages in the atmosphere. The addition of non-BC species significantly impacts the light adsorption properties of BC particles by acting as a lens and focusing light into the BC core of the agglomerate (Bergstrom et al., 1982). A recently developed method to remove coatings on BC has suggested that coatings on aged aerosols can increase the MACS of bare BC particles by a factor of three (Cui et al., 2016). Consequently, these physical and chemical changes can amplify absorption of solar radiation and enhance the atmospheric warming processes induced by BC. Mixing with hydrophilic compounds will also enhance the cloud nucleation effects of particles and induce further cloud interactions.

1.2.2. Impacts to the Arctic

First introduced by Manabe and Stouffer (1980), Arctic amplification describes the phenomenon in which the increase in surface air temperature due to rising atmospheric greenhouse gas concentrations is amplified in the Arctic as compared to the Northern Hemisphere as a whole. Paleoclimate reconstructions have demonstrated that warming in the Arctic has consistently exceeded global changes by a factor of three to four (Miller et.al, 2010). The intensified response in the Arctic is attributed to a range of positive feedbacks associated with increased radiative forcing and reductions in sea ice, terrestrial ice and snow cover. Decreases in snow and ice surface reflectivity, or albedo, contribute to the accelerated melt of the cryosphere which, in turn, perpetuates the causes and consequences of climate change.

Climate models indicate that emissions of atmospheric particles such as BC and organic matter cause significant increases to the net solar warming of the snow-atmosphere column (Flanner et. al, 2009 and Hansen & Nazarenko, 2004). These impacts are due to atmospheric warming through radiative forcing as well as the lowered reflectivity of snow and ice. The albedo of fresh, clean snow is very high at visible wavelengths (0.75-0.90), allowing nearly all incoming light to be reflected (Warren 1982). BC levels of 5-50 ng per gram of snow, typical for Arctic snowpack, can reduce the albedo of snow by as much as 4% (Warren and Wiscombe, 1980), thus increasing the absorption of solar radiation. Albedo reductions of such magnitudes can greatly impact snow and ice melt, as reductions of only 1% are estimated to increase surface mass loss of the Greenland Ice Sheet by 27 Gt/yr (Dumont et al., 2014). They can also have significant contributions to climate forcing, as Hansen and Nazarenko (2004) have estimated a 1 W/m^2 climate forcing at middle and high latitude areas in the Northern Hemisphere due exclusively to albedo reductions of 2.5% and 5% in the Arctic and terrestrial Northern Hemisphere, respectively.

Lowered surface albedo causes warming of the troposphere and top of the cryosphere, which accelerates snow and ice melt and amplifies radiative forcing. The morphology of snow is altered as it warms, typically increasing grain size. Albedo is highly dependent on such morphological properties and decreases with increasing grain size (Warren and Wiscombe, 1980). In addition, carbonaceous impurities are more effective in reducing albedo when the snow grains are larger (Chýlek et al., 1983). Only 3 ng/g of BC would cause a 1% albedo reduction in melting old snow as compared to 15 ng/g necessary for the same reductions in fresh snow (Warren and Wiscombe, 1985). Snowpack thickness also decreases as the melt season begins. Albedo is dependent on the thickness of the snowpack and decreases dramatically as the snowpack becomes too thin to scatter back incoming light (Warren, 1982). As the snow melts or sublimates, it leaves most BC particles behind, thus increasing the impurity concentration at the surface and the absorption of solar radiation. This feeds the positive feedback loop of BC-induced albedo reductions of surface snow.

Reduction in snow, glacier and sea ice coverage, particularly during the summer season, greatly impact the total energy budget of the Arctic. Exposing a greater area of dark underlying surfaces with low reflectivity, such as rock, vegetation and sea water, increases the total amount of solar radiation that is absorbed and contained within the troposphere. This is particularly important at

the start of the melt season, when the stabilization of the atmospheric boundary layer in springtime inhibits heat exchange with the upper troposphere, thus containing warming to the Earth's surface.

A further consequence of glacial and ice sheet melt is rising sea level. For example, yearly losses in mass from the Antarctic and Greenland ice sheets have increased significantly in the last decades and have the potential to raise global sea levels by 32 cm by the year 2050 if acceleration continues at the current rate (Rignot et al., 2011). In Greenland, the leading contributor to accelerated mass loss from the ice sheet has been identified as increased surface melt and runoff (Box et al., 2012), driven primarily by impurities that reduce surface albedo (Tedstone et al., 2017).

As an additional consequence, retreating glaciers have the potential to expose vast subsurface hydrocarbon reserves in the Arctic which may release significant concentrations of methane to the atmosphere, a potent greenhouse gas. Permafrost and glaciers provide high enough pressures and low enough temperatures to entrap methane gas in the form of hydrates, preventing the gas from evading to the atmosphere. The lattice structure of hydrates provides a very concentrated source of methane that is stable within the geologic environments of the Arctic. Melting of the cryosphere can dissociate these stores, allowing methane gas to be released to the atmosphere along boundaries of glacial retreat and permafrost thaw (Anthony et al., 2012). It is widely agreed that a release of even a small fraction of the methane stored in the Arctic could contribute significantly to rising global greenhouse gas concentrations (McGuire et al., 2009).

1.3. Emission Sources of Black Carbon

Ice core studies have revealed that natural emission sources of BC existed prior to the onset of the industrial revolution in the mid 1800's. Prior to 1850, the major source of BC to the Arctic was from coniferous forest fires (McConnell et al., 2007). Today, while natural forest fires are still a predominant emissions source, a significant portion of atmospheric BC concentrations are derived from anthropogenic activities (Bond et al., 2013). BC measurements in a Greenland ice core show that industrial emissions after 1850 led to a sevenfold increase in BC concentrations from pre-industrial levels (McConnell et al., 2007). Global emissions are continually changing, vary greatly by region and are very difficult to quantify. Greater demand for energy and industry worldwide is

increasing total emissions, while implementation of cleaner technologies is concurrently working to reduce them. Anthropogenic and natural emission sources that are high in BC content and have a positive component of climate forcing include diesel engines, industrial activities, residential solid fuel and open burning. These activities represent about 90% of global BC emissions. Bond et al. (2013) summarizes current estimates of regional emissions as described in the following five subsections.

1.3.1. Diesel Engines

Within Europe, North America and Latin America, diesel engines contribute about 70% of the BC emissions. This includes on-road engines such as cars and trucks, and off-road machinery such as that used in agriculture and construction. Globally, diesel engines contributed to only 20% of BC emissions in the year 2000.

1.3.2. Industrial Activities

Industrial activities include coal combustion for coke-making in the steel industry, petrochemical flaring and process heat for brick and lime kilns. While technology is available to make coal combustors relatively clean, simple combustors still used in small industry and developing countries produce high levels of BC. It is estimated that 9% of global BC emissions is sourced from these industrial activities, taking place predominately in East Asia.

1.3.3. Residential Solid Fuels

Solid fuels such as coal and biomass are commonly burned for residential cooking and heating in developing countries. Simple ovens are typically used and result in high emissions of BC particles. These activities contribute between 60-80% of BC emissions throughout Asia and Africa, and 25% globally.

1.3.4. Open Burning

Open biomass burning is the largest source of global BC emissions, estimated at about 40% of the total. This includes predominately natural burning during forest and savannah wildfires, but also accounts for anthropogenic burning of agricultural fields. Open burning is higher in equatorial to

low southern latitudes, specifically Africa and Latin America, where forest and grassland fires are common.

1.3.5. Other Emission Sources

The remaining ~10% of BC emissions are largely attributed to shipping, flaring in the oil and gas industry and industrial and residential use of biofuels. In addition, an increasingly significant source of high-altitude BC emissions is coming from the growing number of hydrocarbon-fueled rocket launches occurring each year. The radiative forcing caused by the aerosol emissions from these launches has already reach a quarter of that caused by global aviation (Ross & Sheaffer, 2014). It is also worth noting that sectors such as shipping, aviation and rocket launches are capable of emitting pollutants in remote regions that would otherwise have little to no emission sources, such as the Arctic.

1.3.6. Emission Sources in the High Arctic

Local emission sources in the Arctic are considerably low compared to lower latitudes but are still prevalent. Flaring in the Arctic oil and gas industries accounts for two-thirds of the BC emissions north of 66ºN, but only 3% of global emissions (Stohl et al., 2013). However, significant uncertainties exist in determining BC emission values from flaring. Most of this is concentrated in oil and natural gas fields being drilled in northwestern Russia. Arctic shipping also contributes to emissions, as reductions in sea ice in the Northwest and Northeast Passages have allowed for more ship traffic (Cramer et al., 2014). Air traffic crosses over the Arctic region frequently, providing far-reaching supplies of emissions. Coal mining and coal burning for power generation exist as additional sources of BC on the Svalbard archipelago and have significant impacts on the localized concentrations (Aamaas et al., 2011 & Khan et al., 2017).

1.4. Atmospheric Transport to and Deposition in the Arctic

1.4.1. Atmospheric Transport to the Arctic

Although emission sources in the Arctic are quite low compared to other regions of the world, short-lived climate forcers can be readily transported from sources at lower latitudes to the Arctic. BC particles deposited in the Arctic originate predominately from lower latitudes (AMAP, 2015).

Prevailing winds can carry black carbon thousands of kilometers, both regionally and intercontinentally, away from emission sources (Bond et al., 2013). Larger particles typically settle out of the atmosphere by gravity nearer to the emission source, but smaller particles can remain in the atmosphere for weeks. The concentrations of BC reaching the Arctic will depend greatly on the transport and precipitation history of the air mass in which they're carried. For example, on the Svalbard archipelago, air arriving from the east contains more than 2.5 times higher BC concentrations than air arriving from the northern, northwestern or southern transport paths (Forsström et al., 2009). Higher concentrations in the east can be attributed to substantial emission sources in Europe and North Asia. However, the lower concentrations arriving on other trajectories are likely more influenced by atmospheric removal of contaminants and deposition processes prior to arriving in the Arctic.

1.4.2. Atmospheric Deposition in the Arctic

The average atmospheric lifespan of BC is limited to about a week before being removed through wet or dry deposition (Bond et al., 2013). Dry deposition is the direct contact of particles to a terrestrial surface due to gravity or impact to surfaces. Larger particles, traveling shorter distances, settle out more readily through dry deposition. Wet deposition, which accounts for 85-91% of BC deposition in the Arctic (Wang et al., 2011), includes in-cloud and below-cloud scavenging of particles in snow or rainfall. Smaller particles, which have a greater ability to travel to the Arctic, are typically deposited during precipitation events.

The atmospheric lifetime of BC is also dependent on its interactions with other aerosols. An aerosol particle is a colloid of solid particles or liquid droplets that are suspended in air. Newly emitted BC particles are hydrophobic, small in diameter and chemically inactive in the atmosphere. As they age and mix internally or externally with other aerosol components such as sulphates, nitrates and organics, their particle size and hygroscopicity increases. This makes them more efficient cloud-condensation and ice-forming nuclei (Bond et al., 2013), subsequently enhancing the wet deposition process and influencing their rate of removal.

1.4.3. Arctic Haze

A reddish-brown haze, known as Arctic haze, is visible in the atmosphere at high latitudes during the springtime. Anthropogenic emissions rich in contaminants are transported from Europe and Russia to the Arctic during winter (Quinn et al., 2007). They are trapped in the Arctic air mass due to a surface-based temperature inversion during the polar night that causes stratifications in the atmosphere to stabilize and prevent overturning. The stability of the atmosphere also inhibits cloud formation and precipitation, so contaminants are not readily removed through scavenging and instead accumulate (Barrie et al.,1981). Solar heating initiated at the return of the sun during spring causes mixing near the surface, which disrupts the inversion and leads to wet deposition through precipitation. The haze is typically made of a mixture of contaminants such as sulfates, particulate organic matter, black carbon and heavy metals (AMAP, 2006). The presence of aerosol particles makes the haze light-absorbing and has a significant effect on the springtime Arctic radiation balance (Shaw & Stamnes, 1980). Increased levels of particulate pollutants such as sulfate aerosols and nitrate have repeatedly been observed across the Arctic during winter and spring (AMAP, 2006).

1.4.4. Post-Deposition Processes

While the concentration of BC in falling snow is dependent only on wet deposition, BC concentrations in the snowpack depend on initial concentrations from wet and dry deposition and are further altered by post-deposition processes. Often, post-deposition processes increase the surface concentration of BC and thus amplify its warming effects. Sublimation can occur as snow ages, which removes vapor water, leaving behind an increased concentration of non-volatile BC on the surface. Melting of snow can create a positive feedback and increase the BC surface concentration due to inefficient scavenging of particles in melting snowpack (Doherty et al., 2010 and Flanner et al., 2007). Melt water usually does not flush the hydrophobic particles through the snow column but rather leaves them on the surface (Doherty et al., 2013).

Snow drifting also induces changes in contaminant content in surface snow and can be particularly influential in glacial areas impacted by katabatic winds and dry, cold, windy regions such as the Arctic. In addition to enhancing sublimation in the snowpack, this phenomenon contributes to small-scale, horizontal variability in impurity levels by redistributing contaminants bonded to the

blowing snow particles. Additionally, the turbulent transport of snow can introduce other impurities, particularly in glaciated areas with nunataks or other exposed rock, where minerals and organic materials can be blown and incorporated into the snowpack.

1.5. Source Attribution of Black Carbon

1.5.1. Levoglucosan

Levoglucosan ($C_6H_{10}O_5$, see Figure 1.1) is a monosaccharide derivative that is used as a highly specific chemical tracer for particulate matter emissions from biomass burning. It is the thermal degradation product of cellulose and is thus exclusively found in BC materials derived from the combustion of biomass (Kuo et al., 2008). Levoglucosan can be used to identify potential BC sources to the Arctic such as boreal forest fires, agricultural or municipal waste incineration and residential wood burning. However, the levels of levoglucosan yielded in the combustion process are highly dependent on several factors and thus make source attribution difficult. The combustion temperature is the most influential factor, with levoglucosan only present in samples burned between 150-350°C, while plant species type is also determinative (Kuo et al., 2008).

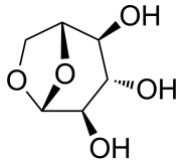

Figure 1.1. Chemical structure of levoglucosan

Using laboratory studies, levoglucosan has been shown to undergo oxidative degradation by reactions with OH radicals during atmospheric transport and may only have an atmospheric lifespan of 0.7 to 2.2 days when exposed to typical summertime atmospheric chemistry conditions (Hennigan et al., 2010). However, wintertime conditions at high latitude may prolong the stability of the compound. Therefore, it is necessary to consider seasonal variation in the compound's extent of degradation when completing temporal studies using levoglucosan as a biomarker.

1.5.2. Trace Elements

Source identification of BC particles or individual soot agglomerates can be conducted by analyzing for trace elements that the particles may be coated or mixed with. Coal-derived carbonaceous particles can be associated with inorganic species containing alkali and alkaline earth elements including Na, Mg, Ca and Ba (Chen et al., 2005). In addition, high levels of P have been consistently linked to soot from coal burning in Barentsburg, Svalbard (Weinbruch et al., 2018). Residual oil-derived carbonaceous particles can be linked with external species containing transition metals such as V, Fe, Ni and Zn. Although this is not conclusive, as these transition metals were not observed by Vander Wal et al. (2010) in their analysis of oil burning soot. Diesel-derived particles have fewer inorganic inclusions (Chen et al., 2005) and thus the concentrations are too low for unambiguous source identification (Weinbruch et al., 2018). Carbonaceous particles derived from biomass and wood burning are typically enriched in K (Tumolva et al., 2010).

It is important to note, however, that aged atmospheric particles tend to show greater levels of trace elements, indicating that the particles become coated, coagulated or mixed with other chemical species during post-emission atmospheric processing (Tumolva et al., 2010). Although the extent and type of processing may be influenced by the origin of the particles, this can make drawing conclusions based on trace element analysis difficult regardless. This is particularly true with long-range transported particles in the Arctic, as their long atmospheric lifespan would offer ample opportunity to mix and coagulate with other aerosols.

1.5.3. Air Trajectory Models

The potential geographical origins of contaminant-containing air masses can be determined using back-trajectory analysis. The Hybrid Single-Particle Lagrangian Integrated Trajectory model (HYSPLIT) created by the National Oceanic and Atmospheric Administration (NOAA) Air Resources Laboratory (ARL) computes and models air parcel trajectories based on a selected point and time of termination. The model applies both a Lagrangian approach, using a moving frame of reference to compute advection and diffusion of air masses, as well as the Eulerian methodology, which applies a fixed three-dimensional grid as the frame of reference for calculations of pollutant air concentrations (Stein et al., 2015).

1.5.4. Source Attribution to Svalbard

Emission sources that are situated north of the polar front allow for rapid, low-level transport of BC to the Arctic without having to penetrate the polar dome. Various air trajectory analyses have concluded that atmospheric transport of BC to Svalbard originates mostly from Russia and Northern Eurasia (Eleftheriadis et al., 2009; Hirdman et al., 2010; Wang et al, 2011), driven by circulation patterns around the Icelandic Low and Siberian High pressure centers. Differences in source regions vary by seasons and are dependent on changes in air circulation patterns and storm tracks in the Northern Hemisphere.

Various studies using levoglucosan as a chemical tracer for biomass burning have been conducted on the Svalbard archipelago. It has been found that spring and summertime concentrations of BC on Svalbard can be heavily influenced by emissions from boreal forest fires in Siberia due to their close proximity to the Arctic (Stohl 2006 & Stohl et al., 2007). In contrast, a study analyzing levoglucosan levels at Zeppelin observatory, located at 474 m a.s.l. on Svalbard, indicated elevated ambient levels of the chemical tracer during winter compared to summer months (Yttri et al., 2013). However, the seasonal variation was attributed to the Arctic haze phenomenon, and despite elevated levels of levoglucosan it was determined that fossil fuel sources dominated the European Arctic BC concentrations in winter. As the frequency and extent of global forest fires grows as a consequence of climate change, the Arctic may be increasingly impacted by such emissions.

A study using transition electron microscopy to identify sources of atmospheric soot particles in Svalbard supported the notion that fossil fuel combustion is the main contributor (Weinbruch et al., 2018). While local sources of BC such as ship emissions and coal burning had impacts to contaminant levels within the major Svalbard settlements, it was determined that they did not contribute significantly to the atmospheric levels found at the Zeppelin observatory. The study determined that aircraft emissions, diesel exhaust and long-range transport of coal burning emissions were the most prevalent sources of BC to Svalbard.

1.6 Black Carbon Trends

A global assessment of anthropogenic emissions of particulate matter, including BC, was conducted by Klimont et al. (2017). The study revealed that global emissions of BC increased by 15% from 1990 to 2010, however changes in regional emission trends were varied. Increases were primarily observed in more southerly regions, including Asia and Africa, due to growth in residential combustion and the transport sector. These emissions, however, would not likely impact BC levels in the Arctic as the atmospheric residence time of BC is not long enough for the particles to travel such distances. Most regions at mid to high latitudes in the Northern Hemisphere, where emissions are more prone to reach the Arctic, have managed to reduce their emissions since 1990.

Long terms studies have revealed a general decrease in BC levels in Arctic snowpack over the last decades (Eleftheriadis et al., 2009; Hirdman et al., 2010; Sharma et al., 2004 & Sharma et al., 2013). These reductions have been explained predominantly by the decreasing emission trends at source regions and to a much lesser extent, changing atmospheric transport patterns. Hirdman et al. (2010) determined that only 4.9% of BC concentration decreases at Zeppelin, Svalbard could be attributed to circulation changes, while the majority was driven by emission reductions. Therefore, further reductions in global BC emissions could have significant impacts on the levels of BC deposited in the Arctic.

1.7. The Study Site

1.7.1. Svalbard

Svalbard is a Norwegian archipelago that lies within the European sector of the high Arctic (see Figure 1.2). The islands are situated approximately 800 km north of mainland Norway between 71° and 84° north latitude and 10° and 35° east longitude. The maritime Arctic climate is heavily influenced by the warm waters of the North Atlantic current system, which maintain unusually high surface air temperatures with respect to the archipelago's high latitude. The warm Atlantic water also regulates sea ice and keeps the surrounding waters ice-free and navigable throughout most of the year. Nearly 60% of the total area of Svalbard is covered by glaciers (Liestøl 1993).

The melt season for Svalbard ice caps generally begins between late May and late June and finishes by the beginning of October (Sharp and Wang, 2009).

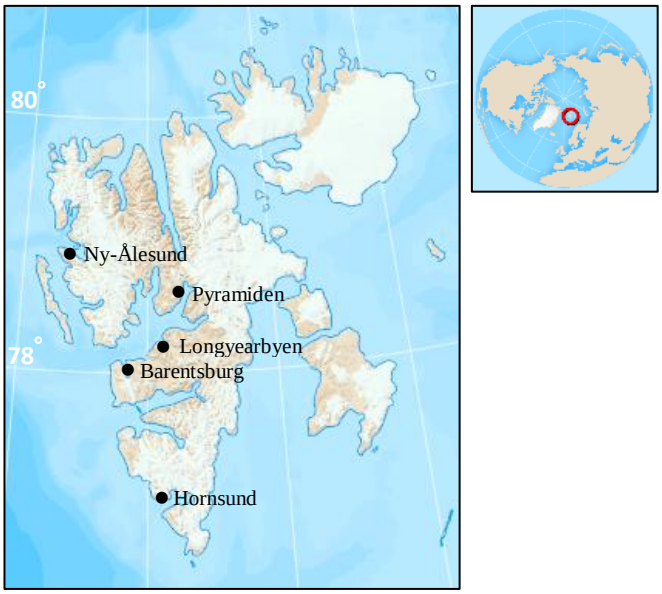

Figure 1.2. Map of Svalbard with settlements identified

The population of Svalbard is approximately 2,300 people spread out among the settlements of Longyearbyen, Barentsburg, Ny-Ålesund and Hornsund (Statistics Norway, 2018). Several people also live in Pyramiden, a deserted mining town that is attracting a growing number of tourists by ship and snowmobile each year. Coal mining activities have been present on Svalbard since the early 20th century with two active mines still remaining today in Longyearbyen and Barentsburg. Coal is the main source of power for the settlements of Longyearbyen and Barentsburg, both with active coal power plants. The tourism industry has grown in recent decades to supplement the shrinking mining industry and brings over 60,000 tourists per year (Visit Svalbard, 2018). Scientific research is also a growing industry and attracts many scientists and students to the University Centre of Svalbard as well as research bases situated throughout Svalbard each year.

1.7.2. Ny-Ålesund

Ny-Ålesund, a former coal mining settlement, is now a base for international scientific Arctic research and environmental monitoring. Ten countries are represented with permanent research

stations, three of which are staffed year-round. The scientific community lies on the northwest coast of Spitsbergen, the largest island of the Svalbard archipelago, within the Kongsfjord. The average surface air temperature in this region ranges from -12.4°C during the coldest month to +5.3°C in the warmest month. The average annual total precipitation is 423 mm with minimum levels during April through July (Serreze et al., 2015). However, the amount of snowfall can exhibit significant spatial variabilities in the region due to orographic effects and meteorological conditions.

Ny-Ålesund is considered to be a well-suited location for the study of long-range transport of pollutants to the Arctic, as the local sources of pollution are minimal. The population of Ny-Ålesund is limited only to support staff and researchers, consisting of 35 people in the winter and a maximum of 180 in the summer. There are a limited number of weekly flights connecting Ny-Ålesund with Longyearbyen year-round and regular ship traffic within the fjord during summer. Restrictions in shipping traffic set in 2015 have prohibited ships running on heavy oil from entering the Kongsfjord. However, cruise ships running on light fuel or electric power are able to visit the settlement during the summer and bring about 13,000 tourists per year. Automobile traffic is minimal throughout the year, but regular snowmobile traffic is prevalent throughout the winter. Typical snow scooters used in the area are powered by 600 and 1200cc 4-stroke gasoline engines. The power supply to Ny-Ålesund is no longer provided by coal, but rather by a diesel powerplant located within the settlement. However, two active coal mines and coal power plants are located approximately 110 km southeast of Ny-Ålesund in Longyearbyen and Barentsburg.

1.7.3. Glaciers Near Ny-Ålesund

The Brøgger peninsula on which Ny-Ålesund is situated is covered by a variety of high-Arctic valley glaciers, tidewater glaciers and icefields. Five of these glaciers, representing a range of glacier types and altitudes, have been continually monitored through yearly mass balance studies by the Norwegian Polar Institute. All have revealed a reduction in mass throughout their respective monitoring periods, which extend as far back as 1967 (Norwegian Polar Institute, 2019). The mass balance of a glacier is dependent on the amount of precipitation received throughout the winter and the extent of melt during the summer. Thus, yearly snow accumulation on these glaciers is not sufficient to overcome the rate of seasonal melt.

1.8. The Present Study

The region around Ny-Ålesund is generally considered a pristine Arctic site and the area is often used as an indicator for background levels of contaminants in the European Arctic. The objective of this work was to determine if the anthropogenic activity in Ny-Ålesund is having a measurable impact on the surrounding region and leading to contaminant levels exceeding that which would be expected from long range atmospheric transport alone. The spatial distribution of BC on glaciers within the Ny-Ålesund region was used as a proxy to investigate the potential extent and impacts of local emission sources. Surface snow samples were collected from glaciers at varying altitudes and distances from Ny-Ålesund during spring 2018. Samples were also taken from layers within snow pits dug in the accumulation area of each glacier. The samples were analyzed for BC and organic carbon (OC) content, as well as levoglucosan and selected trace elements, and compared to a similar dataset gathered during spring 2017. It was hypothesized that samples closer to Ny-Ålesund would exhibit a higher concentration of BC, inferring an impact from the settlement's activities. It was also thought that samples at lower altitudes would exhibit higher concentrations of BC due to a greater extent of scavenging in the air column during wet deposition and the containment of aerosols below the atmospheric boundary layer.

2. Methods

2.1. Sample Collection

The snow sampling was conducted over several field campaigns within the Kongsfjord region from late March to early May of 2018. A total of 67 snow samples were collected from sites on five glaciers; Kongsvegen (KV), Holtedahlfonna (HDF), Edithbreen (EB), Midtre Lovènbreen (ML) and Austre Brøggerbreen (BR); as well as the Gruvebadet (GVB) area between Zeppelin mountain and the settlement of Ny-Ålesund (see Figure 2.1). The campaigns concentrated on sampling surface snow along transects running from the snout of each glacier to the accumulation areas. Most sampling days were selected the day after large snowfall events. In addition, snow pits were dug in the accumulation area of each glacier in order to sample the entire seasonal snow column. Details of all 2018 sampling sites can be found in Appendix A.

All sampling procedures followed the snow sampling protocols published by the Norwegian Polar Institute (NPI) (Gallet et al., 2018). BC concentrations are typically very low in polar snow and thus the risk of contamination during sampling can be high. Appropriate precautions were taken to avoid potential contamination from vehicle exhaust and clothing. The glacier sampling sites were accessed by snowmobile and the Gruvebadet site was reached by electric car or snowmobile. Samples were taken upwind from vehicles and at least 50 m from any snowmobile tracks. Extra-large non-particulating coverall suits were worn over snowmobile suits during sampling as well as plastic gloves.

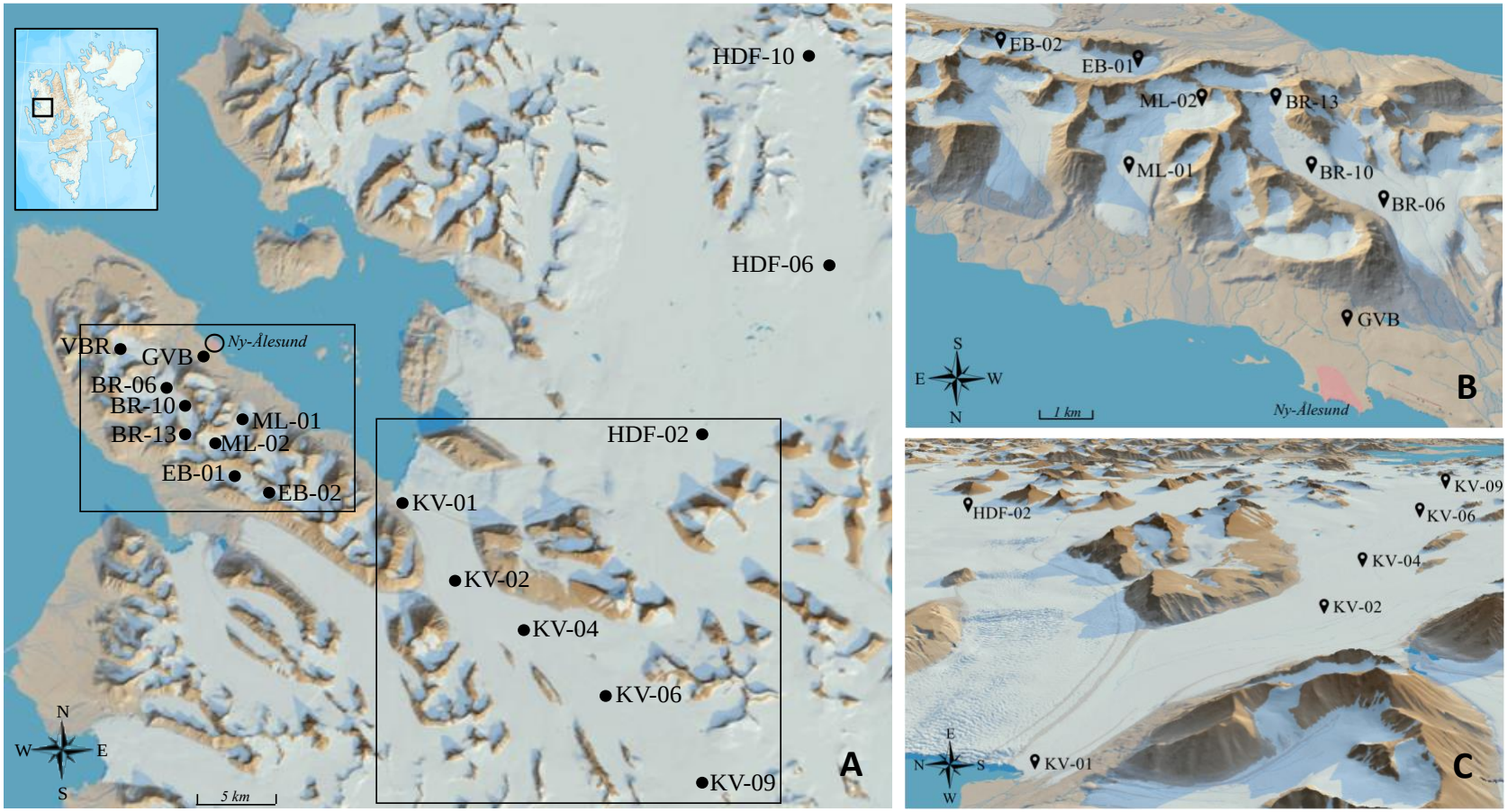

Figure 2.1. Map of sampling sites
a) Map of all 2018 sampling sites; b) detailed map of sampling sites on Brøgger peninsula; c) detailed map of sampling sites on Kongsvegen glacier. (*Map data and cartography: Norwegian Polar Institute, 2019*)

2.1.1. Snow Surface Sampling

When possible, surface snow sampling was conducted the day after a large snowfall event in order to minimize potential alterations in the snowpack due to post-deposition processing and to identify the spatial variability of contaminant levels within one weather event. However, samples were also taken on days without recent precipitation. Meteorological conditions were noted at each sampling site and potential influences, such as exposed moraine or topographical obstacles, were identified. Stainless steel or plastic scoops were used to collect the top layer of fresh snow, typically the top 2-10 cm. Approximately 5 L of snow was collected for samples for BC analysis and placed into 5.4 L transparent polyethylene Whirl-Pak bags. Samples for levoglucosan and trace element analysis were collected directly into 50 mL plastic centrifuge tubes. One Whirl-Pak bag was collected for BC and two vials were collected for levoglucosan and trace element analysis at each sampling site.

2.1.2. Snow Pit Sampling

Snow pits were dug according to the NPI sampling protocol, as described below. Pits were dug in the accumulation zone of each glacier, spanning the entire winter snowpack, until reaching the firn or the previous year's layer of superimposed ice. All pits were sampled in April and thus completed prior to the onset of seasonal surface melt. Pits were dug on days with minimal wind and all snow excavated from the pit was disposed of on the downwind side of the digging site to avoid it drifting back. The snow pits were large enough to sample within them comfortably without brushing against and contaminating the snow wall. The sun-shaded side of the snow pit was selected as the sampling face on sunny days to avoid melt or changes in snow morphology while sampling.

A folding plastic ruler was placed on the face of the pit and snow stratigraphy data was recorded for each layer, starting with the temperature profile. Snow temperatures were measured every 10 cm starting near the surface. The stratigraphic sequence and thickness of each distinct layer was recorded, including hardness and snow grain shape and size. The 'hand test' was used to measure hardness of each layer according to the scale described by Fierz et al. (2009). The snowpack density for snow water equivalent (SWE) was measured along the whole snowpack at 20 cm intervals using a 20 cm long, 2.75 cm inner diameter cylindrical snow cutter. The cylinder was inserted vertically into the snowpack from the surface of each 20 cm segment and stopped using a

metal spatula. The snow collected within the cylindrical cutter was emptied into a plastic bag of known weight and weighed onsite by a scale. Densities were calculated by dividing the collected snow weight by the volume of the cylinder. All snow stratigraphy recordings can be found in Appendix A.

Before taking snow samples, a clean face was made on the sampling wall by removing the outer 10-20 cm. First, a surface sample was taken of the topmost layer, as described by the Snow Surface Sampling section above. Proceeding vertically down the snowpack, the next sample was collected from a segment approximately 50 cm thick, starting and ending at distinct layers. Blocks of snow were cut vertically with a metal knife, spanning the 50 cm segment to ensure a representative sample of each layer. This continued until the bottom of the seasonal snowpack. One 5 L BC sample was collected from each 50 cm segment and two 50 mL tubes were filled for levoglucosan and trace elements from the surface snow only.

2.1.3. Filtering

Samples for levoglucosan and trace element analysis were kept frozen and shipped to Ca' Foscari University of Venice, Italy where they were stored at -18°C for seven months. All BC snow samples were kept frozen in their Whirl-Pak bags within a cool box that was left outside in weather consistently below 0°C. Samples were not stored longer than two days before being taken inside the NPI Sverdrup station at Ny-Ålesund to melt at room temperature. Melted samples were filtered with quartz-fiber filters (pre-baked at 400°C and stored in aluminum foil in the refrigerator). All glassware was rinsed with ultrapure Milli-Q water and filters were placed with tweezers onto a glass filter funnel. The full volume of the liquid samples was pumped through the filters using a hand vacuum pump. The liquid volume of each sample was recorded before rinsing the Whirl-Pak bags with Milli-Q water to remove any particles left in the bag and adding this liquid through the filter. Filters were transferred with tweezers to plastic Petri dishes where they were left to dry overnight in the laboratory with tops loosely covering them. Once the filters were dried, Petri dishes were taped shut, wrapped in aluminum foil and stored in the refrigerator. All BC filter samples were hand carried back to Italy for analyses.

2.2. Determination of Carbon Content

Thermal optical analysis (TOA) following the EUSAAR_2 thermal evolution protocol (Cavalli et al., 2010) was used to determine the carbonaceous aerosol fraction of each filtered snow sample and further classify it into organic carbon (OC) and elemental carbon (EC). In this study, and consistent with many other studies, BC levels are determined by measurement of EC, which is defined as the refractory portion of soot particles that remain stable at high temperatures. In the thermal optical method, the carbonaceous aerosol particles deposited on the quartz filters are thermally desorbed first in an inert atmosphere with He and then in an oxidizing atmosphere with He and O_2. Theoretically, the OC is evaporated in the inert gas environment, while the EC combusts within the oxidizing atmosphere. However, thermally unstable organic compounds can pyrolyze in the inert atmosphere to form pyrolytic organic carbon (POC), which will desorb along with EC in the oxidizing atmosphere. In order to correct for this, a laser diode with a photo detector is used to monitor the transmittance of light through the filter throughout the analysis. The EUSAAR_2 protocol has optimized the stepwise heating process of TOA in order to improve the accuracy of discrimination between OC and EC by reducing pyrolysis and by minimizing early evolution of EC and incomplete evolution of OC during the inert phase (Cavalli et al., 2010). It is used widely in studies analyzing for BC content.

2.2.1. Determination of Carbon Content on the Filter

A square punch with in an area of 1 cm^2 was made in each filter to remove a representative portion of the sample for analysis. If particles did not appear to be evenly distributed on the filter, one or two additional punches were made and analyzed separately. The particle loaded filters were heated in a stepwise fashion from 200 to 650°C in a stream of pure helium gas as per the EUSAAR_2 protocol, described in Table 2.1. No oxidation of carbon takes place during this stage due to the inert atmosphere. Rather, OC compounds evaporate while EC remains on the filter. However, thermally unstable OC compounds may break down, or pyrolyze in the inert atmosphere and remain on the filter as POC. The evaporated OC compounds were oxidized to carbon dioxide by a catalyst and thereafter reduced to methane. The amount of methane was then determined by a flame ionization detector (FID). Next, oxygen was introduced over the filter in a stream of 98% He and 2% O_2 gas during a second stepwise heating process from 500 to 850°C (see Table 2.1). The remaining EC and POC were oxidized during this stage and subsequently reduced to methane

for measurement by FID. At the end of each analysis, a fixed volume of gas (5% methane in He) was injected into the instrument as an internal calibration. The corresponding FID signals formed the calibration peaks which were used, along with a calibration constant, to calculate the mass measurements of EC and OC in each sample.

Table 2.1. Thermal evolution protocol as per EUSAAR_2 (Cavalli et al., 2010)

Inert Atmosphere (He)		
	Temperature (°C)	*Time (sec)*
Step 1	200	120
Step 2	300	150
Step 3	450	180
Step 4	650	180

Oxygenated Atmosphere (O2/He)		
	Temperature (°C)	*Time (sec)*
Step 1	500	120
Step 2	550	120
Step 3	700	70
Step 4	850	80

2.2.2. Differentiation of OC and EC

Optical transmittance was used to differentiate between OC, POC and EC content on the filters. A 658 nm laser beam with a photo detector was used to measure the transmittance of light through the filters throughout the heating process. The amount of EC present on the filters at the start of the process determined their initial transmittance. When OC was pyrolyzed during the inert heating phase and left on the filters as POC, the filters darkened and their transmittance decreased. When oxygen was introduced to the system and the carbon was oxidized, the filters became lighter and their transmittance increased again. Once the filters returned to their initial transmittance level, it was assumed that all pyrolyzed OC had been oxidized and the remaining carbon oxidized thereafter was regarded as EC.

2.2.3. Calculation of OC and EC Concentration in Snow Samples

The EC and OC measurements produced by the TOA were reported in micrograms of EC or OC per punched area of filter (1 cm^2). These values were the filter loadings (L_{EC} and L_{OC}) and were in terms of mass per unit area ($\mu g/cm^2$). For most samples it was assumed that the particles were evenly distributed on the filter, and thus the total mass of particles (m_{EC} and m_{OC}) retained during the filtration of meltwater samples was given by:

$$m_{EC} = L_{EC} \times A_{filt} \text{ and } m_{OC} = L_{OC} \times A_{filt}$$

where A_{filt} is the total area of the filter through which the meltwater passed. The filter area in this study was 9.079 cm^2. In cases in which homogenous particle distribution was not assumed and multiple punches were analyzed, the average of L_{EC} and L_{OC} values from all punches were used in the above equation. It was further assumed that all EC and OC particles present in the snow samples were retained on the filter and thus the mean concentration of EC and OC particles within the samples were calculated by:

$$[EC] = \frac{m_{EC}}{V_{MW}} \text{ and } [OC] = \frac{m_{OC}}{V_{MW}}$$

where V_{MW} is the total volume in liters of snow meltwater that was filtered. Thus, the units of *[EC]* and *[OC]* were in μg/L, equivalent to ng/g using the density of water as 1 g/mL.

2.2.4. Calculation of Total Seasonal BC Flux in Snow Pit Samples

The total seasonal flux of BC was calculated from BC concentrations of layers within the snow pits and their corresponding SWE. Starting below the surface snow layer, representative snow samples were taken for approximately every 50 cm vertical sections within the snow pit, yielding an average BC concentration across each section. Density measurements were taken every 20 cm in the snowpack. Thus, the SWE and BC load ($L_{EC,i}$) was calculated for each segment of the snowpack with individual densities and BC concentrations:

$$SWE_i = z_i \rho_i$$

$$L_{EC,i} = [EC]_i \times SWE_i$$

where z_i is the thickness and ρ_i is the measured density of each segment, i. The total seasonal flux of BC and OC within one snow pit (F_{EC} and F_{OC}) was calculated by summing the $L_{EC,i}$ of all n segments of the snow pit and was reported in ng/cm^2:

$$F_{EC} = \sum_{i=1}^{n} L_{EC,i} \text{ and } F_{OC} = \sum_{i=1}^{n} L_{OC,i}.$$

2.3. Levoglucosan Analysis

2.3.1. Sample Preparation

Quantification of levoglucosan was conducted at the Ca' Foscari University of Venice in November 2018 using high-performance liquid chromatography (HPLC) coupled with a triple quadrupole mass spectrometer (MS/MS). Samples for levoglucosan analysis were removed from the freezer and left to melt in their tubes at room temperature. To avoid potential adsorption of levoglucosan onto glass, 1 mL polypropylene vials were used in the sample analysis. All vials were washed with ultrapure water (UPW; produced by Purelab Ultra system, Elga, High Wycombe, UK) for 15 minutes in a sonic bath. This was repeated with new UPW in a clean laboratory equipped with Class 100 vertical laminar flow hoods. The remaining pre-analytical procedures were carried out in this environment.

Samples and internal standards were transferred to the 1 mL vials in set volumes using Eppendorf pipettes with polyethylene tips rinsed with UPW. Volumes were determined in order to yield a final concentration of 250 pg/mL of internal standards in each sample. Each individual sample consisted of 675 μL of melted snow and 25 μL of internal labeled standard of levoglucosan $^{13}C_6$ (*6.91 ng levoglucosan*/mL,* Cambridge Isotope Laboratories Inc., Andover, MA, USA). Response factor (RF) samples were generated with 595 μL UPW, 25 μL labeled levoglucosan $^{13}C_6$ and 80 μL native standard (*2.18 mg levoglucosan/mL,* Sigma-Aldrich, Steinheim, Germany), yielding 250 pg/mL concentrations of both the labeled and native standards. Five lab blank samples were also generated using 675 μL UPW and 25 μL labeled internal standard.

2.3.2. HPLC and MS/MS

An Agilent 1100 Series HPLC system (Agilent, Waldbronn, Germany) with a binary pump, vacuum degasser, autosampler and thermostatted column compartment was used for chromatographic analysis. The HPLC system was purged with water in the mobile phase A line and with methanol in the mobile phase B line. The HPLC pump was manually purged with a post column injection solution of 100 mL methanol and 700 μL 25% ammonium hydroxide solution. A Synergi 4u Hydro-PR 80A column (50 mm length x 4.6 mm i.d.) was installed with a 0.2 μm

metal filter in order to on-line filter the samples and prevent any contamination occurring with a common filtration.

For the analysis, 100 μL of the prepared samples was injected into the column and the flow of the chromatographic run was 500 μL/min. The gradient run started with an initial mobile phase composition of 15% B (methanol) and an isocratic hold of 4 minutes, followed by a 2-minute gradient time from 15% to 100% B. The system was purged from 6-13 minutes at 100% B to elute highly retained components from the column and then re-equilibrated from 15-25 minutes at 15% B to return the whole analytical column to the initial gradient composition prior to the next run. The mobile phase compositions of the gradient run are detailed in Table 2.2. The analysis queue started with UPW samples, followed by two response factors, UPW, lab blanks and then the snow samples mixed intermittently with response factors and UPW. The retention time of levoglucosan was at 1.98 minutes and the run lasted 4 minutes.

Table 2.2. Mobile phase composition gradient of the HPLC run

Time (min)	*A (%)*	*B (%)*
0	85	15
4	85	15
6	0	100
13	0	100
15	85	15
25	85	15

An API 4000 triple quadrupole MS system (Applied Biosystems/MDS SCIEX, Toronto Ontario, Canada) with Turbo V^{TM} source was used for quantification of levoglucosan in the melted snow samples. In order to achieve high selectivity and increased sensitivity, the system was operated in negative ion mode by multiple reaction monitoring (MRM) with 150 ms dwell time per transition. The first quadrupole (Q1) of the MRM acquisition mode selected the precursor ion of interest, while the third (Q3) selected the product ion of interest produced in the second quadrupole (Q2), or collision cell. The collision energy (CE) within the collision cell and the collision cell exit potential (CXP) were optimized previously for each transition. Instrumental conditions are

reported in Table 2.3 and a summary of the transitions monitored with CE and CXP parameters are given in Table 2.4. The transitions 161/112.9 *m/z* for levoglucosan and 167/117.8 *m/z* for labeled levoglucosan were used in the quantification of the samples due to strength of signal and minimal noise.

Table 2.3. Instrumental conditions and measurement parameters for MS system

API 4000	
Collision gas (psi)	8
Curtain gas (psi)	50
Ion source gas 1 (psi)	60
Ion source gas 2 (psi)	40
Ionization voltage (V)	-4500
Temperature (°C)	450

Table 2.4. Transitions monitored and compound parameter collision energy (CE) and collision cell exit potential (CXP) settings for levoglucosan and labeled levoglucosan

Levoglucosan			
Q1 m/z	*Q3 m/z*	*CE (V)*	*CXP (V)*
161	113	-14	-8.4
161	101	-14	-3
161	71	-17	-7

Levoglucosan ^{13}C			
Q1 m/z	*Q3 m/z*	*CE (V)*	*CXP (V)*
167	118	-14.4	-8.2
167	105	-15.7	-15
167	74	-19.6	-11.2

2.3.3. Calculation of Method Detection Limit and Limit of Detection

The five lab blank samples were used to calculate the method detection limit (MDL) of the levoglucosan analysis with the following equation:

$$MDL = 3 \cdot \sigma_{LB}$$

where σ_{LB} is the standard deviation of the measured levoglucosan concentrations of the lab blank samples. The 'cut-off' approach was used to determine the limit of detection (LOD) of the instrument and was calculated at the concentration when the signal to noise ratio (S/N) was equal to three.

2.4. Trace Element Analysis

2.4.1. Sample Preparation

All polypropylene vials used for the trace metal analysis (samples, standard, instrumental washing solutions) were cleaned by filling each with 3% HNO_3 solution (diluted using 69% HNO_3 ultrapure grade solution, UPA, Romil, Cambridge and UPW, Purelab Ultra system, Elga, High Wycombe, UK) and leaving overnight at room temperature. The HNO_3 solution was then poured out of the vials and each vial was rinsed three times with UPW. Vials were left in a laminar flow hood in a clean room to dry. Samples for trace element analysis were removed from the freezer and left to melt in their tubes at room temperature. Once melted, 5 mL of melted sample was transferred to each vial along with 100 µL of 69% HNO_3 ultrapure grade solution (UPA, Romil, Cambridge). The vials were stored at -18°C until analysis could begin.

2.4.2. ICP-SFMS

All trace metal measurements were completed with an Inductively Coupled Plasma Sector Field Mass Spectrometer (ICP-SFMS; Element2, ThermoFischer, Bremen, Germany) equipped with a cyclonic Peltier-cooled spray chamber (ESI, Omaha, USA) at the Ca' Foscari University of Venice. The sample flow was maintained at 0.4 mL/min. The sample solution was introduced into the system by self-aspiration and then nebulized by a microconcentric nebulizer (MCN-100, Cetac Technologies, Omaha, NB, USA). A 2% v\v solution of ultrapure HNO_3 (diluted using 69% HNO_3 ultrapure grade solution, UPA, Romil, Cambridge and UPW, Purelab Ultra system, Elga, High Wycombe, UK) was allowed to flow through the sample introduction system for two hours prior to the measurement session to avoid potential contamination. A 90 second cleaning step using the 2% HNO_3 solution was also flushed between each sample to avoid a possible memory effect.

The flow rate of the aerosol carrier gas was optimized by obtaining the maximum signal response with a 1.0 ng/g HNO_3 acidified UPW solution of indium. Sensitivities ranged during the analysis between 180,000 and 300,000 counts/s in low resolution mode and between 9000 and 15,000 counts/s per ng/g of indium in medium resolution mode. A calibration was completed at the start of the measurement session in both low and medium resolution modes with a 1.0 ng/g multi-element standard solution (Merck, Darmstadt, Germany) containing Li, B, Na, Sc, Fe, Co, Ga, Y,

In, Rh, Ba, Lu, Tl and U. A mass calibration was completed in medium resolution mode when drift in the *m/z* values exceeded 0.003. An external calibration curve was obtained by analysis of one blank and six standards and was used in the quantification of each analyte. All instrument conditions and measurement parameters are detailed in Table 2.5.

Table 2.5. Instrumental conditions and measurement parameters for the ThermoFischer ICP-SFMS

Finnigan MAT Element	
Forward power	1300 W
Plasma flow rate	14.5 L/min
Intermediate gas flow rate	0.7 L/min
Sample uptake rate	40-80 μL/min
Washing time	3 min
Take up time	40 s
Acquisition mode	E-scan
Number of scans	50
Dwell time per acquisition point	10 ms
Total acquisition time	0.5 s per mass segment scan
Number of acquisition points per mass segment	50
Run and passes	5, 5
Acquisition window	100%
Search window	100%
Integration window (low resolution)	60
Integration window (medium resolution)	50

2.5. Ambient BC Measurements

Atmospheric measurements of BC were taken at the Sverdrup station within the settlement of Ny-Ålesund with a single wavelength particle soot absorber photometer (3-λ PSAP, Radiance Research, Seattle) operating at 525 nm. A pump drew air through a filter and the absorption of the filter was measured every 10 minutes. The difference between absorption levels at each measurement along with the volume of air filtered during that time were used to calculate absorption in units of m^{-1}. In order to convert absorption to concentration, the mass absorption coefficient (MAC) was used, which characterizes how easily a beam can penetrate a material and is dependent on the properties of the material and the wavelength of the beam used in the measurement. The MAC used in this study was 6.6 m^2/kg, which accounts for the absorbance of both BC particles and the aerosols that typically coat BC particles. Dividing absorption by the MAC produced BC concentration values for every 10 minutes, which were averaged into hourly values.

3. Results and Discussion

A dataset of BC and OC content in snow surface samples collected in the Ny-Ålesund region during spring 2017 were added to the 2018 dataset. The 2017 dataset used similar sampling locations to the 2018 study and were also analyzed by the TOA method using the EUSAAR_2 thermal evolution protocol. The 2017 study included a sampling site on an additional glacier not included in the 2018 campaign, Vestre Brøggerbreen (VBR), which is northwest of Austre Brøggerbreen and southwest of Ny-Ålesund and is labeled in Figure 2.1.a. All details of sampling locations from the 2017 campaign can be found in Appendix A.

3.1. 2017 and 2018 EC and OC Surface Snow Concentrations

For the initial analysis, all surface snow sampling locations were divided into two groups based on wind patterns in the Ny-Ålesund region. Wind in the Ny-Ålesund region most often flows from the southeast and is influenced strongly by katabatic winds bringing cold, heavy air from inland glaciers downwards towards the Kongsfjord (Argentini et al., 2003). Based on this information, *Group 1* sampling sites included the GVB sampling site and all sampling sites on KV as these areas are generally under the same prevailing wind pattern, driven by katabatic winds flowing down KV and into the fjord. *Group 2* consisted of the remaining glaciers (BR, EB, HDF, ML and VBR) which experience weather patterns that are highly influenced by orography. Their local, complex topography can lead to highly variable localized wind and weather patterns; thus, these sites are considered separately from the *Group 1* sites.

3.1.1. Measured EC and OC Concentration Results

Measured [EC] of surface snow ranged from 0 ng per gram of snow to 9.8 ng/g in the 2018 samples, with mean and median concentrations of 1.9 ng/g and 0.75 ng/g, respectively. The 2017 [EC] ranged from 0 to 68 ng/g with mean and median concentrations of 14 ng/g and 9.1 ng/g, respectively. Measured [OC] of 2018 surface snow ranged from 14 to 730 ng/g and from 18 to 7200 ng/g in 2017.

Two samples were excluded from the data analysis due to potential error or sample contamination. The April 22 GVB sample from the 2017 dataset was removed due to its extraordinarily high [EC]

value (1700 ng/g). The explanation for such a high value is unknown, but potentially due to sample contamination during collection. The April 10 KV-01 sample from the 2018 dataset was removed due to potential error during analysis. The sampling site was in the moraine of KV where the snow was hard and windblown and there were areas of exposed rock. The fresh snow had been blown away and thus the sample was not representative of the recent snowfall. In addition, the snow sample contained an excessive amount of dirt and other organic material that overloaded the filter. This causes a great deal of pyrolysis during the TOA method and potentially led to an inaccurate measurement.

[EC] and [OC] of surface snow samples from both years were plotted against their sampling sites' distance from Ny-Ålesund (Figures 3.1 and 3.5 for *Group 1* and *Group 2* sites, respectively) and altitude (Figures 3.3 and 3.7 for *Group 1* and *Group 2* sites, respectively). Distances were determined using TopoSvalbard maps provided by NPI and were measured as the straight-line distances between Ny-Ålesund center and the sampling site. Thus, topography was not taken into consideration. Figures 3.2, 3.4, 3.6 and 3.8 provide a graphical depiction of the variability in concentrations in each of the scenarios. All measured [EC] and [OC] from 2017 and 2018 sampling campaigns can be found in Appendix B.

Figure 3.1 plots the [EC] and [OC] of *Group 1* sampling sites against their distance from Ny-Ålesund. The plot shows clearly that the EC and OC concentrations from 2017 sampling were higher than 2018 concentrations. In addition, the plot indicates that sampling sites closer to Ny-Ålesund yielded much higher variability in measured [EC] and [OC] as well as higher values. A radius was made at 15 km around Ny-Ålesund and all *Group 1* samples within that distance were displayed in a box plot and compared to those outside of the designated radius. This was done for 2017 and 2018 samples separately, as well as for [EC] and [OC] separately, as shown in Figure 3.2. The box plots corroborate the higher variability and higher concentrations at sampling sites closer to Ny-Ålesund, aside from the 2018 [EC] which appear to be variable at all distances.

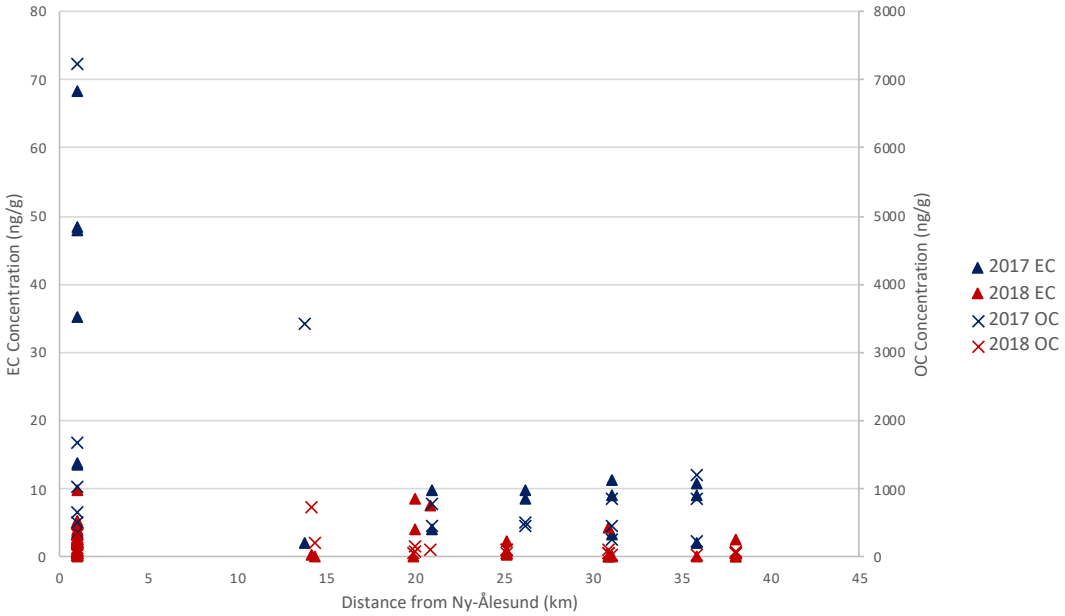

Figure 3.1. [EC] and [OC] from *Group 1* sampling sites as a function of sampling site distance from Ny-Ålesund

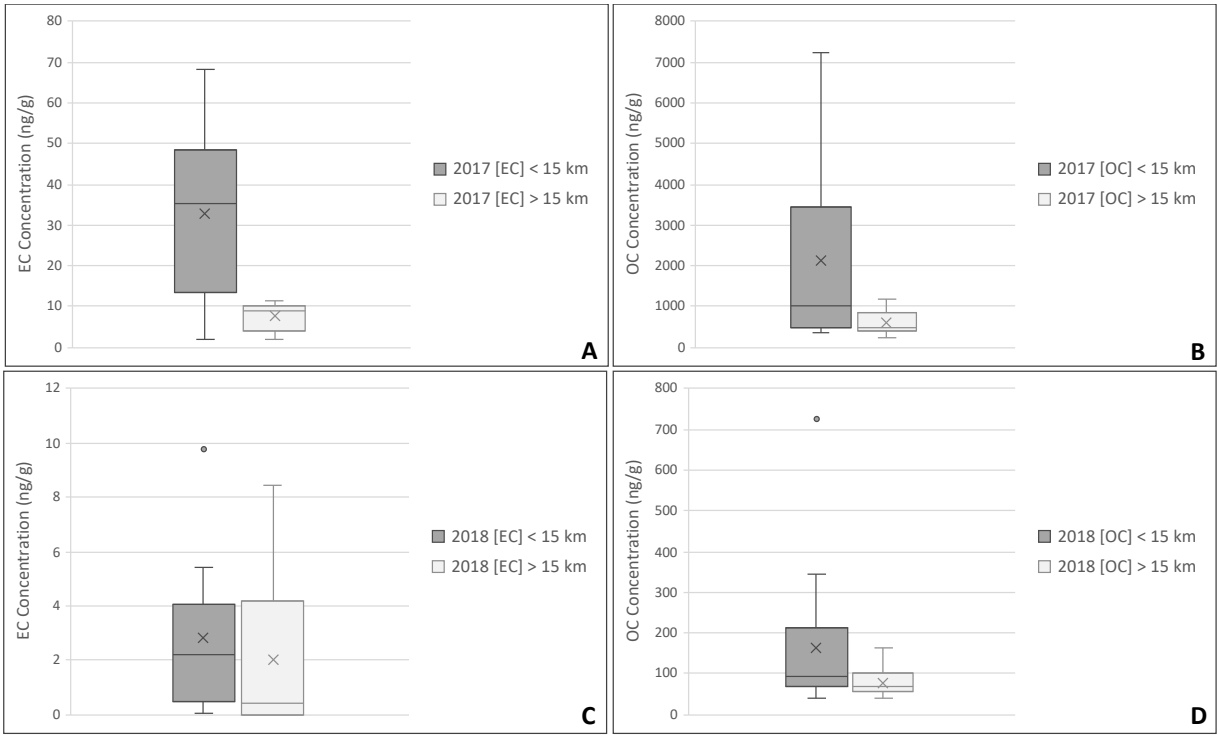

Figure 3.2. [EC] and [OC] variability dependent on *Group 1* sampling site distance from Ny-Ålesund
a) 2017 [EC], b) 2017 [OC], c) 2018 [EC] and d) 2018 [OC] Dark grey boxes represent concentrations of all *Group 1* sites within a 15 km radius while light grey boxes represent concentrations of all *Group 1* sites further than 15 km. Number of samples (n) for sites < 15 km is 7 and 15 for 2017 and 2018, respectively; n for sites > 15 km is 10 and 15 for 2017 and 2018, respectively.

Figure 3.3 plots the [EC] and [OC] of *Group 1* sampling sites against their altitude. The plot indicates that *Group 1* sampling sites at lower altitudes yielded much higher variability in measured [EC] and [OC] as well as higher values. A threshold was made at 450 m altitude and all *Group 1* samples below that were displayed in a box plot and compared to those above the designated altitude. The threshold was determined based on dominant wind flow patterns in the Ny-Ålesund region, which typically show a change in wind direction at altitudes between 300 and 600 m (Argentini et al., 2003). Thus, higher altitudes may experience air originating from different sources than lower altitudes and could potentially be less influenced by ground-based aerosol emission sources in Ny-Ålesund. The separation of sampling sites based on altitude was done for 2017 and 2018 samples separately, as well as for [EC] and [OC] separately, as shown in Figure 3.4. The box plots corroborate the higher variability and higher concentrations at sampling sites below 450 m.

The *Group 1* sampling locations located within 15 km from Ny-Ålesund include the GVB site and the KV-01 site, which is situated within the moraine area of KV. The sampling locations at altitudes below the 450 m threshold include the GVB site, KV-01, KV-02 and KV-04; but the sampling sites below 100 m, which show the highest variability and concentrations include only GVB and the KV-01 site.

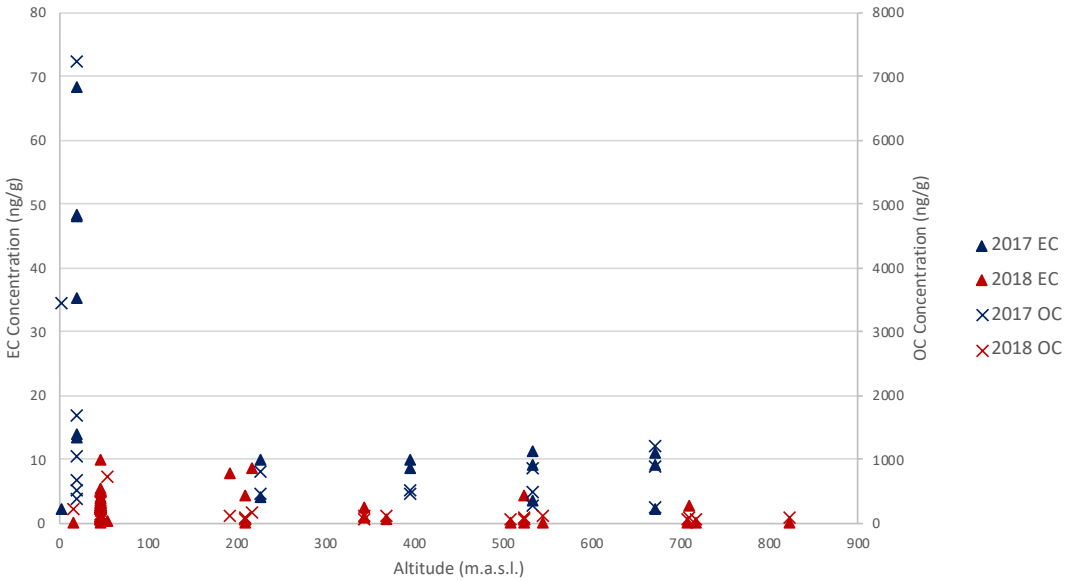

Figure 3.3. [EC] and [OC] from *Group 1* sampling sites as a function of sampling site altitude

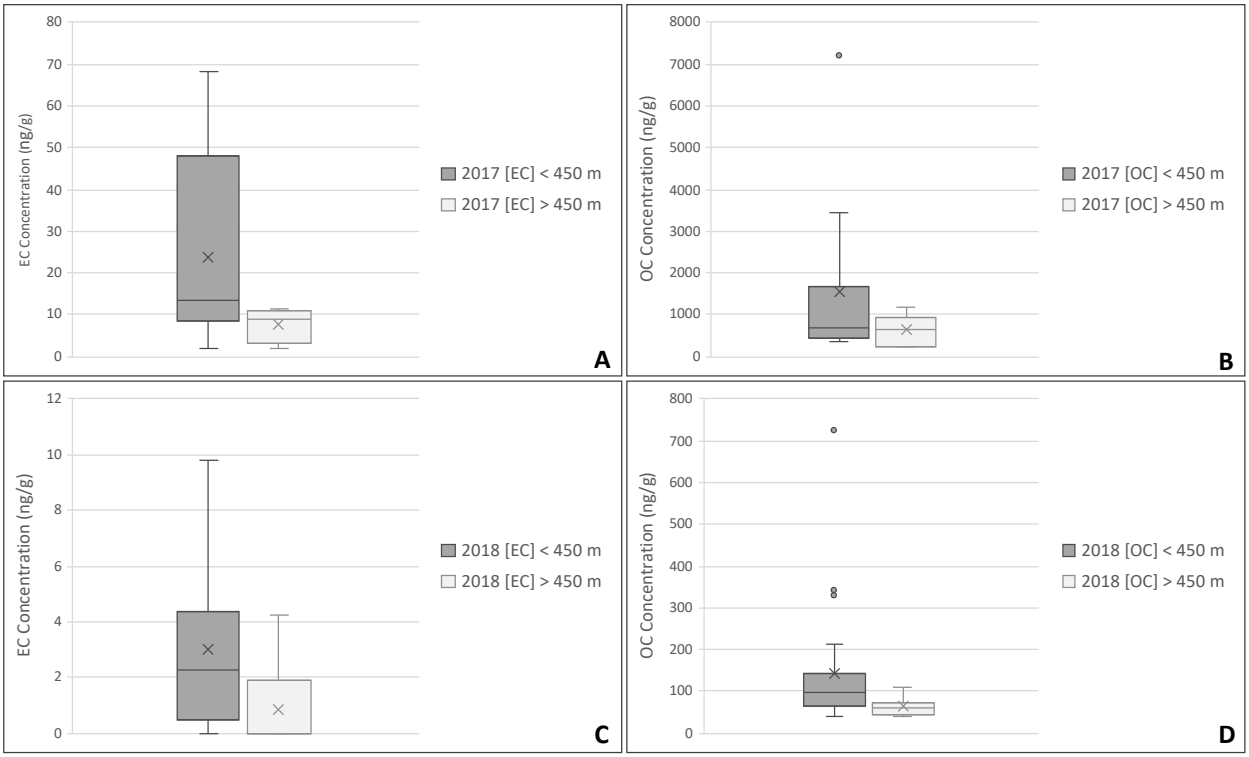

Figure 3.4. [EC] and [OC] variability dependent on *Group 1* sampling site altitude

a) 2017 [EC], b) 2017 [OC], c) 2018 [EC] and d) 2018 [OC]. Dark grey boxes represent concentrations of all *Group 1* sites under 450 m altitude while light grey boxes represent concentrations of all *Group 1* sites above 450 m altitude. Number of samples (n) for sites < 450 m is 11 and 22 for 2017 and 2018, respectively; n for sites > 450 m is 6 and 8 for 2017 and 2018, respectively.

Figure 3.5 plots the [EC] and [OC] of *Group 2* sampling sites against their distance from Ny-Ålesund. Similar to the *Group 1* sampling sites, the plot shows clearly that the EC and OC concentrations from 2017 sampling were higher than 2018 concentrations. The plot also indicates higher variability and higher values in measured [EC] and [OC] at distances closer to Ny-Ålesund. Again, all *Group 2* samples within a 15 km radius were displayed in a box plot and compared to those outside of the designated radius. This was done for 2017 and 2018 samples separately, as well as for [EC] and [OC] separately, as shown in Figure 3.6. The box plots corroborate the higher variability and higher concentrations at sampling sites closer to Ny-Ålesund.

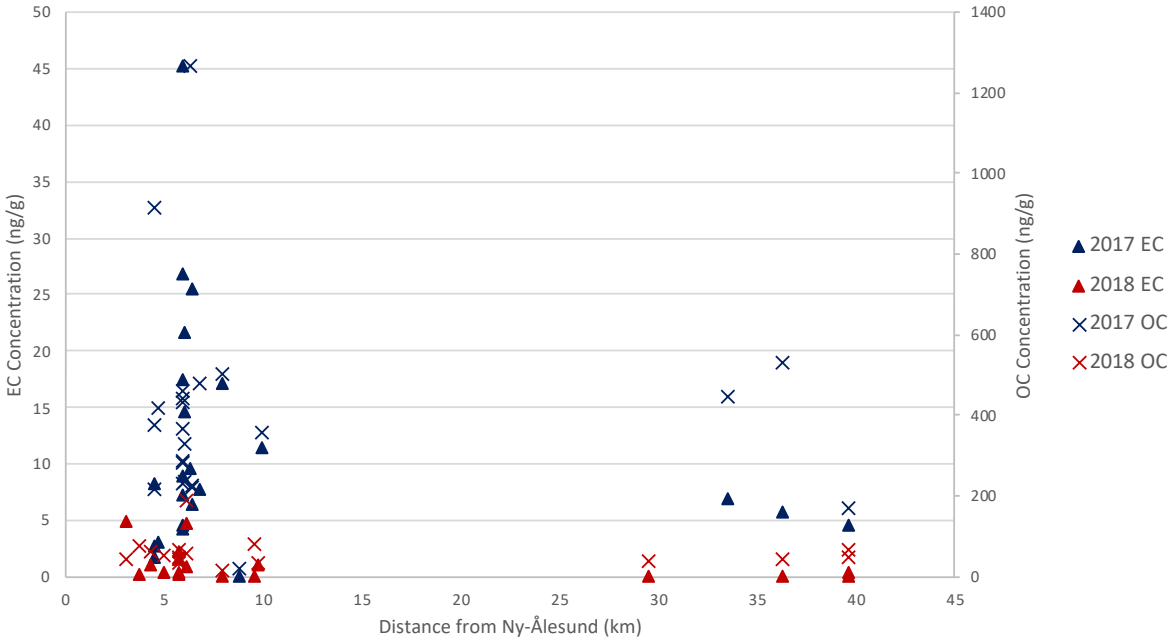

Figure 3.5. [EC] and [OC] from *Group 2* sampling sites as a function of sampling site distance from Ny-Ålesund

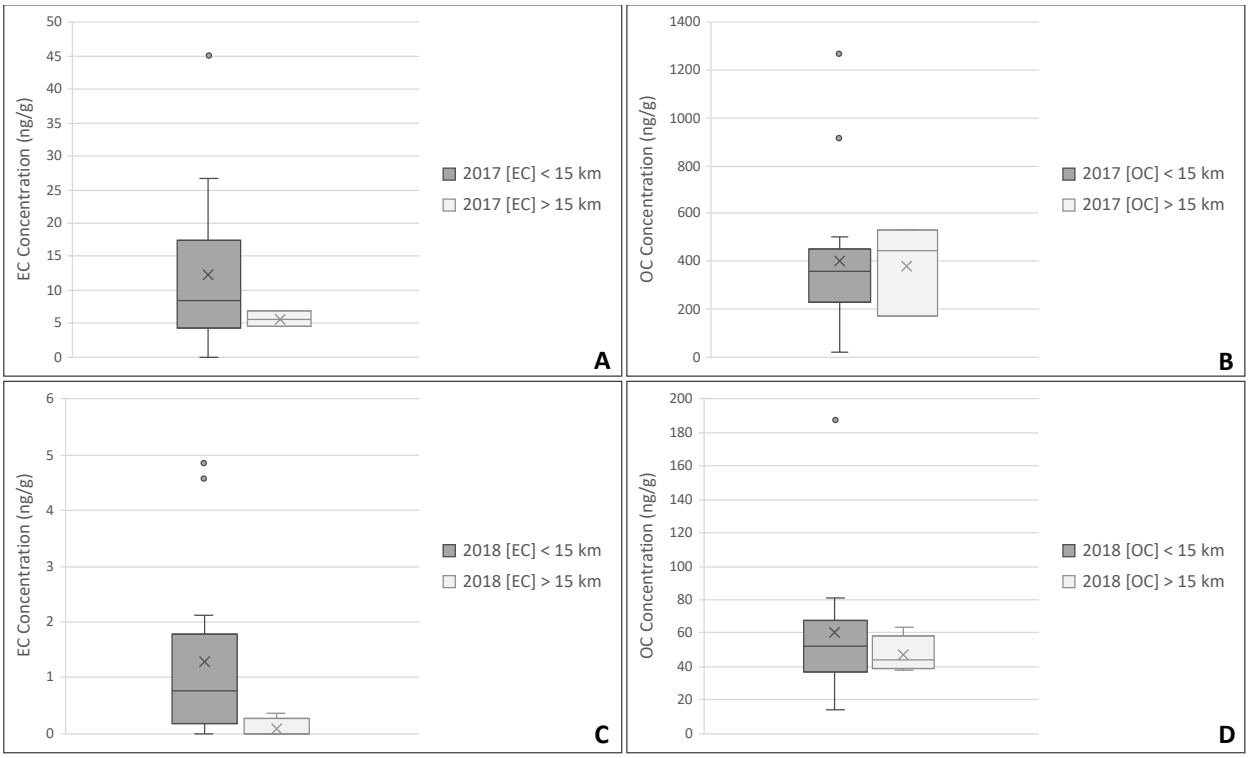

Figure 3.6. [EC] and [OC] variability dependent on *Group 2* sampling site distance from Ny-Ålesund
a) 2017 [EC], b) 2017 [OC], c) 2018 [EC] and d) 2018 [OC]. Dark grey boxes represent concentrations of all *Group 2* sites within a 15 km radius while light grey boxes represent concentrations of all *Group 2* sites further than 15 km. Number of samples (n) for sites < 15 km is 20 and 13 for 2017 and 2018, respectively; n for sites > 15 km is 3 and 4 for 2017 and 2018, respectively.

Figure 3.7 plots the [EC] and [OC] of *Group 2* sampling sites against their altitude. Similar to the *Group 1* sampling sites, the plot indicates that *Group 2* sampling sites at lower altitudes yielded higher variability and higher values in measured [EC] and [OC]. Again, a threshold was made at 450 m altitude based on the atmospheric stratigraphy typically observed in the Ny-Ålesund region, and samples above and below 450 m were displayed in box plots and compared. The separation of sampling sites based on altitude was done for 2017 and 2018 samples separately, as well as for [EC] and [OC] separately, as shown in Figure 3.8. The box plots corroborate the higher variability and higher concentrations at sampling sites below 450 m. The *Group 2* sampling locations located within 15 km from Ny-Ålesund are comprised of all the valley glaciers on the Brøgger peninsula (BR, EB, ML and VBR), while the sites further away are exclusively from HDF. The sites at altitudes below the 450 m threshold include the lower sampling locations on all the valley glaciers as well as the accumulation area on ML.

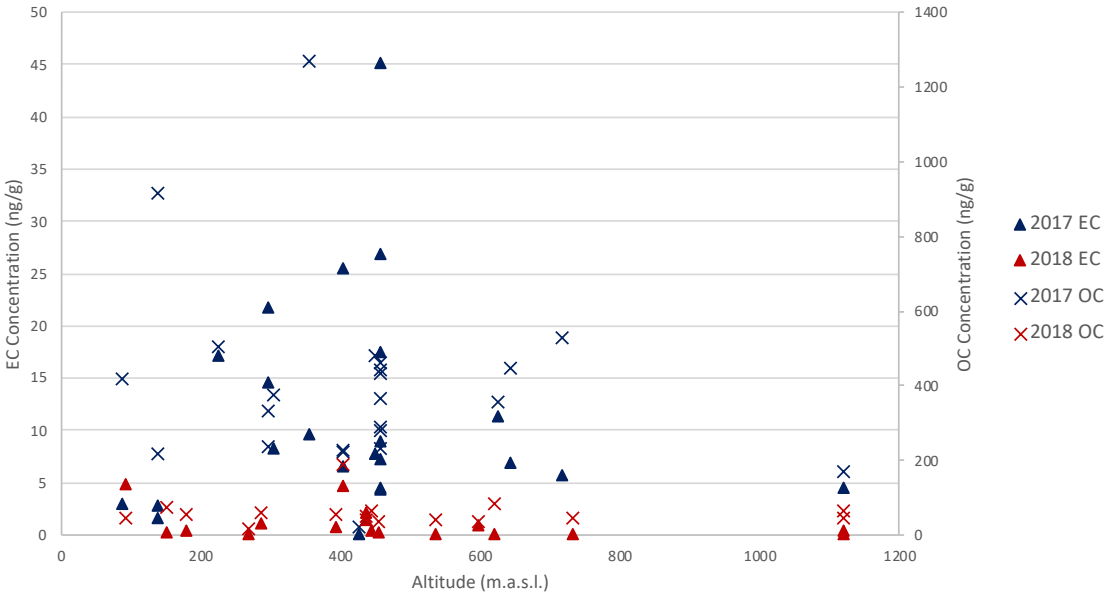

Figure 3.7. [EC] and [OC] from *Group 2* sampling sites as a function of sampling site altitude

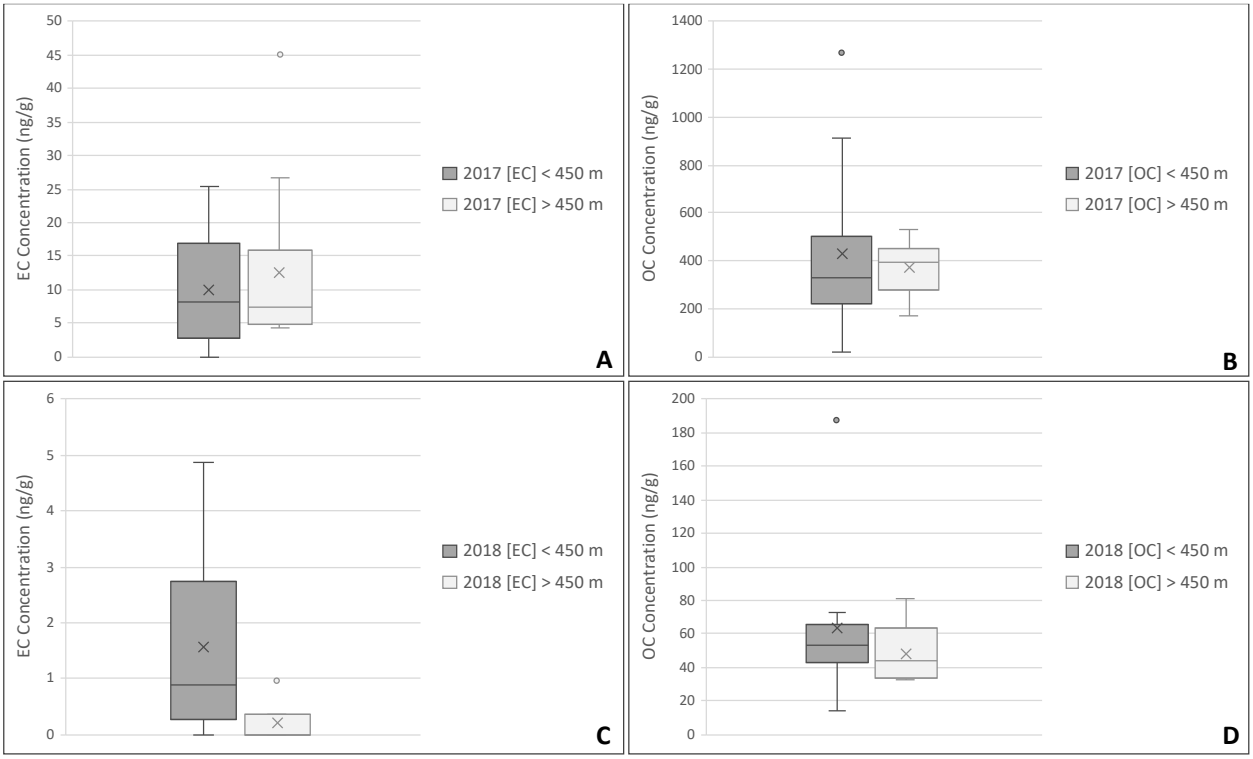

Figure 3.8. [EC] and [OC] variability dependent on *Group 2* sampling site altitude

a) 2017 [EC], b) 2017 [OC], c) 2018 [EC] and d) 2018 [OC]. Dark grey boxes represent concentrations of all *Group 2* sites under 450 m altitude while light grey boxes represent concentrations of all *Group 2* sites above 450 m altitude. Number of samples (n) for sites < 450 m is 11 and 10 for 2017 and 2018, respectively; n for sites > 450 m is 12 and 7 for 2017 and 2018, respectively.

3.1.2. 2017 and 2018 Concentration Comparison

As the samples were collected during different field campaigns across two spring seasons, the complete dataset cannot be considered a mapping of BC concentrations in Svalbard, but rather it provides an insight into the range of variability. The heterogeneity in sampling timing and the limited number of samples will have contributed to the variability in measured concentrations. As indicated in Figures 3.1, 3.3, 3.5 and 3.7, the 2017 [EC] and [OC] were significantly higher than those measured in 2018. Table 3.1 summarizes the factor difference of average concentrations between the two years for different sampling areas.

Table 3.1. Comparison of 2017 and 2018 arithmetic means of [EC] and [OC]

Average Measured EC Concentrations (Arithmetic Mean)					
	Number of 2017 samples	*[EC] 2017 (ng/g)*	*Number of 2018 samples*	*[EC] 2018 (ng/g)*	*Factor Difference*
GVB	6	38	13	3.2	12
KV	11	7.3	17	1.8	4.1
Other Glaciers [+]	23	11	17	1.0	11
Sites < 15 km from Ny-Ålesund	27	18	28	2.1	8.3
Sites > 15 km from Ny-Ålesund	13	7.3	19	1.6	4.6
Sites < 450 m altitude	22	17	32	2.6	6.5
Sites > 450 m altitude	18	11	15	0.56	20

Average Measured OC Concentrations (Arithmetic Mean)					
	Number of 2017 samples	*[OC] 2017 (ng/g)*	*Number of 2018 samples*	*[OC] 2018 (ng/g)*	*Factor Difference*
GVB	6	1900	13	120	16
KV	11	864	17	150	5.7
Other Glaciers [+]	23	400	17	60	6.6
Sites < 15 km from Ny-Ålesund	27	850	28	120	7.1
Sites > 15 km from Ny-Ålesund	13	560	19	72	7.8
Sites < 450 m altitude	22	990	32	120	8.3
Sites > 450 m altitude	18	460	15	56	8.2

[+] *Refers to BR, EB, HDF, ML and VBR*

The 2017 and 2018 [EC] are within the values expected for a remote Arctic site based on published data. Surface snow samples collected within a 5 km radius of Ny-Ålesund in 1984 by Clarke and Noone (1985) reported [EC] values ranging from 4.6 to 36 ng/g with a mean of 18 ng/g. In the

same study, seven samples collected across all of Svalbard in 1983 at elevations between 200 and 800 m above sea level yielded [EC] ranging from 6.7 to 52 ng/g with a mean of 31 ng/g. More recent studies have reported much lower average values of [EC] on Svalbard, such as Forsström et al. (2009), which found [EC] values ranging from 0 to 81 ng/g across all of Svalbard in 2007, but averaging 8.7 ng/g. Among the samples collected by Forsström et al. in the same sampling areas as the present study, [EC] ranged from 0 to 23 ng/g, which much lower averages (4.1 ng/g, 2.2 ng/g and 2.1 ng/g for the Brøgger peninsula, KV and HDF, respectively). While the 2018 data appears to be even lower than the 2007 findings, the 2017 [EC] values are slightly higher on average.

The significantly higher [EC] and [OC] in 2017 can likely be attributed to a building project that was underway within the Ny-Ålesund settlement during spring 2017. Due to thawing permafrost, a new foundation was needed for a scooter garage. This required moving the building so that the foundation could be dug and laid, and then returning the building to the new foundation. Observers present in Ny-Ålesund at this time reported high emissions of BC and dust, which consists of both BC and OC. These aerosol impurities would likely have been contained in the region due to the cold, stable atmosphere during the springtime Arctic haze period until being washed out of the air column during a snowfall event. It is believed that this building activity provided a significant source of BC and OC emissions and was the primary cause of unusually high [EC] and [OC] in the Ny-Ålesund region in 2017.

Based on meteorological data from MET Norway, precipitation levels during the 2017 and 2018 sampling periods (late March to early May) were comparable. Ny-Ålesund received 22.8 mm of precipitation during April 2017 and 20.2 mm during April 2018. In addition, air temperature throughout April was similar for both years, averaging -8.4°C and -8.1°C for 2017 and 2018, respectively. Thus, increased concentration of impurities due to less snowfall or more snow melt can be ruled out as major contributing factors to the high surface snow concentrations in 2017.

3.1.3. Sampling Site Distance from Ny-Ålesund

A spatial difference in BC levels was found when considering sample distances from Ny-Ålesund. When in the vicinity of a BC emission source, larger particles will have a shorter atmospheric

lifespan and settle out of the atmosphere through dry deposition close to the source. Smaller particles will remain in the atmosphere and travel further before eventually being removed from the atmosphere through wet deposition. Particles have a greater chance of being scavenged before reaching sampling sites further from emission sources. As displayed in Table 3.1, the average 2017 factor differences of [EC] values at GVB (12) and sites within 15 km of Ny-Ålesund (8.3) were greater than the factor difference at KV (4.1) and sites greater than 15 km away (4.6). Larger particles originating from Ny-Ålesund activities likely settled out of the atmosphere close to the settlement, while smaller particles were dispersed by wind and air currents, diluting their atmospheric concentrations before being wet-deposited on the snow surface. Sinha et al. (2018) has observed that dry deposition is typically a small contributor to the total BC deposition in the Ny-Ålesund region. Thus, these factor differences between 2017 and 2018 [EC] demonstrate that when a strong emission source is present within the settlement, as observed in 2017, it can provide a source of dry-deposited BC that significantly influences the snow contamination levels close to Ny-Ålesund.

Figures 3.1 and 3.5 plot [EC] and [OC] against the sampling sites' distances from Ny-Ålesund and demonstrate that samples closer to the settlement exhibit higher, more variable [EC] and [OC] values. It is necessary to consider the post-deposition processing that can alter the chemistry of the snowpack and lead to horizontal variability in contaminant levels at small scales. Wind-induced snow drifting would be expected at most sampling sites due to katabatic winds acting on glaciers and the orographic effects of steep mountain ridges. This phenomenon works to both physically and chemically alter the snowpack by enhancing sublimation and redistributing surface snow. Thus, localized variability in impurity content will have contributed to wide-scale variability across the sampling sites.

When comparing the [EC] averages for all sampling sites within the 15 km radius around Ny-Ålesund (18 ng/g and 2.1 ng/g for 2017 and 2018, respectively) to the average concentrations outside the radius (7.3 ng/g and 1.6 ng/g for 2017 and 2018, respectively), it is clear that the region around the settlement experiences higher levels of surface snow contamination. This is true for 2017, when significant building activities were underway, as well as for 2018 when no major activities were reported. Regular activities within Ny-Ålesund provide year-round emission

sources of BC such as snow scooter, airplane and ship traffic, combustion of diesel at the power plant and the use of motor vehicles in town. Excluding ship traffic, all of these emission sources would have been present during the sampling periods. As the 2018 concentrations suggest, it is likely that these normal activities are also producing a measurable impact to the localized contaminant levels.

3.1.4. Sampling Site Altitude

A variability trend in BC levels was also found when considering sampling sites' elevation above sea level. Figures 3.3 and 3.7 plot [EC] and [OC] against the sampling site altitude and demonstrate that during both sampling years, samples at lower elevations exhibited higher, more variable [EC] and [OC] values. In addition, when comparing the [EC] averages for all sampling sites below 450 m altitude (17 ng/g and 2.6 ng/g for 2017 and 2018, respectively) to the average concentrations above 450 m (11 ng/g and 0.56 ng/g for 2017 and 2018, respectively), it is clear that surface snow at lower altitudes contains higher levels of contamination.

This trend can be due in part to the nearness of low-altitude sampling sites to Ny-Ålesund. Most sites below 450 m elevation are within the 15 km radius around the settlement, excluding KV-02 and KV-04, and thus likely influenced by local sources of BC emissions. To illustrate this relationship, all sampling sites' altitudes have been plotted as a function of their distance from Ny-Ålesund in Figure 3.9. It is therefore difficult to differentiate between the influences from sampling site elevation and nearness to Ny-Ålesund and both should be considered contributing factors. Additionally, snow scooter traffic in the region is more frequent at lower altitudes and common tracks run at the bases of BR, VBR, ML and along the KV sampling sites. High [EC] values measured at the base of BR and at KV-02 during 2018 are likely attributed to common snow scooter routes.

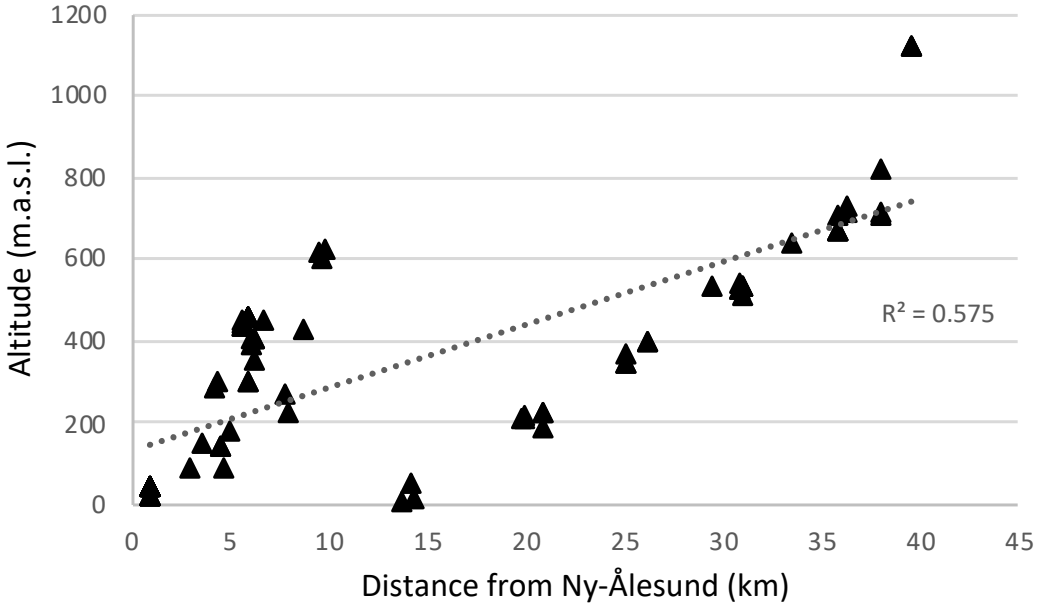

Figure 3.9. Sampling site altitude plotted against sampling site distance from Ny-Ålesund for all 2017 and 2018 surface snow samples

There are various other physical and meteorological factors that may contribute to the altitudinal variance expressed by the data. BC can accumulate in the lower boundary layer of the troposphere, particularly in springtime due to the Arctic haze phenomenon. As meteorological observations in the Ny-Ålesund region have demonstrated, the lower atmospheric boundary layer is typically at 300 to 600 m altitude (Argentini et al., 2003). Thus, the emissions from the settlement would likely be contained below this boundary layer during springtime until being washed out of the air column by wet deposition. This would lead to higher concentrations of BC below the atmospheric boundary layer, whereas sampling sites above the layer would be less influenced by local sources of emissions and more representative of contaminant levels brought by long range transport. It should be noted that weekly airplane traffic to and from Ny-Ålesund would emit BC into the atmosphere above the atmospheric boundary layer and could be a potential local source of contamination to high altitude locations.

Snowfall at high altitudes may contain lower concentrations of contaminants than at lower altitudes due to a shorter depth of air column that is available for scavenging of particles during wet deposition. Additionally, higher altitudes tend to receive greater amounts of precipitation due to topographical changes that influence precipitation processes and often induce precipitation events.

The amount of precipitation on BR has been shown to increase by 100 mm with every 100 m increase in altitude (Hagen & Lefauconnier, 1995). Other small valley glaciers on Svalbard have demonstrated even higher accumulation gradients, with up to 440 mm increase in precipitation with every 100 m increase in altitude (Grabiec et al., 2011). Precipitation in central areas of BR is 45% higher than in Ny-Ålesund (Førland 1997). Higher precipitation levels can dilute contaminant concentrations in snowfall due to progressive scavenging of species, which decreases solute concentrations in an exponential manner with time (Davies et al. 1992). These are likely contributing factors to the difference in BC levels observed between low and high-altitude sampling sites.

An accumulation gradient has been observed when looking at a singular snowfall event during the 2018 sampling campaign. A large snowfall occurred on 12 April 2018 and a widespread sampling campaign was conducted on 13 April, covering GVB, BR, EB, ML, KV and HDF sampling sites and sampling only the entire top layer of soft, fresh snow. The depth of the top layer was measured and considered to be the amount of precipitation received during the snowfall event. The top layer was very distinguishable from lower layers in terms of snow crystal morphology and was composed of fresh, recognizable precipitating snowflakes. The sample depth is plotted against altitude in Figure 3.10, which demonstrates a general trend of increasing depth with increasing altitude, implying nearly 10 mm of increased precipitation for every 100 m increase in altitude during this particular snow event. It is difficult to generally compare the [EC] of the sampling sites with their altitudes from this snowfall event due to variations caused by topographical influences. However, the spatial variability of BC levels observed from this snow event are discussed further in section 3.4.

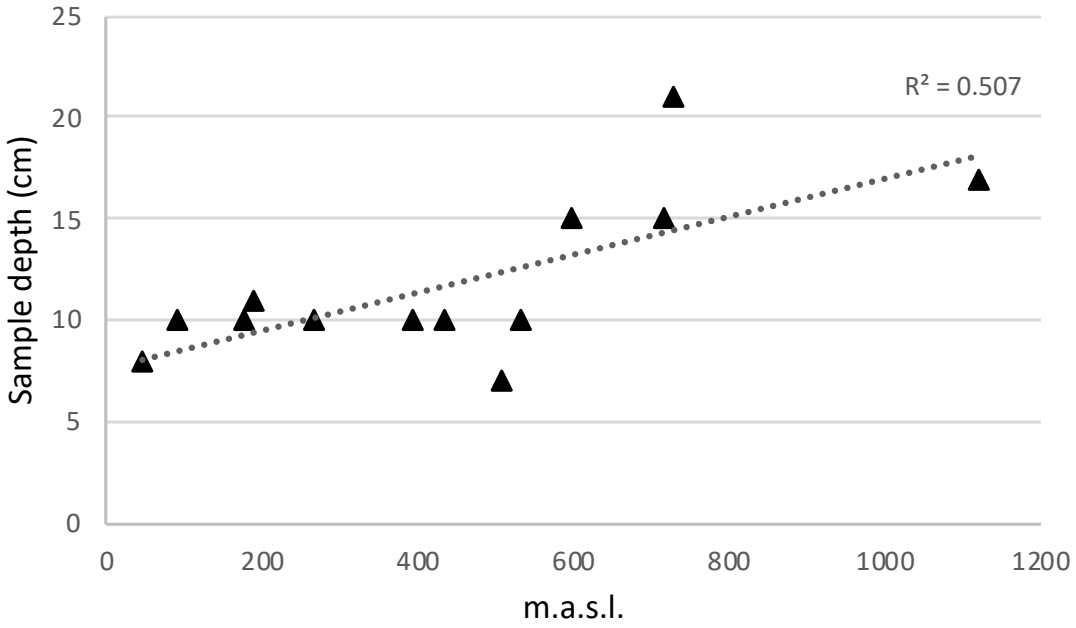

Figure 3.10. Sample depth plotted against altitude of sampling site for all snow surface samples collected on 13 April 2018
Sampling depth represents the top layer of fresh snow and is considered to be the amount of snow received during one precipitation event on 12 April 2018.

Variability in [EC] is high for the valley glaciers on the Brøgger peninsula (BR, EB, ML and VBR), as demonstrated in Figure 3.7, which plots the [EC] and [OC] of *Group 2* sampling sites against altitude. The local topography of these glaciers plays an important role in the distribution and amount of precipitation they receive, ultimately resulting in inhomogeneous deposition of contaminants. They are surrounded by steep mountain ridges that act as orographic barriers, encouraging formation of orographic clouds during pressure decreases from rising airmasses along the mountainous terrain. Formation of such clouds often leads to precipitation events once the cloud has reached saturation level or is 'fed' by a higher altitude cloud (Førland et al., 1997). More frequent precipitation may cause lower concentrations of contaminants in the snowpack, but it may also lead to greater total mass deposition of BC throughout the snow season. In addition to influences from orographic precipitation, circulation patterns and wind direction are highly variable in mountainous areas and play a large role in determining if air masses with contaminants from local emission sources will reach the glaciers. Thus, it is difficult to generalize spatial and altitudinal variability of BC deposition on small valley glaciers.

3.1.5. Overall Observations

The 2017 and 2018 datasets of [EC] and [OC] in surface snow samples exhibit spatial trends and it is evident that local emission sources from Ny-Ålesund are having an impact on the contaminant levels in the region. Points within 15 km from Ny-Ålesund or at an altitude below 450 m have higher and more variable EC concentrations than sampling sites further away or at higher altitudes. This is very likely due to anthropogenic activities within the settlement, as well as common snow scooter traffic routes in the area. The 2017 dataset further substantiated this theory by exhibiting greater measurable impacts to contaminant levels within the 15 km radius when strong anthropogenic activities were undertaken in Ny-Ålesund.

All [EC] values measured in surface snow in 2018 were within the levels expected for Svalbard. The highest values were from the GVB sampling site closest to Ny-Ålesund and sites close to commonly used snow scooter traffic routes. Most of the [EC] values measured in 2017 exceeded the background contaminant levels expected for the Svalbard region, but the region outside the 15 km radius and above 450 m altitude was less impacted. The Ny-Ålesund region is commonly used to study long range transport of contaminants to the Arctic, with the assumption that there is little to no local emission sources. However, the collected dataset clearly shows that when strong activities are undertaken within the settlement, contaminant levels can be strongly affected. Thus, it is advised that scientists travel further than 15 km away from Ny-Ålesund when sampling to measure for background levels of contaminants if the logistical, financial, timing and safety challenges are not too great.

3.2. Impact of Air and Snow Temperature on BC Levels

BC levels in snow can be influenced by air and snow temperature, both during and after the deposition process. The efficiency of wet deposition increases with increasing temperature and is most efficient when the air is moist and the temperature is near freezing (Garrett et al., 2011). Thus, warmer snowfall events may be more effective at scavenging BC particles from the air column. Warmer temperatures also encourage post-depositional processing within the snowpack such as melting and sublimation, which virtually increase [EC] due to decreasing the total SWE. As BC is hydrophobic, it tends to remain on the surface and does not percolate through the

snowpack during snow melt (Doherty et al., 2013). Thus, high [EC] levels could be attributed to increased air or snow temperature that has induced snow melt. Figure 3.11 plots 2018 BC levels against air temperature and snow temperature and demonstrates a weak trend towards increasing [EC] with increasing temperatures.

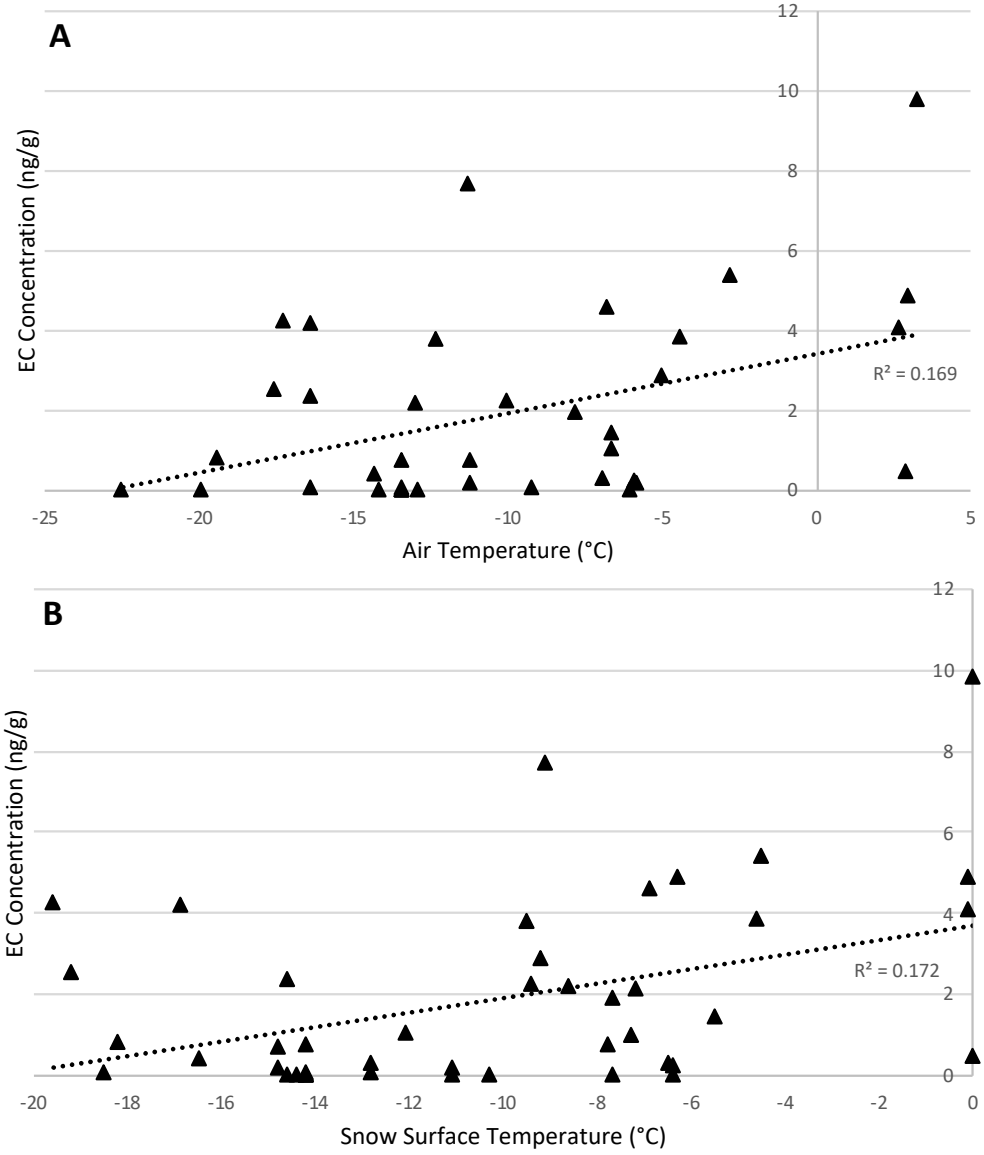

Figure 3.11. [EC] in all 2018 surface snow samples as a function of air and snow surface temperature

This trend is particularly strong when looking only at [EC] at the GVB sampling site during the 2018 campaign. Figure 3.12 plots 2018 BC levels at GVB against air temperature and snow temperature. The consequences of warmer temperatures on snow, including the concentration of

contaminants on the surface and increased snow grain size, create a positive feedback by reducing the surface albedo. This perpetuates melt and enhances the increase in surface [EC]. The stronger trend observed at the GVB site, implying a greater influence of temperature on [EC], is likely attributed to the greater initial levels of BC which feed and intensify the positive feedback loop. Ultimately, these trends indicate that some of the high [EC] values may be partially attributed to concentrated containment levels due to snow melt or sublimation, particularly at GVB and other low altitude sites that are more often exposed to warmer temperatures.

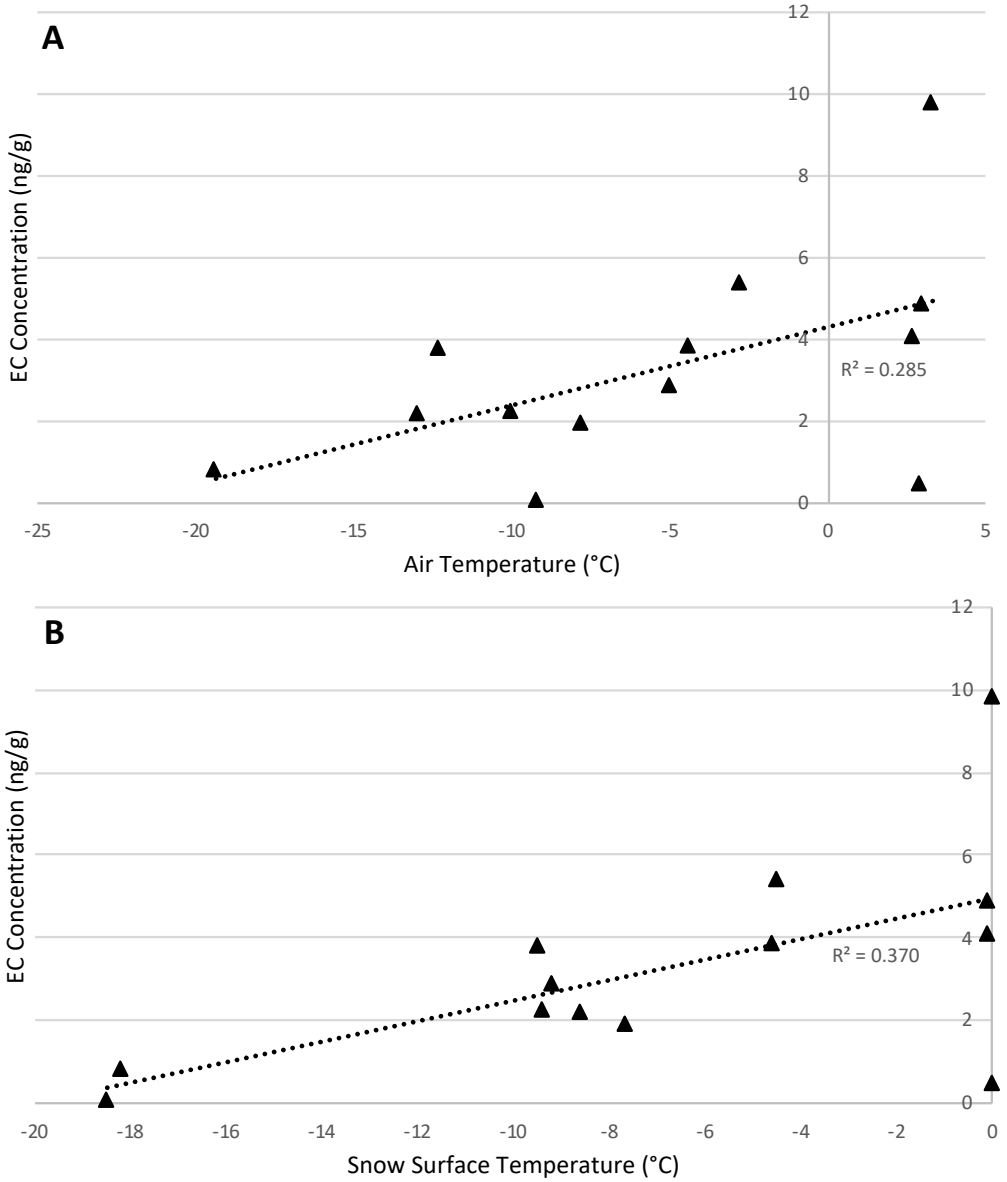

Figure 3.12. [EC] in all 2018 GVB surface snow samples as a function of air temperature and snow surface temperature

3.3. Ambient BC Concentrations in Ny-Ålesund

Hourly atmospheric BC measurements were available for the full winter and spring seasons of 2017, however only a limited dataset was available for 2018 and comparisons can only be made on the months of January and March. The available data is displayed in Figure 3.13. Ambient BC levels for January were higher in 2017 than 2018. There was a general increase of BC between January 2018 and March 2018, likely due to the Arctic haze phenomenon. Values at the start of March appear to be comparable between the years, however 2017 values begin to increase significantly in the middle of the month and remain high throughout the rest of April. This is likely due to the building activities going on within the settlement and coincides with the higher [EC] in snow samples during spring 2017. It is also interesting to note that precipitation in March 2017 was very high compared to 2018. Total precipitation for the month as reported by MET Norway was 52.0 mm in 2017 and only 19.5 mm in 2018. Thus, the ambient BC levels remained high in 2017 despite progressive washout of the air column due to extensive precipitation.

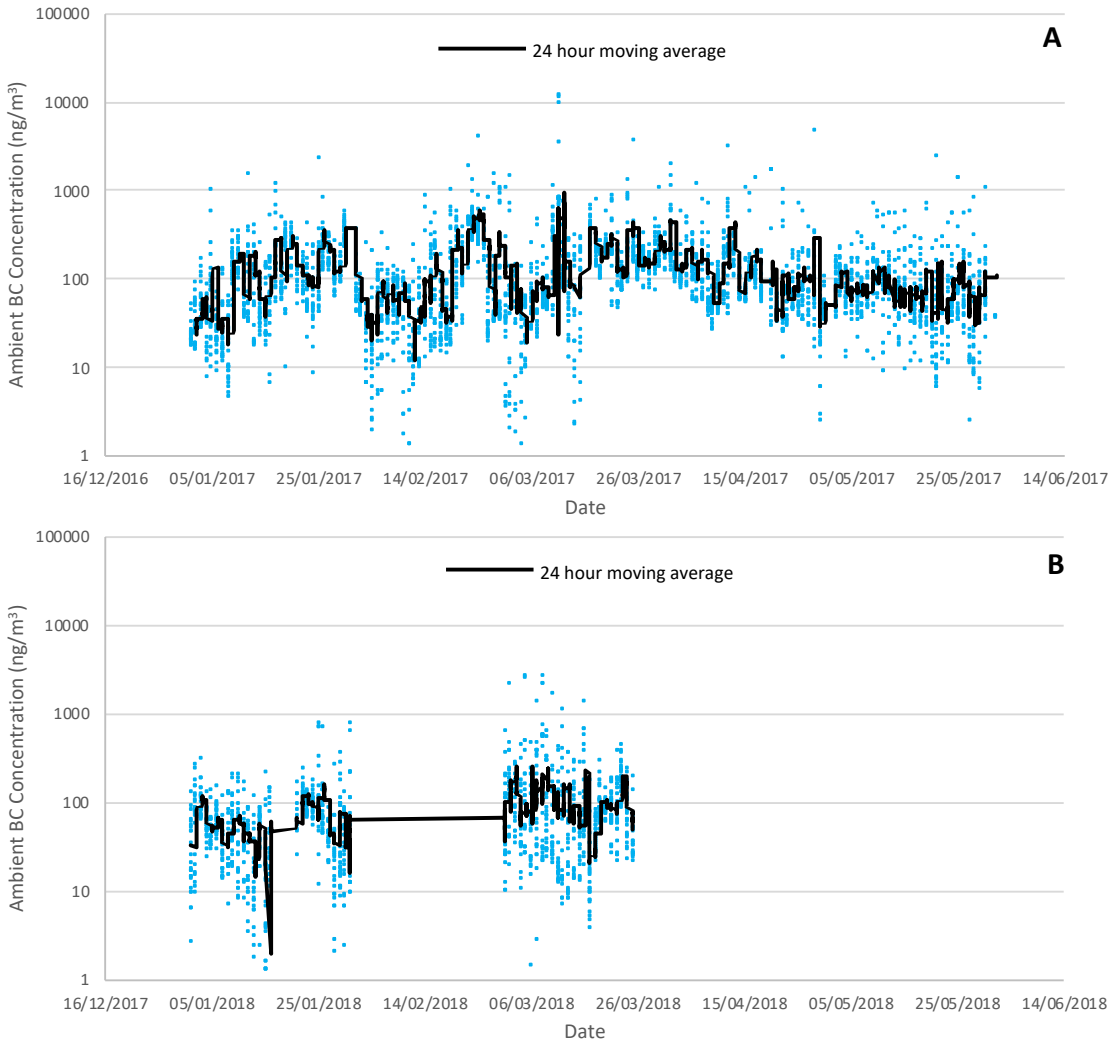

Figure 3.13. Ambient winter and spring BC concentrations measured within the settlement of Ny-Ålesund in a) 2017 and b) 2018

3.4. Spatial Variability of BC in a Fresh Snow Event

There was a large snowfall event on 12 April 2018. While MET Norway reported only 3.2 mm of precipitation in Ny-Ålesund during the event, significantly larger amounts were observed at higher altitudes. A widescale sampling campaign was completed on 13 April 2018 to sample the whole top layer of soft, fresh snow at the GVB, BR, EB, ML, KV and HDF sampling sites. Very little to no wind was observed during the sampling campaign on 13 April and thus the top layer of snow was assumed to be intact from the previous day's snow event with very little post-depositional processing. The BC measurements obtained from these samples were used to assess the spatial

variability of BC within a singular snow event. The data is displayed in Figures 3.14 and 3.15 as a function of distance from Ny-Ålesund and altitude, respectively.

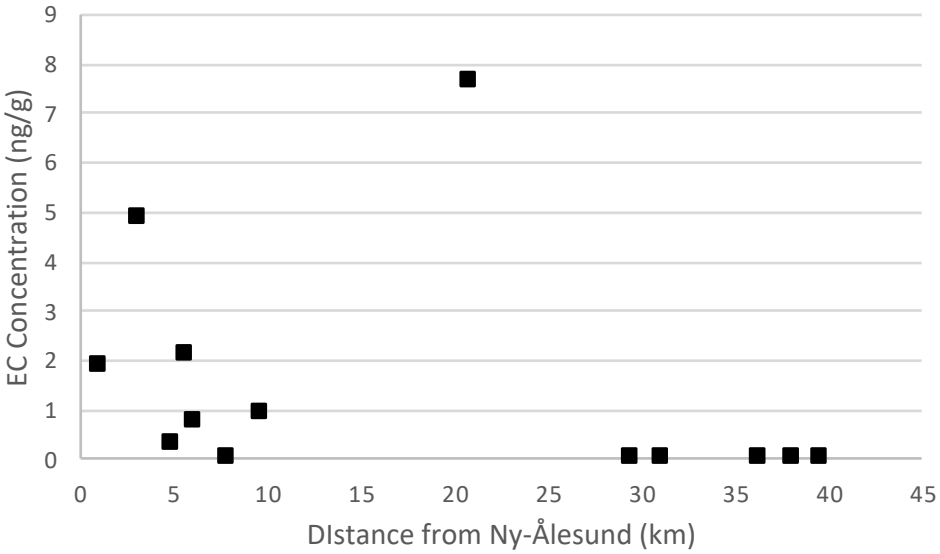

Figure 3.14. [EC] in surface snow samples as a function of sampling site's distance from Ny-Ålesund during sampling campaign on 13 April 2018

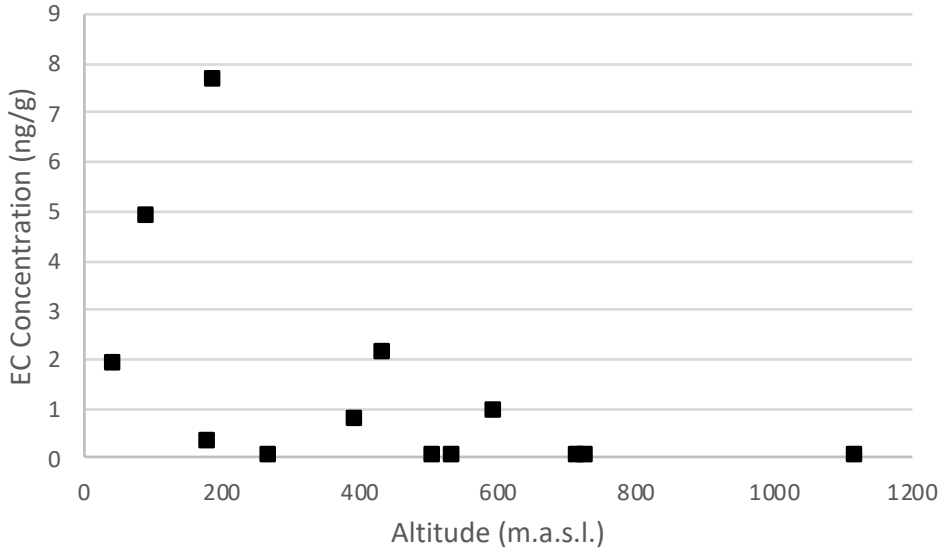

Figure 3.15. [EC] in surface snow samples as a function of altitude during sampling campaign on 13 April 2018

3.4.1. Spatial Variability Analysis

The measured concentrations are within the range of observed background values with no strong variability. There were several snowfalls prior to the 12 April snow event (8, 9 and 11 April) and thus much of the locally-sourced BC in the atmosphere may have been washed out through wet deposition in the days prior. Progressive scavenging from these previous snowfalls likely yielded lower ambient BC concentrations and consequently lowered spatial variability and BC concentrations in the snowfall. Unfortunately, atmospheric BC concentrations from this time period are not available for confirmation.

Figures 3.14 and 3.15 show a similar trend to the complete surface snow dataset presented in section 3.1. Sampling sites closer to Ny-Ålesund and at lower altitudes yielded higher, more variable [EC] values. One [EC] value (7.67 ng/g) did not fit this trend and is from the lower part of KV at 191 m.a.s.l. and 21 km from Ny-Ålesund. This sample was collected at 19:45 at the end of the day. It was noted that there was 2 cm of fresh snow on the top of the snowpack, then a 0.5 cm ice layer, followed by 8 cm of soft, recently fresh snow beneath. The snow sample was taken from the top 10.5 cm and thus included the ice layer. The weather on KV throughout the day of 13 April was mostly clear skies and sunny. The air temperature at the time of sampling was -11.3°C, however it is known that temperatures exceeded 0°C in Ny-Ålesund during the snowfall event on 12 April. Thus, during the 24 hours preceding the collection of the sample, the snow surface was exposed to sunshine and above-freezing temperatures. It is likely that post-depositional processing within the snowpack, such as melting and refreezing, concentrated the BC particles. This was the only sample from the day that included an ice layer. The other samples were only taken from the uppermost layer of soft, fresh snow.

There was another [EC] value (4.86 ng/g) that was slightly higher than the rest, which was from the base of BR at 92 m.a.s.l. and 3.1 km from Ny-Ålesund. This sample was also taken at the end of the day, after the snow surface was exposed to sunshine throughout the day. Thus, it is possible that post-depositional processing modified the snowpack and increased the [EC]. It is also worth noting that both of the sampling sites with slightly higher [EC] values were near to usual snow scooter traffic paths that are frequently used and may have been a local source of BC emissions.

3.4.2. Back Trajectory Analysis of the Airmass

A backward trajectory of the airmasses arriving to Ny-Ålesund on the 12th of April was created using NOAA's HYSPLIT model and is displayed in Figure 3.16. Trajectories were obtained for airmasses at 50, 300 and 600 m.a.s.l. to identify potential for long range transport of BC. The model shows that the airmasses both above and below the atmospheric boundary layer arrived from the southwest. It has been shown that air arriving to Svalbard from the southwest tends to carry lower levels of contaminants than air arriving from the east (Forrström et al, 2009). Air originating from the eastern sector can contain more than two and half times higher levels of soot than air arriving from south to west. Lower concentrations in these airmasses is likely due to scavenging of particles through precipitation prior to their arrival to the Svalbard archipelago, as the air has further to travel from emission sources and is exposed to warmer weather patterns along the way. Thus, long range transport of BC in this airmass was likely low and the very low levels of BC measured from this snowfall event are not surprising. The slight difference between the average [EC] measured within 15 km of Ny-Ålesund (1.0 ng/g, excluding the high value on BR) and the average [EC] measured further than 15 km (0.0 ng/g, excluding the high value on KV) could be attributed to local emission sources within Ny-Ålesund.

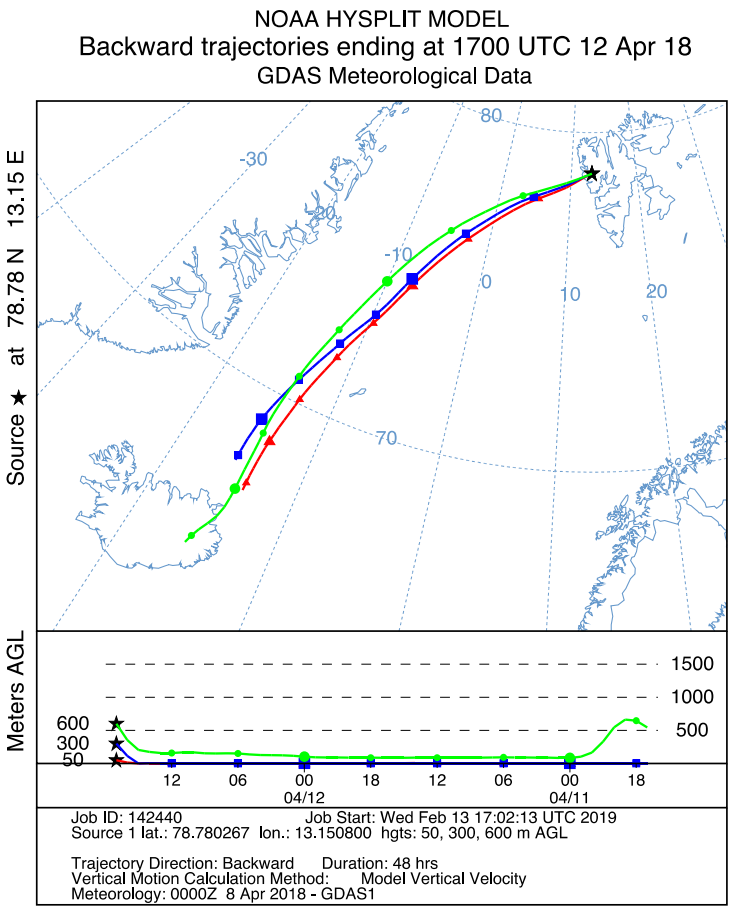

Figure 3.16. 48-hour backward trajectory of airmasses arriving to Ny-Ålesund on 12 April 2018 produced by NOAA's HYSPLIT model

3.5. Seasonal Flux of BC

Snow pits were dug in the accumulation area of each glacier during late spring 2018 and spanned the entire winter 2017/2018 snowpack. Measured [EC] from samples obtained along the vertical layers of the snowpack were used to calculate the total BC flux, reported in μg/m^2, for the entire snowfall season on each glacier and at GVB. Calculations are available in Appendix B and the calculated values are displayed in Table 3.2. The BC flux values are considered to represent the total accumulation of BC deposited throughout the snowfall season. While several snow pits were dug at the GVB sampling site during the spring, measurements obtained from the latest sampling date were used for comparison as it was closest to the sampling dates of the other snow pits.

Table 3.2. Total 2018 seasonal flux of BC calculated using [EC] obtained from snow pit sampling in the glacier accumulation area

Total Seasonal Flux of BC				
	Date of Sampling	*Altitude (m.a.s.l.)*	*Distance from Ny-Ålesund (km)*	*Total BC Flux ($\mu g/m^2$)*
GVB	17-Apr-18	46	1.0	390
BR	14-Apr-18	453	5.7	50
ML	14-Apr-18	403	6.1	68
EB	15-Apr-18	620	9.6	45
KV	19-Apr-18	708	36	86
HDF	18-Apr-18	1121	40	25

3.5.1. Seasonal BC Flux of Gruvebadet

Accumulation of BC throughout the snow season in the GVB area is significantly higher than the glacier snow pit locations. This is likely due to a range of factors, most notably its proximity to Ny-Ålesund and the influence of wet and dry deposition of locally sourced emissions. Situated only 1.0 km away from the settlement, the GVB site is exposed to regular anthropogenic activity such as snow scooter traffic, vehicle traffic and emissions from the diesel power plant.

Meteorological conditions may also play a role in the GVB area's high BC flux value. The site experiences warmer air temperatures than the accumulation areas of the glaciers due to its position close to the sea and at a significantly lower altitude. Warmer temperatures during snowfall events can increase the aerosol scavenging efficiency of the snowflakes and lead to snowfalls more concentrated with pollutants (Garrett et al., 2011). GVB can also experience melting and a loss of material, with BC being preferably stored in the remaining material, which could also explain the much higher load of BC at this site. While it is difficult to differentiate the impacts of natural meteorological trends from the impacts of local anthropogenic emissions on the BC levels at GVB, it is concluded that both play a significant role.

3.5.2. Overall BC Flux Trends

The BC flux values of the glacier sites follow the general trend of higher BC deposition within 15 km of Ny-Ålesund and lower altitudes, aside from the values measured at KV. Lower values of total BC seasonal flux were expected at the sampling sites within high altitude accumulation areas due to the presence of the atmospheric boundary layer that may prevent locally sourced emissions

from reaching the sites. Additionally, the higher elevation accumulation areas were located further distances from Ny-Ålesund, giving aerosols emitted in the settlement more opportunity to be scavenged from the air column before reaching the sites. Lower seasonal flux of BC was observed at two of the three highest sampling sites, EB (620 m.a.s.l.) and HDF (1121 m.a.s.l.).

The flux of BC at KV is higher than what would be expected for its distance from the settlement (36 km) and its high altitude (708 m). KV has regular but light scooter traffic in its accumulation area throughout the late winter and spring season due to field work for ongoing mass balance studies of the glacier. This is opposed to BR, EB, ML and HDF which generally receive little to no scooter traffic in their accumulation areas. Additionally, the KV site is generally within the same prevailing winds as Ny-Ålesund and may receive more regular BC emissions from the settlement when the wind is coming from the west along the fjord and up the glacier.

It is important to also consider the natural meteorological influences that may add to the total seasonal flux of BC for high altitude sites. Accumulation areas at high elevations experience summer temperatures cold enough to receive snow year-round, making the snowfall season start earlier than at lower altitudes. Thus, the area may receive precipitation in the form of snow while lower altitude sites are still receiving rain in the autumn. The smaller valley glaciers with accumulation areas low in altitude (BR, ML and EB) experience warmer temperatures in summer and autumn and receive more rain. The snow melts nearly completely on these glaciers, exposing glacial ice. Any BC deposited during this time accumulates and concentrates on surface of the ice and is preserved in a layer of superimposed ice rather than incorporated into the snowpack. Thus, BC deposited during the summer or early autumn on low altitude glaciers would not likely be included in the seasonal flux calculations. Conversely, BC deposited during this time on high altitude glaciers, such as HDF and KV, would likely remain dispersed within the snowpack and thus be incorporated into seasonal flux calculations. This could potentially be a significant amount of BC, as it would include emissions from regular ship traffic which is present only during summer and early autumn in the region.

The meteorological differences between high and low altitude accumulation areas also influence the potential impact that BC can have on the glaciers. Snow melt at higher elevations is less

extensive and ensures that the BC remains dispersed vertically throughout the snowpack, which lessens its potential to induce surface melt through reduction in surface albedo. Lower altitude glaciers, which experience more summer snow melt and expose greater areas of glacial ice may be more impacted by BC deposition in the summer. BC particles will concentrate on the surface of the snow and ice, subsequently lowering albedo and enhancing summer melt. The impacts are particularly strong during summer, when there is 24-hour daylight and the sun is at its highest.

The lowest concentrations of BC within the snowpack were at the base of the snow pits for each of the glacial sites. The snow accumulated at the bases of each snow pit would be from early in the snow season. For lower altitude glaciers, this was later in the autumn season when there was very little or no sunlight, thus minimizing potential for surface melt. The snowpack is better preserved without surface melt, and the low concentrations of BC are maintained rather than being concentrated on the surface layer. Snow layers higher up in the snow pack would have fallen when sunlight was more prevalent and thus post-depositional processes such as surface melt and sublimation would have more effect on BC concentrations. Conversely, the GVB site had a 22 cm thick melt refreeze layer at the base of its snow pit with very high concentrations of BC (23 ng/g). This can be attributed to repeated fluctuations in temperature above and below freezing during the spring that concentrated BC particles into a lower ice layer.

3.6. Levoglucosan

Levoglucosan content was analyzed in 38 of the 2018 surface snow samples. Measured levoglucosan values ranged from 0 pg/mL to 427 pg/mL of melted snow with mean and median concentrations of 164 pg/mL and 162 pg/mL, respectively. Four samples were measured below the MDL (47.0 pg/mL) and remained in the dataset with an assigned levoglucosan concentration of 0 pg/mL. The data is presented in Appendix C and plotted as a function of sampling site distance from Ny-Ålesund in Figure 3.17.

It was observed that the snow samples intended for levoglucosan analysis were in the form of ice rather than snow when removed from the storage freezer prior to analysis. This suggested that the samples had melted previously and refrozen during transportation or storage. A few samples had

burst their tubes and leaked during the refreezing process and were thus discarded. It was determined that the samples having melted at an earlier point should not impact the levoglucosan analysis, as the compound is highly soluble in water and thus the analysis proceeded with the remaining 38 snow surface samples.

A trend is observed of decreasing levels of levoglucosan with increasing distance from the settlement and higher, more variable values within the 15 km radius. Wood burning emissions contain a wide distribution of particle sizes (Rau, 1989) and thus some larger particles will settle out of the atmosphere quickly while smaller particles may travel further from the emission source. Similar to the spatial variability observed with BC, this trend indicates an influence of emissions from Ny-Ålesund on contaminant levels in the surrounding region. However, the obvious potential sources of wood-burning emissions in the area are limited to approximately ten cabins that contain wood-burning stoves. These cabins are not located within Ny-Ålesund but are situated throughout the Brøgger peninsula and thus the spatial variability of their emissions would not necessarily be centered around the settlement. The observed trend is likely due to the KV and HDF sampling sites, which are all greater than 15 km from Ny-Ålesund, being significantly further away from regularly used wood-burning cabins than the other sampling sites.

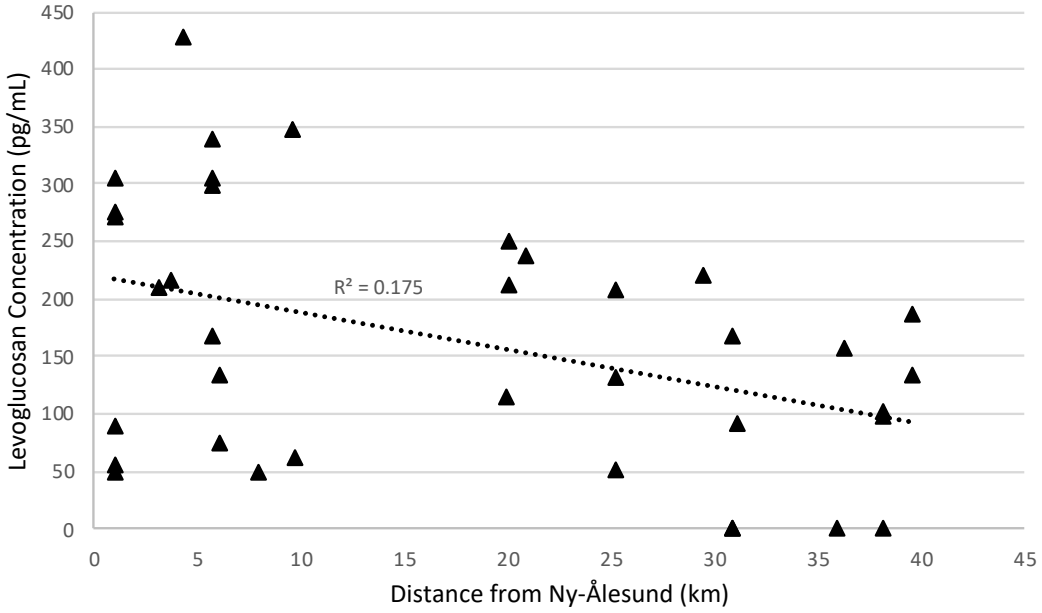

Figure 3.17. Concentration of levoglucosan in 2018 snow surface samples as a function of sampling site distance from Ny-Ålesund
(Four samples measured below the MDL and reported as 0 pg/mL)

3.7. Trace Elements

The concentrations of selected trace elements were measured in 39 of the 2018 snow surface samples and were used to augment the findings from the BC dataset. Sample concentrations of Pb, Cd, K, Al and Zn are plotted as a function of sampling site distance from Ny-Ålesund in Figure 3.18 and sampling site altitude in Figure 3.19. All samples with measured concentrations below the elemental LOD were removed from the dataset, which amounted to four samples for Cd. All measured trace element concentrations, in addition the LOD of each element, are provided in Appendix D. Similar to the levoglucosan samples, it was apparent that the snow samples intended for trace element analysis had melted and refrozen during transport or storage prior to analysis. Samples that had burst were discarded and the analysis proceeded with the remaining samples.

Three samples were excluded from the dataset used to create Figures 3.18 and 3.19 due to exceptionally high concentrations of nearly all measured trace elements. All three samples were from the KV-01 sampling site within the moraine of the KV glacier. There were areas of windblown, exposed rock near to the sampling site and it was noted that the snow samples contained high levels of sedimentary material. It was therefore assumed that the trace element contents of these samples were heavily enriched by mineral materials blown into the snow from exposed rock and soil.

The plots in Figures 3.18 and 3.19 express a spatial variability in the deposition of trace metals on the region's snowpack. Concentrations of all elements decrease with increasing distance from Ny-Ålesund and all elemental concentrations excluding Zn decrease with increasing altitude. The five elements measured are commonly emitted alongside BC during a variety of anthropogenic activities. Pb, Cd and Zn are typically emitted during energy production from coal and oil combustion and are also present in emissions from diesel and gasoline combustion engines (Le Roux et al., 2016). Al and K are also commonly emitted by diesel combustion engines (Cheung et al., 2010) and emissions from biomass and wood burning are typically enriched with K (Tumolva et al., 2010). The data indicates that emission sources of these trace elements within Ny-Ålesund, such as the diesel power plant and vehicle and snow scooter traffic, are leading to increased levels in the surrounding region.

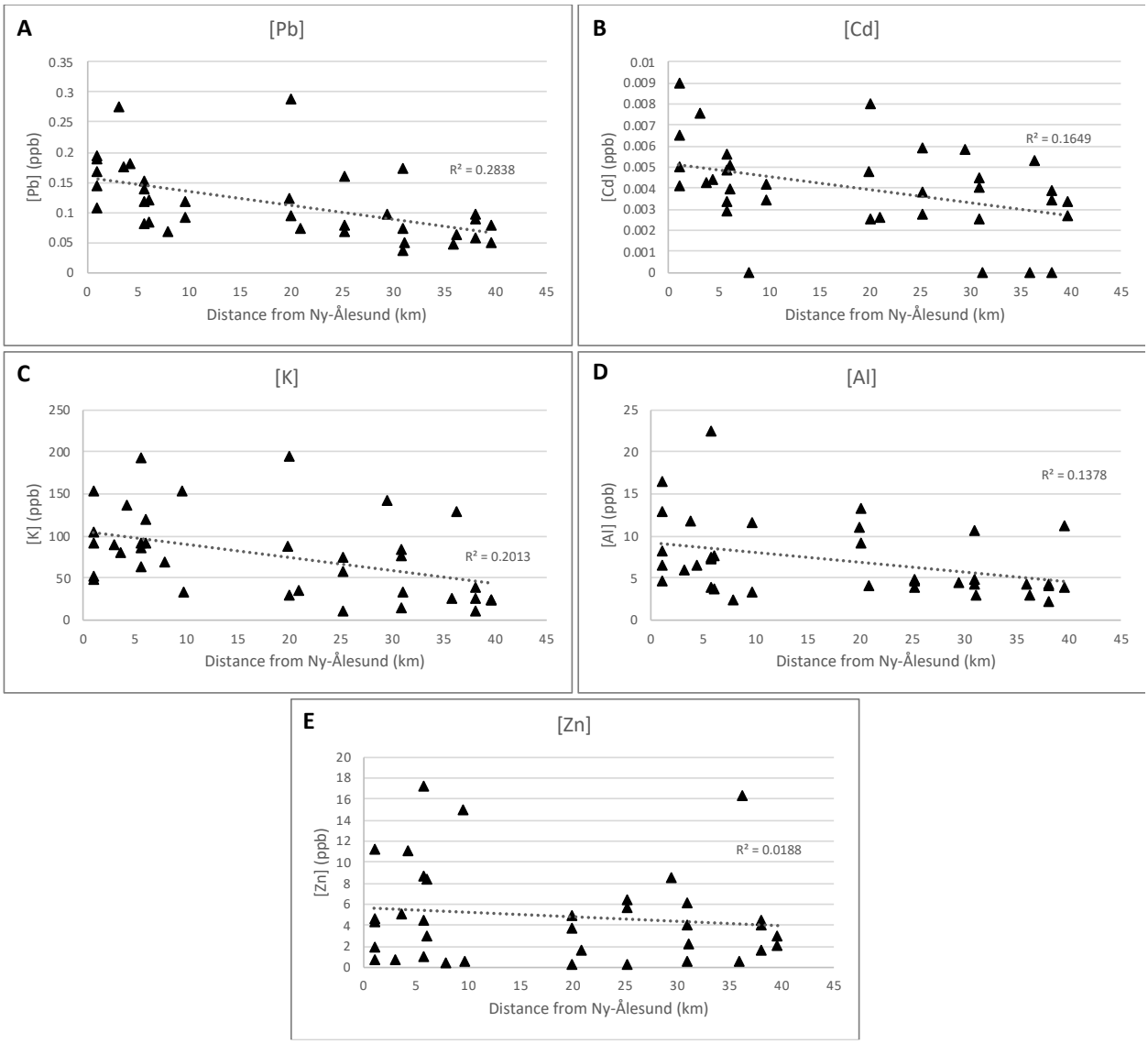

Figure 3.18. Measured ppb concentration of selected trace elements in 2018 surface snow samples as a function of sampling site distance from Ny-Ålesund

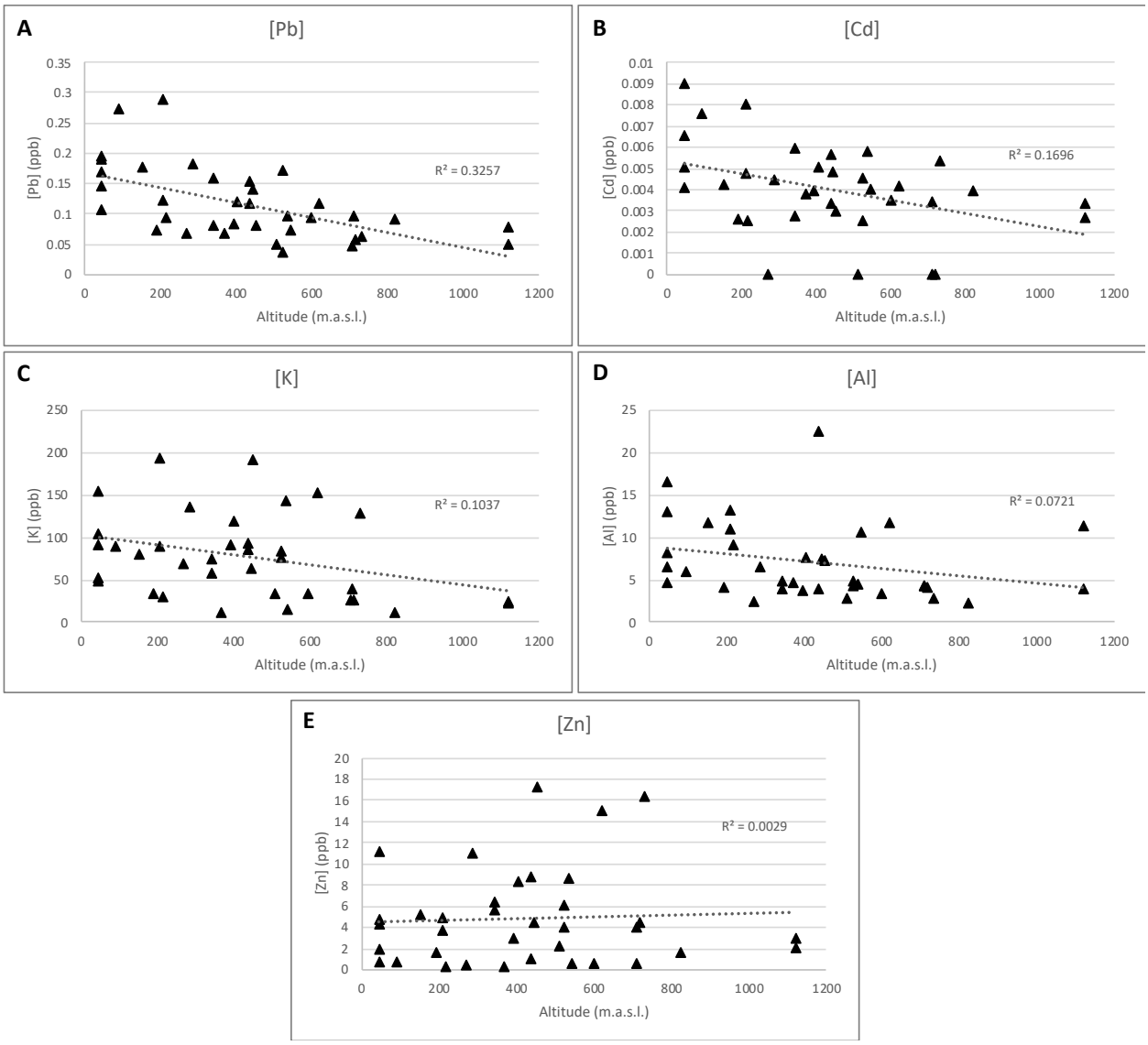

Figure 3.19. Measured ppb concentration of selected trace elements in 2018 surface snow samples as a function of sampling site altitude

It is also necessary to consider the sampling sites' distances from the sea, as saltwater spray contains ions and trace elements that may influence the chemistry of the snow near to shore. Through the duration of the sampling campaign, sea ice was either not present in Kongsfjord or present only as open drift ice, thus influences from sea spray were possible. The K^+ ion is a major constituent of saltwater and traces of Al and Zn can also be found in seawater (Turekian, 1968). There is a very strong correlation between sampling sites' distances from Ny-Ålesund and their closest distance to the sea, as plotted in Figure 3.20. Distances from the sea were determined by measuring straight-line distances from the sampling sites to the closest shoreline using

TopoSvalbard maps provided by NPI. Topography was not considered in the measurements. This correlation makes it difficult to differentiate between anthropogenic impacts from activities in Ny-Ålesund and natural impacts from seawater spray. Due to the high content of K in seawater, it is likely that the K content in snow was due in part to sea spray and these measurements should not be used as evidence for anthropogenic impact. However, it is not suspected that sea spray had substantial impacts to the concentrations of Pb, Cd, Al and Zn in snow due to the typically low levels of these elements in sea water (Turekian, 1968).

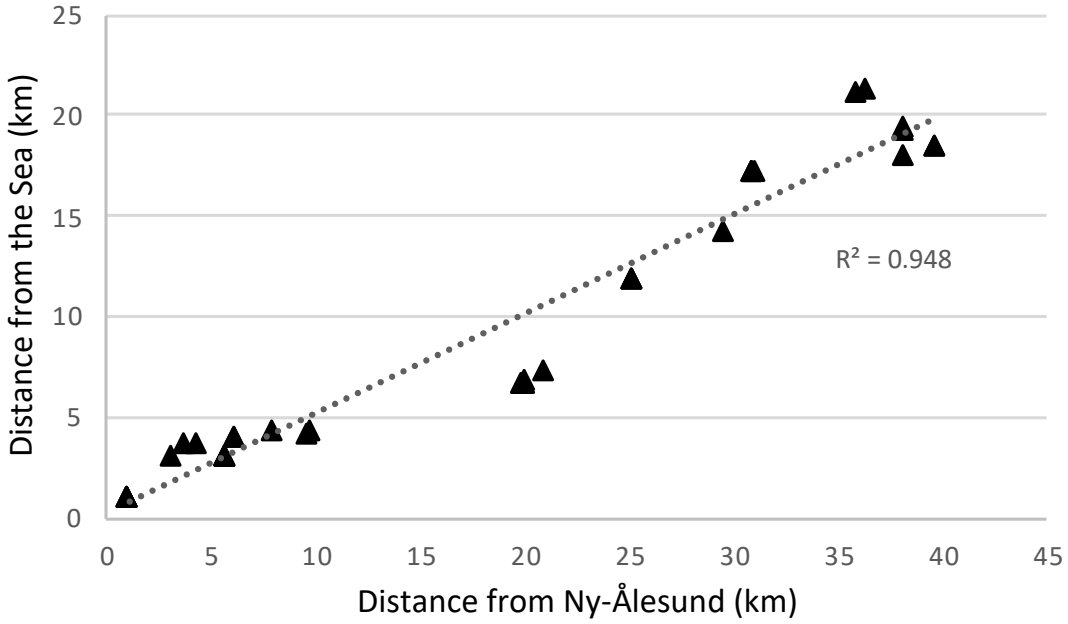

Figure 3.20. Sampling sites' distance from the sea as a function of their distance from Ny-Ålesund

The concentrations of Pb, Cd, K and Al were normalized by the concentration of Mn in each of the snow samples, which showed no spatial variance between sample concentrations. Mn concentrations ranged from 0.18 ppb to 1.5 ppb with mean and median concentrations of 0.51 ppb and 0.38 ppb, respectively. Bedrock in the southern region of Kongsfjord along the Brøgger peninsula consists primarily of conglomerates, sandstones, carbonates and spiculitic rocks that are high in Mn content (Hjelle, 1993 and Wehrmann et al., 2014). Therefore, it was assumed that the Mn content in the snow was representative of the natural background levels and could be used to normalize the data.

The ratio of each trace metal concentration to the Mn concentration was determined for each snow sample. Average ratios were calculated for all samples within 15 km from Ny-Ålesund and all samples outside of the 15 km radius. These average ratios were compared to the ratios of the average abundance of each element in the continental crust, as summarized by Taylor (1964), in order to determine an enrichment factor (EF). The EF describes the minimum factor by which the element concentration is greater than its average occurrence in the Earth's crust. For example, the EF of Pb was calculated as follows:

$$EF = \frac{[Pb]/[Mn]_{snow\ samples}}{[Pb]/[Mn]_{average\ crustal\ abundance}}$$

An exception was made for Al due to its very low ratios in snow samples compared to the average crustal abundance. Therefore the EF for Al was calculated based on the average ratio of the KV-01 sites. The KV-01 samples excluded from the earlier analysis were used as indicators of trace element content in the local bedrock. It was assumed that the chemical makeup of these samples was dominated by the inclusion of local sedimentary materials. Therefore, the average ratios of the element concentrations to the samples' Mn concentrations were used as a baseline for the region's natural background levels. All ratios and EFs are summarized in Table 3.3.

Table 3.3. Comparison of average trace element ratios of snow samples and ratios of average trace element abundance in the continental crust

Trace Element Ratios			**Sites < 15 km from Ny-Ålesund**		**Sites > 15 km from Ny-Ålesund**	
	Ratio of Average Crustal Abundance [+]	*Average ratio of KV-01 sites*	*Average Ratio*	*Enrichment Factor*	*Average Ratio*	*Enrichment Factor*
[Pb]/[Mn]	0.013	0.015	0.36	27	0.20	16
[Cd]/[Mn]	2.1E-04	4.2E-04	0.012	57	0.0093	44
[K]/[Mn]	22	22	250	11	140	6.4
[Al]/[Mn]	87	9.9	21	2.1[++]	13	1.3[++]

[+] *Referenced from Taylor, 1964*

[++] *Enrichment factors for [Al]/[Mn] were calculated based on average ratio of KV-01 sites rather than average crustal abundance*

The average ratios calculated for the three KV-01 sites are comparable to the ratios of the average crustal abundance for Pb, Cd and K, and are thus considered to be representative of the naturally occurring ratios. The [Al]/[Mn] ratios for the KV-01 sites and all other snow samples are

significantly lower than what was expected according to the average crustal abundance of the elements. This is likely attributed to naturally low levels of Al in the region's bedrock and thus the [Al]/[Mn] ratio for the KV-01 sites is still considered to be representative of natural background levels.

The EFs of the snow samples are greater than 1.0, indicating an additional source of Pb, Cd, K and Al to the snowpack. This could be from local emission sources within Ny-Ålesund, long-range transport of the chemical elements from lower latitudes or, in the case of K, from seawater spray. Furthermore, the EFs of the sites within 15 km of Ny-Ålesund are greater for each of the trace elements than the ratios for sites further away. Pb and Cd appear to be highly enriched, particularly in the snow located close to Ny-Ålesund. There are a variety of ongoing activities within Ny-Ålesund that typically produce Pb- and Cd-rich emissions including energy production and operation of snow scooters and other diesel or petrol vehicles. This substantiates the notion that emission sources present in Ny-Ålesund are leading to increased deposition of contaminants on the region's snowpack, with the most intense impacts observed closer to the settlement.

3.8. Potential Errors

Several potential errors may have arisen during sample preparation and analysis. Using a hand pump to filter the melted snow samples made it difficult to distribute particles homogeneously on the filter. It was observed that particles were not evenly distributed on the filters of many of the samples. In order to account for this, two or three punches were made and analyzed from the filters and the measured concentrations were averaged together. This may not have yielded accurate results. Additionally, some of the hydrophobic BC particles may have attached to the walls of the polyethylene Whirl-Pak sampling bags while the samples were left to melt. This has been observed in studies using high-density polyethylene containers (Ogren et al., 1983) and would lead to lower measured [EC] values. In order to prevent such losses, each sample was filtered within 24 hours of being fully melted to reduce BC absorbance potential and each emptied bag was rinsed with Milli-Q water to recover remaining particles.

When analyzing samples with low EC levels, as is typical for Arctic regions, pyrolysis of OC during analysis can have implications on measured EC. OC measurements are less impacted because OC levels are generally much higher, and the potential error is proportionally small. However, the EUSAAR_2 heating protocol has been optimized to reduce pyrolysis during TOA and thus minimizes this potential error.

3.9. Future Research

Typically, snow samples in the Ny-Ålesund region do not allow us to account for emissions from ship traffic because ships are in the region primarily during the summer and snow sampling is completed in springtime. The snow is melted during the summer at low altitudes and thus BC emissions from ships are deposited onto exposed rock or glacial ice and not incorporated into the snowpack. These emissions may have significant impacts on summer glacial melt as they would be deposited directly onto the ice surface, lowering albedo when the sun is at its strongest. Thus, it is important to understand the extent of BC emissions from ship traffic in the region. This could be done by measuring BC levels in glacial ice cores. It would be expected that the yearly accumulation of BC measured in the ice core would be higher than that calculated by snow pit measurements due to the preservation of BC deposited directly onto the exposed glacial ice during the summer months. This would include ship emissions that are not accounted for in seasonal flux calculations using snow samples. A future study comparing seasonal flux calculated from the snowpack to seasonal flux measured from an ice core could give an indication of how much BC is being deposited on glaciers during the summer.

The limited number of samples in this study and the inherit variability caused by heterogeneity in sampling timing pose challenges to the confidence of the results. There is clear evidence that activities in Ny-Ålesund are influencing the region's impurity content and this study has suggested an impact radius. However, more systematic sampling campaigns covering individual snowfall events would be necessary to better understand the distribution of contaminants. This could provide a more confident impact radius to scientists looking to study background levels of impurities on Svalbard.

Extended BC monitoring at high temporal resolution in the Ny-Ålesund region and at Zeppelin observatory would provide a better understanding of seasonal variations. Additionally, it would indicate if there are unusual periods of time with heightened levels of contaminants, such as in 2017, suggesting that measurements during that time should be taken with extreme caution. Such occurrences may become more common in Ny-Ålesund and other remote Arctic scientific sites due to permafrost thawing. Reductions in permafrost present issues in stability for aging infrastructure and thus replacement of foundations and construction of new buildings will likely be required at many locations in the coming years. This is an important consideration for Ny-Ålesund, but also other scientific locations as environmental sampling is often conducted close to such facilities.

4. Conclusions

Measured [EC] of 2018 surface snow samples were within the range expected for a remote Arctic site. Samples from 2018 ranged from 0 ng per gram of snow to 9.8 ng/g, with mean and median concentrations of 1.9 ng/g and 0.75 ng/g, respectively. The 2017 [EC] values were much higher and ranged from 0 to 68 ng/g with mean and median concentrations of 14 ng/g and 9.1 ng/g, respectively. The higher levels of BC in the 2017 samples were very likely due to emissions from building activities underway within Ny-Ålesund during the spring of 2017.

A comparison of the 2017 and 2018 datasets of [EC] in surface snow has confirmed that when strong anthropogenic activities are present in Ny-Ålesund, there is a clear, measurable impact on the contaminant levels of the surrounding region. Areas within a 15 km radius of the settlement are most impacted and exhibited 2.3 times higher average [EC] values than locations further away in 2017 (17 ng/g at < 15 km and 7.3 ng/g at > 15 km), when extensive building works were underway. In 2018, when no extraordinary activities were present in the settlement, average [EC] values for sites within the 15 km radius were 1.3 times higher than sites further away (2.1 ng/g at < 15 km and 1.6 ng/g at > 15 km), which could be attributed both to natural variability and anthropogenic activities. Normal activities in Ny-Ålesund such as snow scooter, vehicle and airplane traffic, as well as emissions from the diesel power plant are year-round local sources of BC to the region. The spatial variability of BC observed in the area is attributed to progressive atmospheric scavenging of particles from these emissions as they are transported further away from Ny-Ålesund.

Altitude of sampling locations was also a major contributing factor, leading to 1.5 times higher average [EC] values for sites lower than 450 m.a.s.l. in 2017 (17 ng/g at < 450 m and 11 ng/g at > 450 m) and 4.6 times higher average values in 2018 (2.6 ng/g at < 450 m and 0.56 ng/g at > 450 m). The presence of the atmospheric boundary layer, which is particularly stable in springtime and throughout the Arctic haze period, inhibits mixing of the lower and upper troposphere and keeps locally sourced contaminants at low altitudes. Higher altitude sites are thus influenced less by local sources of emissions and are more representative of contaminant levels brought by long range atmospheric transport.

The conclusion that BC levels are higher within 15 km of Ny-Ålesund and at altitudes below 450 m.a.s.l. was further confirmed by analysis of a singular snowfall event in spring 2018 and seasonal BC flux calculations on each of the glacier sites. Enrichment of trace elements Pb and Cd and the chemical tracer, levoglucosan, in surface snow near to Ny-Ålesund also indicated similar spatial and altitudinal trends. It is therefore suggested that the anthropogenic activities within Ny-Ålesund are having a measurable impact on the contaminant levels of the surrounding region. Based on the results of this study, it is recommended that sampling campaigns are completed further than 15 km from Ny-Ålesund and at altitudes greater than 450 m for future studies aiming to measure long range transport of contaminants to Svalbard or background levels of contaminants in the Arctic.

References

Aamaas, B., Bøggild, C. E., Stordal, F., Berntsen, T., Holmén, K. I. M., & Strùm, J. (2011). Elemental carbon deposition to Svalbard snow from Norwegian settlements and long-range transport. *Tellus B: Chemical and Physical Meteorology*, *63*(3), 340-351.

AMAP Assessment 2006: Acidifying Pollutants, Arctic Haze, and Acidi cation in the Arctic. Arctic Monitoring and Assessment Programme (AMAP), Oslo, Norway. xii + 112pp.

AMAP Assessment 2015: Black carbon and ozone as Arctic climate forcers. Arctic Monitoring and Assessment Programme (AMAP), Oslo, Norway. vii + 116 pp.

Anthony, K. M. W., Anthony, P., Grosse, G., & Chanton, J. (2012). Geologic methane seeps along boundaries of Arctic permafrost thaw and melting glaciers. *Nature Geoscience*, *5*(6), 419.

Argentini, S., Viola, A. P., Mastrantonio, G., Maurizi, A., Georgiadis, T., & Nardino, M. (2003). Characteristics of the boundary layerat Ny-Ålesund in the Arctic during the ARTIST field experiment. *Annals of Geophysics*, *46*(2).

Barrie, L. A., Hoff, R. M., & Daggupaty, S. M. (1981). The influence of mid-latitudinal pollution sources on haze in the Canadian Arctic. *Atmospheric Environment (1967)*, *15*(8), 1407-1419.

Bergstrom, R. W., Ackerman, T. P., & Richards, L. W. (1982). Optical Properties of particulate elemental carbon. Particulate carbon: atmospheric life cycle, edited by: Wolff, GT and Klimisch, RL.

Bond, T. C., & Bergstrom, R. W. (2006). Light absorption by carbonaceous particles: An investigative Review. *Aerosol Science and Technology, 40* (1), 27-67. doi:10.1080/02786820500421521.

Bond, T. C., Doherty, S. J., Fahey, D. W., Forster, P. M., Berntsen, T., Deangelo, … Zender, C. S. (2013). Bounding the role of black carbon in the climate system: A scientific assessment. *Journal of Geophysical Research: Atmospheres, 118* (11), 5380-5552. doi:10.1002/jgrd.50171.

Box, J. E., Fettweis, X., Stroeve, J. C., Tedesco, M., Hall, D. K., & Steffen, K. (2012). Greenland ice sheet albedo feedback: thermodynamics and atmospheric drivers. *The Cryosphere*, *6*(4), 821-839.

Cavalli, F., Viana, M., Yttri, K. E., Genberg, J., & Putaud, J. P. (2010). Toward a standardised thermal-optical protocol for measuring atmospheric organic and elemental carbon: the EUSAAR protocol. *Atmospheric Measurement Techniques*, *3*(1), 79-89.

Chen, Y., Shah, N., Braun, A., Huggins, F. E., & Huffman, G. P. (2005). Electron microscopy investigation of carbonaceous particulate matter generated by combustion of fossil fuels. *Energy & Fuels*, *19*(4), 1644-1651.

Cheung, K. L., Ntziachristos, L., Tzamkiozis, T., Schauer, J. J., Samaras, Z., Moore, K. F., & Sioutas, C. (2010). Emissions of particulate trace elements, metals and organic species from gasoline, diesel, and biodiesel passenger vehicles and their relation to oxidative potential. *Aerosol Science and Technology*, *44*(7), 500-513.

Chýlek, P., Ramaswamy, V., & Srivastava, V. (1983). Albedo of soot-contaminated snow. *Journal of Geophysical Research: Oceans*, *88*(C15), 10837-10843.

Ciais, P., C. Sabine, G. Bala, L. Bopp, V. Brovkin, J. Canadell, … P. Thornton. (2013). Carbon and Other Biogeochemical Cycles. In: Climate Change 2013: The Physical Science Basis. Contribution of Working Group I to the Fifth Assessment Report of the Intergovernmental Panel on Climate Change. Cambridge University Press, Cambridge, United Kingdom and New York, NY, USA.

Clarke, A. D., & Noone, K. J. (1985). Soot in the Arctic snowpack: A cause for perturbations in radiative transfer. *Atmospheric Environment (1967)*, *19*(12), 2045-2053.

Cramer, W., G.W. Yohe, M. Auffhammer, C. Huggel, U. Molau, M.A.F. da Silva Dias, … L. Tibig. (2014). Detection and attribution of observed impacts. In: Climate Change 2014: Impacts, Adaptation, and Vulnerability. Part A: Global and Sectoral Aspects. Contribution of Working Group II to the Fifth Assessment Report of the Intergovernmental Panel on Climate Change. Cambridge University Press, Cambridge, United Kingdom and New York, NY, USA, pp. 979-1037.

Cui, X., Wang, X., Yang, L., Chen, B., Chen, J., Andersson, A., & Gustafsson, Ö. (2016). Radiative absorption enhancement from coatings on black carbon aerosols. *Science of The Total Environment*, 551-552, 51-56. doi:10.1016/j.scitotenv.2016.02.026.

Davies, T. D., Tranter, M., Jickells, T. D., Abrahams, P. W., Landsberger, S., Jarvis, K., & Pierce, C. E. (1992). Heavily-contaminated snowfalls in the remote Scottish Highlands: a consequence of regional-scale mixing and transport. *Atmospheric Environment. Part A. General Topics*, *26*(1), 95-112.

Doherty, S. J., Warren, S. G., Grenfell, T. C., Clarke, A. D., & Brandt, R. E. (2010). Light-absorbing impurities in Arctic snow. *Atmospheric Chemistry and Physics*, *10*(23), 11647-11680.

Doherty, S. J., Grenfell, T. C., Forsström, S., Hegg, D. L., Brandt, R. E., & Warren, S. G. (2013). Observed vertical redistribution of black carbon and other insoluble light-absorbing particles in melting snow. *Journal of Geophysical Research: Atmospheres*, *118*(11), 5553-5569. doi:10.1002/jgrd.50235.

Dumont, M., Brun, E., Picard, G., Michou, M., Libois, Q., Petit, J. R., ... & Josse, B. (2014). Contribution of light-absorbing impurities in snow to Greenland's darkening since 2009. *Nature Geoscience*, *7*(7), 509.

Eleftheriadis, K., Vratolis, S., & Nyeki, S. (2009). Aerosol black carbon in the European Arctic: measurements at Zeppelin station, Ny-Ålesund, Svalbard from 1998–2007. *Geophysical Research Letters*, *36*(2).

Fierz, C., Armstrong, R., Durand, Y., Etchevers, P., Greene, E., McClung, D., ... & der Künste ZHdK, Z. H. (2009). IACS international classification for seasonal snow on the ground. *International Association of Cryospheric Sciences, UNESCO, Paris*.

Flanner, M. G., Zender, C. S., Randerson, J. T., & Rasch, P. J. (2007). Present-day climate forcing and response from black carbon in snow. *Journal of Geophysical Research: Atmospheres*, *112*(D11).

Flanner, M. G., Zender, C. S., Hess, P. G., Mahowald, N. M., Painter, T. H., Ramanathan, V., & Rasch, P. J. (2009). Springtime warming and reduced snow cover from carbonaceous particles. *Atmospheric Chemistry and Physics*, *9*(7), 2481-2497.

Forsström, S., Ström, J., Pedersen, C. A., Isaksson, E., & Gerland, S. (2009). Elemental carbon distribution in Svalbard snow. *Journal of Geophysical Research*, *114*(D19). doi:10.1029/2008jd011480.

Forster, P., V. Ramaswamy, P. Artaxo, T. Berntsen, R. Betts, D.W. Fahey, … R. Van Dorland. 2007. Changes in Atmospheric Constituents and in Radiative Forcing. In: Climate Change 2007: The Physical Science Basis. Contribution of Working Group I to the Fourth Assessment Report of the Intergovernmental Panel on Climate Change. Cambridge University Press, Cambridge, United Kingdom and New York, NY, USA.

Førland, E. J., Hansen-Bauer, I., & Nordli, P. Ø. (1997). Orographic precipitation at the glacier Austre Brøggerbreen. DNMI Rep. 2/97 Klima.

Gallet, J. C., Björkman, M. P., Larose, C., Luks, B., Martma, T., & Zdanowicz, C. (2018). Protocols and recommendations for the measurement of snow physical properties, and sampling of snow for black carbon, water isotopes, major ions and microorganisms.

Garrett, T. J., Brattström, S., Sharma, S., Worthy, D. E., & Novelli, P. (2011). The role of scavenging in the seasonal transport of black carbon and sulfate to the Arctic. *Geophysical Research Letters*, *38*(16).

Grabiec, M., Puczko, D., Budzik, T., & Gajek, G. (2011). Snow distribution patterns on Svalbard glaciers derived from radio-echo soundings. *Polish Polar Research*, *32*(4), 393-421.

Hagen, J. O., & Lefauconnier, B. (1995). Reconstructed runoff from the high Arctic basin Bayelva based on mass-balance measurements. *Hydrology Research*, *26*(4-5), 285-296.

Hansen, J., & Nazarenko, L. (2004). Soot climate forcing via snow and ice albedos. *Proceedings of the National Academy of Sciences*, *101*(2), 423-428.

Hennigan, C. J., Sullivan, A. P., Collett Jr, J. L., & Robinson, A. L. (2010). Levoglucosan stability in biomass burning particles exposed to hydroxyl radicals. *Geophysical Research Letters*, *37*(9).

Highwood, E. J., & Kinnersley, R. P. (2006). When smoke gets in our eyes: The multiple impacts of atmospheric black carbon on climate, air quality and health. *Environment international*, *32*(4), 560-566.

Hirdman, D., Burkhart, J. F., Sodemann, H., Eckhardt, S., Jefferson, A., Quinn, P. K., ... & Stohl, A. (2010). Long-term trends of black carbon and sulphate aerosol in the Arctic: changes in atmospheric transport and source region emissions. *Atmospheric Chemistry and Physics*, *10*(19), 9351-9368.

Hjelle, A. (1993). *Geology of Svalbard*. Oslo, Polarhåndbok no. 7, Norsk Polarinstitutt.

Khan, A. L., H. Dierssen, J. P. Schwarz, C. Schmitt, A. Chlus, M. Hermanson, T. H. Painter, & D. M. McKnight. (2017). Impacts of coal dust from an active mine on the spectral reflectance of Arctic surface snow in Svalbard, Norway. *J. Geophys. Res. Atmos., 122*. doi:10.1002/2016JD025757.

Klimont, Z., Kupiainen, K., Heyes, C., Purohit, P., Cofala, J., Rafaj, P., ... & Schöpp, W. (2017). Global anthropogenic emissions of particulate matter including black carbon. *Atmospheric Chemistry and Physics*, *17*(14), 8681-8723.

Kuo, L. J., Herbert, B. E., & Louchouarn, P. (2008). Can levoglucosan be used to characterize and quantify char/charcoal black carbon in environmental media?. *Organic Geochemistry*, *39*(10), 1466-1478.

Le Roux, G., Hansson, S. V., & Claustres, A. (2016). Inorganic Chemistry in the Mountain Critical Zone: Are the Mountain Water Towers of Contemporary Society Under Threat by Trace Contaminants?. In *Developments in Earth Surface Processes*(Vol. 21, pp. 131-154). Elsevier.

Liestøl, O. (1993). Glaciers of Svalbard, Norway. *Satellite Image Atlas of Glaciers of the World: Glaciers of Europe*, E127-E151.

Liousse, C., Cachier, H., & Jennings, S. G. (1993). Optical and thermal measurements of black carbon aerosol content in different environments: Variation of the specific attenuation cross-section, sigma (σ). *Atmospheric Environment. Part A. General Topics*, *27*(8), 1203-1211.

Manabe, S., & Stouffer, R. J. (1980). Sensitivity of a global climate model to an increase of CO2 concentration in the atmosphere. *Journal of Geophysical Research: Oceans*, *85*(C10), 5529-5554.

McConnell, J. R., Edwards, R., Kok, G. L., Flanner, M. G., Zender, C. S., Saltzman, E. S., ... & Kahl, J. D. (2007). 20th-century industrial black carbon emissions altered arctic climate forcing. *Science*, *317*(5843), 1381-1384.

McGuire, A. D., Anderson, L. G., Christensen, T. R., Dallimore, S., Guo, L., Hayes, D. J., ... & Roulet, N. (2009). Sensitivity of the carbon cycle in the Arctic to climate change. *Ecological Monographs*, *79*(4), 523-555.

Miller, G. H., Alley, R. B., Brigham-Grette, J., Fitzpatrick, J. J., Polyak, L., Serreze, M. C., & White, J. W. (2010). Arctic amplification: can the past constrain the future?. *Quaternary Science Reviews*, *29*(15-16), 1779-1790.

Norwegian Polar Institute, University of Oslo (2019). Cummulative mass balance for glaciers in Svalbard. *Environmental monitoring of Svalbard and Jan Mayen (MOSJ)*. URL: http://www.mosj.no/en/climate/land/mass-balance-glaciers.html

Ogren, J. A., Charlson, R. J., & Groblicki, P. J. (1983). Determination of elemental carbon in rainwater. *Analytical chemistry*, *55*(9), 1569-1572.

Quinn, P. K., Shaw, G., Andrews, E., Dutton, E. G., Ruoho-Airola, T., & Gong, S. L. (2007). Arctic haze: current trends and knowledge gaps. *Tellus B: Chemical and Physical Meteorology*, *59*(1), 99-114.

Rau, J. A. (1989). Composition and size distribution of residential wood smoke particles. *Aerosol Science and Technology*, *10*(1), 181-192.

Rignot, E., Velicogna, I., van den Broeke, M. R., Monaghan, A., & Lenaerts, J. T. (2011). Acceleration of the contribution of the Greenland and Antarctic ice sheets to sea level rise. *Geophysical Research Letters*, *38*(5).

Ross, M. N., & Sheaffer, P. M. (2014). Radiative forcing caused by rocket engine emissions. *Earth's Future*, *2*(4), 177-196.

Serreze, M. C., Crawford, A. D., & Barrett, A. P. (2015). Extreme daily precipitation events at Spitsbergen, an Arctic Island. *International Journal of Climatology*, *35*(15), 4574-4588.

Sharma, S., Lavoué, D., Cachier, H., Barrie, L. A., & Gong, S. L. (2004). Long-term trends of the black carbon concentrations in the Canadian Arctic. *Journal of Geophysical Research: Atmospheres*, *109*(D15).

Sharma, S., Ishizawa, M., Chan, D., Lavoué, D., Andrews, E., Eleftheriadis, K., & Maksyutov, S. (2013). 16-year simulation of Arctic black carbon: Transport, source contribution, and sensitivity analysis on deposition. *Journal of Geophysical Research: Atmospheres*, *118*(2), 943-964.

Sharp, M., & Wang, L. (2009). A Five-Year Record of Summer Melt on Eurasian Arctic Ice Caps. *Journal of Climate*, *22*(1), 133-145. doi:10.1175/2008jcli2425.1.

Shaw, G. E., & Stamnes, K. (1980). Arctic haze: perturbation of the polar radiation budget. *Annals of the New York Academy of Sciences*, *338*(1), 533-539.

Sinha, P. R., Kondo, Y., Goto-Azuma, K., Tsukagawa, Y., Fukuda, K., Koike, M., ... & Førland, E. J. (2018). Seasonal Progression of the Deposition of Black Carbon by Snowfall at Ny-Ålesund, Spitsbergen. *Journal of Geophysical Research: Atmospheres*, *123*(2), 997-1016.

Smallwood, G. J., Bachalo, W. D., & Sankar, S. V. (2003). Particulate Measurement Methods. In *Optical Metrology for Fluids, Combustion and Solids* (pp. 221-257). Springer, Boston, MA.

Statistics Norway. (2018, September 20). Population of Svalbard. Retrieved February 11, 2019, from https://www.ssb.no/en/befsvalbard/

Stein, A. F., Draxler, R. R., Rolph, G. D., Stunder, B. J., Cohen, M. D., & Ngan, F. (2015). NOAA's HYSPLIT atmospheric transport and dispersion modeling system. *Bulletin of the American Meteorological Society*, *96*(12), 2059-2077.

Stohl, A. (2006). Characteristics of atmospheric transport into the Arctic troposphere. *Journal of Geophysical Research: Atmospheres*, *111*(D11).

Stohl, A., Berg, T., Burkhart, J. F., Fjæraa, A. M., Forster, C., Herber, A., ... & Shiobara, M. (2007). Arctic smoke–record high air pollution levels in the European Arctic due to agricultural fires in Eastern Europe in spring 2006. *Atmospheric Chemistry and Physics*, *7*(2), 511-534.

Stohl, A., Klimont, Z., Eckhardt, S., Kupiainen, K., Shevchenko, V. P., Kopeikin, V. M., & Novigatsky, A. N. (2013). Black carbon in the Arctic: the underestimated role of gas flaring and residential combustion emissions. *Atmospheric Chemistry and Physics*, *13*(17), 8833-8855. doi:10.5194/acp-13-8833-2013.

Taylor, S. R. (1964). Abundance of chemical elements in the continental crust: a new table. *Geochimica et cosmochimica acta*, *28*(8), 1273-1285.

Tedstone, A. J., Bamber, J. L., Cook, J. M., Williamson, C. J., Fettweis, X., Hodson, A. J., & Tranter, M. (2017). Dark ice dynamics of the south-west Greenland Ice Sheet. *Cryosphere*, *11*(6), 2491-2506.

Tumolva, L., Park, J. Y., Kim, J. S., Miller, A. L., Chow, J. C., Watson, J. G., & Park, K. (2010). Morphological and elemental classification of freshly emitted soot particles and atmospheric ultrafine particles using the TEM/EDS. *Aerosol Science and Technology*, *44*(3), 202-215.

Turekian, K. K. (1968). *Oceans*. Englewood Cliffs, NJ: Prentice-Hall.

Vander Wal, R. L., Bryg, V. M., & Huang, C. H. (2014). Aircraft engine particulate matter: macro-micro-and nanostructure by HRTEM and chemistry by XPS. *Combustion and Flame*, *161*(2), 602-611.

Visit Svalbard. (2018, May). Svalbard Statistics. Retrieved February 11, 2019, from https://en.visitsvalbard.com/visitor-information/corporate-site/svalbard-statistics

Wang, Q., Jacob, D. J., Fisher, J. A., Mao, J., Leibensperger, E. M., Carouge, C. C., . . . Doherty, S. J. (2011). Sources of carbonaceous aerosols and deposited black carbon in the Arctic in winter-spring: implications for radiative forcing. *Atmospheric Chemistry and Physics, 11*(23), 12453-12473. doi:10.5194/acp-11-12453-2011.

Warren, S. G. (1982). Optical properties of snow. *Reviews of Geophysics, 20*(1), 67-89.

Warren, S. G., & Wiscombe, W. J. (1980). A Model for the Spectral Albedo of Snow. II: Snow Containing Atmospheric Aerosols. *Journal of the Atmospheric Sciences, 37*(12), 2734-2745. doi:10.1175/15200469(1980)037<2734:amftsa>2.0.co;2.

Warren, S. G., & Wiscombe, W. J. (1985). Dirty snow after nuclear war. *Nature, 313*(6002), 467.

Wehrmann, L. M., Formolo, M. J., Owens, J. D., Raiswell, R., Ferdelman, T. G., Riedinger, N., & Lyons, T. W. (2014). Iron and manganese speciation and cycling in glacially influenced high-latitude fjord sediments (West Spitsbergen, Svalbard): evidence for a benthic recycling-transport mechanism. *Geochimica et Cosmochimica Acta, 141*, 628-655.

Weinbruch, S., Benker, N., Kandler, K., Schütze, K., Kling, K., Berlinger, B., ... & Kallenborn, R. (2018). Source identification of individual soot agglomerates in Arctic air by transmission electron microscopy. *Atmospheric Environment, 172*, 47-54.

Yttri, K. E., Lund Myhre, C., Eckhardt, S., Fiebig, M., Dye, C., Hirdman, D., ... & Stohl, A. (2014). Quantifying black carbon from biomass burning by means of levoglucosan–a one-year time series at the Arctic observatory Zeppelin. *Atmospheric Chemistry and Physics, 14*(12), 6427-6442.

Zanatta, M., Gysel, M., Bukowiecki, N., Müller, T., Weingartner, E., Areskoug, H., … Laj, P. (2016). A European aerosol phenomenology-5: Climatology of black carbon optical properties at 9 regional background sites across Europe. *Atmospheric Environment, 145*, 346-364. doi:10.1016/j.atmosenv.2016.0.

Appendices

Appendix A. Sampling Sites

Table A.1. 2018 Snow Surface Sampling Sites

Site	*Date*	*Time*	*Latitude (°N)*	*Longitude (°E)*	*Altitude (m)*	*Distance from Ny-Ålesund (km)*	*Surface Sample Depth (cm)*	*Air Temp (°C)*	*Snow Surface Temp (°C)*	*Wind Speed (m/s)*	*Sky Conditions*	*Precipitation Notes*
GVB	23-Mar-18	15:00	78.91651667	11.89446667	46	1.0	2	-9.2	-18.5	0	Mostly clear	
KV-01	5-Apr-18		78.86283333	12.49815	53	14						
KV-02	5-Apr-18		78.82068333	12.67493333	216	20						
KV-04	5-Apr-18		78.80463333	12.91061667	369	25						
KV-06	5-Apr-18		78.77791667	13.13573333	544	31						
KV-09	5-Apr-18		78.74526667	13.47115	822	38						
GVB	6-Apr-18	9:38	78.91651667	11.89446667	46	1.0	10	-19.4	-18.2	0	Clear	
GVB	8-Apr-18	18:10	78.91651667	11.89446667	46	1.0	2	-5	-9.2	7	Partly cloudy	Fresh snow in the morning
BR-06	8-Apr-18	17:30	78.89478333	11.84158333	152	3.7	2	-5.8	-11.1	0-5	Partly cloudy	Fresh snow in the morning
BR-10	8-Apr-18	16:45	78.88576667	11.90708333	285	4.3	5	-6.6	-12.1	0-5	Partly cloudy	Fresh snow in the morning
BR-13	8-Apr-18	15:50	78.87265	11.91488333	445	5.7	3	-6.9	-12.8	0-5	Partly cloudy	Fresh snow in the morning
KV-01	10-Apr-18	12:00	78.8605	12.50398333	15	14	5	-11.2	-14.8	0	Clear	Heavy snowfall the day before
KV-02	10-Apr-18	13:00	78.82081667	12.67516667	209	20	2	-16.4	-16.9	0	Clear	Heavy snowfall the day before
KV-04	10-Apr-18	13:30	78.80435	12.91051667	343	25	6	-16.4	-14.6	0	Clear	Heavy snowfall the day before
KV-06	10-Apr-18	13:50	78.77795	13.1361	524	31	5	-17.3	-19.6	0	Clear	Heavy snowfall the day before
KV-09	10-Apr-18	14:35	78.74228333	13.41211667	710	38	6	-17.6	-19.2	0-5	Clear	Heavy snowfall the day before
GVB	10-Apr-18	18:00	78.91651667	11.89446667	46	1.0	12	-13	-8.6	0-5	Mostly clear	Heavy snowfall the day before
GVB	11-Apr-18	19:00	78.91651667	11.89446667	46	1.0	10	-2.8	-4.5	0	Overcast	Fresh snow in the morning
GVB	13-Apr-18	21:10	78.91651667	11.89446667	46	1.0	8	-7.8	-7.7	0	Mostly cloudy	Heavy snowfall the day before
EB-01	13-Apr-18		78.8582	12.05491667	269	7.9	10		-6.4			Heavy snowfall the day before
EB-02	13-Apr-18		78.85318333	12.17715	598	9.7	15		-7.3			Heavy snowfall the day before
BR-04	13-Apr-18		78.90196667	11.83063333	92	3.1	10		-6.3			Heavy snowfall the day before
BR-13	13-Apr-18		78.87238333	11.91591667	437	5.7	10		-7.2			Heavy snowfall the day before
ML-01	13-Apr-18		78.88675	12.04713333	180	5.0	10		-6.5			Heavy snowfall the day before
ML-02	13-Apr-18		78.87091667	11.98563333	394	6.1	10		-7.8			Heavy snowfall the day before
HDF-02	13-Apr-18	16:42	78.92863333	13.29738333	536	30	10	-19.9	-11.1	0	Clear	Heavy snowfall the day before
HDF-06	13-Apr-18	15:47	79.02783333	13.53256667	731	36	21	-14.2	-14.4	0	Clear	Heavy snowfall the day before
HDF-10	13-Apr-18	14:07	79.14006667	13.39488333	1121	40	17	-12.9	-14.6	0-5	Mostly clear	Heavy snowfall the day before
KV-02	13-Apr-18	19:45	78.83026667	12.76008333	191	21	11	-11.3	-9.1	0	Mostly cloudy	Heavy snowfall the day before
KV-06	13-Apr-18	19:00	78.78026667	13.1508	509	31	7	-22.5	-10.3	0	Partly cloudy	Heavy snowfall the day before
KV-09	13-Apr-18	18:20	78.74243333	13.41055	717	38	15	-16.4	-12.8	0	Clear	Heavy snowfall the day before
BR-13	14-Apr-18	16:00	78.87248333	11.91513333	453	5.7	8	-5.9	-6.4	5	Overcast	Light snow during collection
ML-02	14-Apr-18	12:50	78.87073333	11.98361667	403	6.1	8	-6.8	-6.9	0	Overcast	Light snow during collection
EB-02	15-Apr-18	17:30	78.85473333	12.1847	620	9.6	5	-6	-7.7	5	Whiteout	Light snow during collection
GVB	17-Apr-18	18:00	78.91651667	11.89446667	46	1.0	12	-10	-9.4	5	Mostly clear	
HDF-10	18-Apr-18	14:00	79.14006667	13.39488333	1121	40	5	-14.3	-16.5	0-5	Clear	
KV-01	19-Apr-18	13:00	78.8605	12.50398333	15	14	4	-13.4	-14.2	0	Clear	
KV-02	19-Apr-18	13:30	78.82081667	12.67516667	209	20	10	-13.4	-14.2	0	Clear	
KV-04	19-Apr-18	13:45	78.80435	12.91051667	343	25	8	-13.4	-14.2	0	Clear	
KV-06	19-Apr-18	14:05	78.77795	13.1361	524	31	7	-13.4	-14.2	0	Mostly clear	
KV-08	19-Apr-18	15:30	78.75556667	13.3363	708	36	4	-13.4	-14.2	0		Light snow during collection
BR-13	21-Apr-18	13:30	78.87238333	11.91591667	437	5.7	17	-6.6	-5.5	0-5	Overcast	Fresh snow the night before
GVB	21-Apr-18	15:30	78.91651667	11.89446667	46	1.0	13	-4.4	-4.6	4-5	Overcast	Fresh snow the night before
GVB	23-Apr-18	19:30	78.91651667	11.89446667	46	1.0	6	-12.3	-9.5	3	Clear	
GVB	1-May-18	10:09	78.91651667	11.89446667	46	1.0	4.5	2.7	-0.1	0	Overcast	
GVB	4-May-18	10:34	78.91651667	11.89446667	46	1.0	7	3	-0.1	5	Cloudy	Light rain during collection
GVB	8-May-18		78.91651667	11.89446667	46	1.0	4	2.9	0	0-5	Mostly clear	
GVB	11-May-18		78.91651667	11.89446667	46	1.0	6	3.3	0	0	Mostly cloudy	

Appendix A. Sampling Sites (continued)

Table A.2. 2018 Snow Pit Sampling Sites

Site	*Date*	*Time*	*Latitude (°N)*	*Longitude (°E)*	*Altitude (m)*	*Air Temp (°C)*	*Wind (m/s)*	*Sky Conditions*	*Precipitation Notes*	*Sample Type*	*Sample Depth Top (cm)*	*Sample Depth Bottom (cm)*	*Snow Temp (°C)*
GVB	23-Mar-18	15:00	78.91651667	11.89446667	46	-9.2	0	Mostly clear		SURFACE	28	26	-18.5
										PIT	26	0	-18.5
GVB	6-Apr-18	9:38	78.91651667	11.89446667	46	-19.4	0	Clear		SURFACE	32	22	-18.2
										PIT	22	0	-18.2
GVB	11-Apr-18	19:00	78.91651667	11.89446667	46	-2.8	0	Overcast	Fresh snow in the morning	SURFACE	35	21	-4.5
										PIT	21	16	-4.5
										PIT	16	0	-4.5
BR-13	14-Apr-18	16:00	78.87248333	11.91513333	453	-5.9	5	Overcast	Light snow during sampling	SURFACE	95	87	-6.4
										PIT	87	30	-9.1
										PIT	30	0	-9.1
ML-02	14-Apr-18	12:50	78.87073333	11.98361667	403	-6.8	0	Overcast	Light snow during sampling	SURFACE	167	159	-6.9
										PIT	159	105	-10
										PIT	105	56	-10.9
										PIT	56	0	-8.7
EB-02	15-Apr-18	17:30	78.85473333	12.1847	620	-6	5	Whiteout	Light snow during sampling	SURFACE	105	100	-7.7
										PIT	100	49	-7.7
										PIT	49	0	-7.7
GVB	17-Apr-18	18:00	78.91651667	11.89446667	46	-10	5	Mostly clear		SURFACE	51	39	-9.4
										PIT	39	22	-9.4
										PIT	22	0	-9.4
HDF-10	18-Apr-18	14:00	79.14006667	13.39488333	1121	-14.3	0-5	Clear		SURFACE	166	160	-16.5
										PIT	160	110	-15
										PIT	110	53	-13.8
										PIT	53	0	-11.9
KV-08	19-Apr-18	15:30	78.75556667	13.3363	708	-13.4	0	Overcast	Light snow during sampling	SURFACE	173	169	-14.2
										PIT	169	105	-13
										PIT	105	47	-11.1
										PIT	47	0	-9.6

Appendix A. Sampling Sites (continued)

Table A.3. 2018 Snow Pit Stratigraphy Details

		Temperature Profile		Snow Stratigraphy				Snow Density		
Site	*Date*	*Depth (cm)*	*Snow Temp (°C)*	*Layer Depth Top (cm)*	*Layer Depth Bottom (cm)*	*Hardness* [+]	*Grain Type*	*Layer Depth Top (cm)*	*Layer Depth Bottom (cm)*	*Density (kg/m^3)*
GVB	23-Mar-18	27	-18.5	28	27	K		28	0	152
		19	-14.8	27	19	4F				
		16	-13.5	19	16	1F				
		13	-11.0	16	13	1F				
		0	-9.8	13	0	K	melt refreeze			
GVB	6-Apr-18	26	-18.2	32	31	4F	fresh snow	32	16	72.0
		21	-16.8	31	30	1F	wind packed	16	0	131
		18	-13.5	30	21	F	faceted / depth hoar			
		10	-11.9	21	19	1F	melt refreeze			
		0	-10.4	19	14	4F	depth hoar			
				14	0	K	melt refreeze			
				0	-10	I	melt refreeze			
GVB	11-Apr-18	31	-4.5	35	27	4F	fresh snow	35	27	70.0
		23	-7.2	27	21	4F	slighly harder fresh snow	27	21	200
		18	-8.2	21	16	1F	fragmented snow	21	16	192
		8	-8.8	16	11	4F	faceted / depth hoar	11	5	230
		3	-8.8	11	5	K	melt refreeze			
				5	0	4F	faceted / depth hoar			
BR-13	14-Apr-18	90	-6.4	95	88	F		95	75	232
		80	-8.3	88	70	4F		75	55	368
		70	-8.9	70	66	1F		55	35	358
		60	-9.1	66	65	K	melt refreeze	35	15	505
		50	-9.4	65	44	4F		15	0	253
		40	-9.5	44	43	1F				
		30	-9.5	43	33	4F				
		20	-9.0	33	32	I	ice lens			
		10	-9.3	32	18	4F				
		0	-9.2	18	10	1F				
				10	0	4F	depth hoar			

[+] *Hardness scale is based on the 'hand test' detailed in Fierz et al. (2009). From softest to hardest: fist (F), 4 fingers (4F), 1 finger (1F), pencil (P), knife blade (K), ice (I).*

Appendix A. Sampling Sites (continued)

Table A.3. *2018 Snow Pit Stratigraphy Details (continued)*

		Temperature Profile		**Snow Stratigraphy**				**Snow Density**		
Site	*Date*	*Depth (cm)*	*Snow Temp (°C)*	*Layer Depth*	*Layer Depth*	*Hardness* [+]	*Grain Type*	*Layer Depth*	*Layer Depth*	*Density*
ML-02	14-Apr-18	159	-6.9	167	159	F	fresh snow	167	147	158
		151	-9.2	159	151	F		147	127	305
		145	-10	151	145	4F		127	107	305
		139	-10.4	145	139	4F		107	87	305
		131	-10.7	139	131	F		87	67	453
		106	-11.1	131	106	4F	depth hoar	67	47	452
		105	-11.0	106	101	P	melt refreeze	47	27	400
		87	-10.9	101	87	1F		27	7	379
		65	-10.5	87	65	P		7	0	391
		55	-9.8	65	55	1F				
		38	-9.1	55	38	K	melt refreeze			
		28	-8.8	38	28	P				
		25	-8.6	28	25	K				
		15	-8.2	25	15	P				
		0	-7.5	15	0	4F	depth hoar			
EB-02	15-Apr-18	100	-7.8	105	100	F	fresh snow	105	85	253
		90	-8.4	100	84	4F		85	65	284
		80	-9.6	84	83	K	melt refreeze	65	45	390
		70	-9.6	83	58	4F		45	25	495
		60	-9.4	58	53	P		25	5	453
		50	-9.5	53	46	4F		5	0	505
		40	-9.6	46	32	1F				
		30	-9.6	32	10	P				
		20	-9.5	10	7	K	melt refreeze			
		10	-9.3	7	0	4F	depth hoar			
		0	-9.1							
GVB	17-Apr-18	48	-9.4	51	50	1F	recent snow, crust	50	48	140
		47	-8.1	50	48	4F	fresh snow	47	39	160
		39	-7.0	48	47	K	melt refreeze	39	30	290
		30	-6.6	47	39	1F	rounded grains	30	28	600
		28	-6.5	39	30	4F	faceted	28	22	200
		22	-6.6	30	28	P	melt refreeze	22	0	700
		0	-6.5	28	22	4F	depth hoar			
				22	0	K	melt refreeze			

[+] *Hardness scale is based on the 'hand test' detailed in Fierz et al. (2009). From softest to hardest: fist (F), 4 fingers (4F), 1 finger (1F), pencil (P), knife blade (K), ice (I).*

Appendix A. Sampling Sites (continued)

Table A.3. *2018 Snow Pit Stratigraphy Details (continued)*

		Temperature Profile		Snow Stratigraphy				Snow Density		
Site	*Date*	*Depth (cm)*	*Snow Temp (°C)*	*Layer Depth Top (cm)*	*Layer Depth Bottom (cm)*	*Hardness* [+]	*Grain Type*	*Layer Depth Top (cm)*	*Layer Depth Bottom (cm)*	*Density (kg/m* ^{3} *)*
HDF-10	18-Apr-18	160	-16.5	166	160	P		166	146	379
		150	-16.0	160	155	1F		146	126	484
		140	-15.1	155	150	P		126	106	421
		130	-14.5	150	125	K		106	86	400
		120	-14.2	125	121	1F		86	66	411
		110	-14.1	121	110	P		66	46	474
		100	-14.1	110	100	1F		46	26	495
		90	-14.0	100	70	P		26	6	400
		80	-13.8	70	56	1F		6	0	386
		70	-13.6	56	50	P				
		60	-13.3	50	48	K	melt refreeze			
		50	-12.9	48	43	K				
		40	-12.5	43	32	P				
		30	-12.1	32	22	K				
		20	-11.8	22	10	1F				
		10	-11.4	10	0	4F	depth hoar			
		0	-10.7							
KV-08	19-Apr-18	170	-14.2	173	158	F	fresh snow	173	153	200
		160	-14.8	158	147	P		153	133	305
		150	-14.1	147	130	1F		133	113	358
		140	-13.0	130	119	P		113	93	379
		130	-12.3	119	117	K		93	73	284
		120	-11.9	117	105	1F		73	53	390
		110	-11.7	105	75	P		53	33	284
		100	-11.4	75	70	K		33	13	273
		90	-11.4	70	69	K	melt refreeze	13	0	178
		80	-11.2	69	47	P				
		70	-11.1	47	40	K				
		60	-10.8	40	37	P	melt refreeze			
		50	-10.5	37	34	1F				
		40	-10.1	34	29	P				
		30	-9.7	29	28	K	melt refreeze			
		20	-9.7	28	18	K				
		10	-9.4	18	13	P				
		0	-9.1	13	7	K	melt refreeze			
				7	0	P	depth hoar			

[+] *Hardness scale is based on the 'hand test' detailed in Fierz et al. (2009). From softest to hardest: fist (F), 4 fingers (4F), 1 finger (1F), pencil (P), knife blade (K), ice (I).*

Appendix B. Measured Elemental and Organic Carbon

Table B.1. Measured EC and OC Concentrations of 2018 Surface Snow Samples

			Punch 1		Punch 2			
Site	*Date*	*Filtered Volume (mL)*	*OC (µg/cm^2)*	*EC (µg/cm^2)*	*OC (µg/cm^2)*	*EC (µg/cm^2)*	***OC (ng/g)*** [+]	***EC (ng/g)*** [+]
GVB	23-Mar-18	2235	81	0.01			329	0.04
KV-01	5-Apr-18	785	63	0.02			727	0.23
KV-02	5-Apr-18	2070	37	1.9			164	8.5
KV-04	5-Apr-18	1795	20	0.08			102	0.40
KV-06	5-Apr-18	2455	30	0.00			111	0.00
KV-09	5-Apr-18	1745	13	0.00			66	0.00
GVB	6-Apr-18	3135	39	0.27			114	0.78
GVB	8-Apr-18	2805	49	0.79	36	0.98	137	2.9
BR-06	8-Apr-18	2385	19	0.04			73	0.15
BR-10	8-Apr-18	1872	12	0.21			60	1.0
BR-13	8-Apr-18	2670	19	0.09			63	0.31
KV-01	10-Apr-18	640	69	0.05			986	0.71
KV-02	10-Apr-18	2215	24	1.2	17	0.86	86	4.2
KV-04	10-Apr-18	2190	14	0.57			60	2.4
KV-06	10-Apr-18	2615	19	1.22			68	4.2
KV-09	10-Apr-18	2760	22	0.8			73	2.5
GVB	10-Apr-18	1930	12	0.49	11	0.43	53	2.2
GVB	11-Apr-18	1750	20	1.0			102	5.4
GVB	13-Apr-18	2420	9.2	0.46	11	0.56	38	1.9
EB-01	13-Apr-18	2180	3.4	0.00			14	0.00
EB-02	13-Apr-18	2485	8.8	0.26			32	0.95
BR-04	13-Apr-18	2185	10	1.2			43	4.9
BR-13	13-Apr-18	2240	12	0.52			48	2.1
ML-01	13-Apr-18	2390	14	0.08			53	0.30
ML-02	13-Apr-18	2385	14	0.20			54	0.76
HDF-02	13-Apr-18	2530	11	0.00			38	0.00
HDF-06	13-Apr-18	1645	7.9	0.00			44	0.00
HDF-10	13-Apr-18	2710	19	0.00			63	0.00
KV-02	13-Apr-18	3180	30	2.5	42	2.8	103	7.7
KV-06	13-Apr-18	2210	10	0.00			42	0.00
KV-09	13-Apr-18	2330	14	0.01			54	0.04
BR-13	14-Apr-18	1730	6.4	0.04			33	0.21
ML-02	14-Apr-18	1575	30	0.84	35	0.75	187	4.6
EB-02	15-Apr-18	2035	18	0.00			81	0.00
GVB	17-Apr-18	3055	27	0.89	21	0.60	71	2.2
HDF-10	18-Apr-18	2670	13	0.11			45	0.37
KV-01	19-Apr-18	3590	91	0.03	77	0.03	213	0.08
KV-02	19-Apr-18	2960	19	0.00			58	0.00
KV-04	19-Apr-18	2940	32	0.24			98	0.74
KV-06	19-Apr-18	2850	18	0.00			58	0.00
KV-08	19-Apr-18	2870	12	0.00			38	0.00
BR-13	21-Apr-18	2420	11	0.38			41	1.4
GVB	21-Apr-18	2560	19	1.1			67	3.8
GVB	23-Apr-18	2750	28	1.1			93	3.8
GVB	1-May-18	3140	26	1.4			74	4.1
GVB	4-May-18	3940	18	2.1			41	4.9
GVB	8-May-18	2160	16	0.11			68	0.48
GVB	11-May-18	1610	61	1.7			344	9.8

[+] *Calculated using the volume of the filtered sample and the total surface area of the filter, 9.079 cm^2, see calculations in section 2.2.3.*

Appendix B. Measured Elemental and Organic Carbon (continued)

Table B.2. Measured EC and OC Concentrations of 2017 Surface Snow Samples

Site	*Date*	*Latitude (°N)*	*Longitude (°E)*	*Altitude (m)*	*Distance from Ny-Ålesund (km)*	*Surface Sample Depth (cm)*	*Filtered Volume (mL)*	***OC (ng/g)***	***EC (ng/g)***
BR-13	21-Mar-17	78.872321	11.915841	456	6.0	5	2820	442	8.8
BR-13	29-Mar-17	78.872321	11.915841	456	6.0	1	1510	227	4.5
GVB	29-Mar-17	78.91754	11.89439	20	1.0	1	1420	366	13
BR-13	2-Apr-17	78.872321	11.915841	456	6.0	1	3210	285	7.2
GVB	2-Apr-17	78.91754	11.89439	20	1.0	2	3630	1026	35
KV-01	2-Apr-17	78.864052	12.491002	3	13.8	13	3740	3425	2.0
KV-02	2-Apr-17	78.83013	12.75878	226	21	5	2870	794	9.9
KV-04	2-Apr-17	78.80279	12.95866	395	26.2	5	3630	505	9.8
KV-06	2-Apr-17	78.778049	13.15344	534	31.1	5	2840	256	3.4
KV-08	2-Apr-17	78.755574	13.336307	672	35.9	5	2910	226	2.1
GVB	5-Apr-17	78.91754	11.89439	20	1.0	3	1850	496	14
BR-13	5-Apr-17	78.872321	11.915841	456	6.0	7	3280	431	17
VBR-01	9-Apr-17	78.911753	11.733951	139	4.5	5	2370	214	2.7
HDF-04	11-Apr-17	78.977785	13.4683	642	33.5	3.5	2490	443	6.8
HDF-06	11-Apr-17	79.029367	13.531009	718	36.3	3	2580	528	5.6
HDF-10	11-Apr-17	79.140312	13.394256	1119	39.6	10	1980	169	4.4
VBR-02	11-Apr-17	78.903914	11.657997	355	6.3	2	3080	1266	9.6
ML-01	12-Apr-17	78.893377	12.061562	87	4.7	2	2590	416	2.9
ML-01b	12-Apr-17	78.876529	12.030603	297	6.0	3	3280	330	15
ML-02	12-Apr-17	78.870736	11.983614	403	6.4	5	2620	224	6.4
BR-10	12-Apr-17	78.885811	11.907174	304	4.5	2	2920	375	8.2
BR-13	12-Apr-17	78.872321	11.915841	456	6.0	2	2590	279	4.2
VBR-01	12-Apr-17	78.911753	11.733951	139	4.5	2	2960	915	1.6
VBR-02	12-Apr-17	78.894918	11.663595	450	6.8	2	3000	477	7.7
KV-02	13-Apr-17	78.83013	12.75878	226	21	6	3230	459	4.0
KV-04	13-Apr-17	78.80279	12.95866	395	26.2	2.5	3620	446	8.6
KV-06	13-Apr-17	78.778049	13.15344	534	31.1	2	3930	856	11
KV-08	13-Apr-17	78.755574	13.336307	672	35.9	3	3360	1198	11
EB-01	13-Apr-17	78.85685	12.04031	225	8.0	1.5	3290	502	17
EB-01b	13-Apr-17	78.85461	12.75	425	8.8	1.5	2880	18	0.0
EB-02	13-Apr-17	78.85299	12.18493	625	9.9	1	3100	355	11
GVB	13-Apr-17	78.91754	11.89439	20	1.0	1	2880	7227	48
GVB	16-Apr-17	78.91754	11.89439	20	1.0	3	2730	668	68
BR-13	16-Apr-17	78.872321	11.915841	456	6.0	4	2765	458	45
GVB	22-Apr-17	78.91754	11.89439	20	1.0	3	3050	9426	1720
ML-01b	4-May-17	78.876529	12.030603	297	6.0	2	2500	234	22
ML-02	4-May-17	78.870736	11.983614	403	6.4	3	2570	221	25
BR-13	4-May-17	78.872321	11.915841	456	6.0	1	2890	364	27
GVB	4-May-17	78.91754	11.89439	20	1.0	4	3590	1683	48
KV-08	5-May-17	78.755574	13.336307	672	35.9	4	3300	868	9.0
KV-06	5-May-17	78.778049	13.15344	534	31.1	7	3128	468	9.2

Appendix B. Measured Elemental and Organic Carbon (continued)

Table B.3. Measured EC and OC Concentrations of 2018 Snow Pit Samples

				Punch 1		Punch 2		Punch 3			
Site	*Date*	*Sample Layer (cm)*	*Filtered Volume (mL)*	*OC (µg/cm²)*	*EC (µg/cm²)*	*OC (µg/cm²)*	*EC (µg/cm²)*	*OC (µg/cm²)*	*EC (µg/cm²)*	***OC (ng/g)*** [+]	***EC (ng/g)*** [+]
GVB	23-Mar-18	28-26	2235	81	0.01					330	0.04
		26-0	2605	33	4.0					120	14
GVB	6-Apr-18	32-22	2944	39	0.27					110	0.78
		22-0	3135	28	4.1	32	6.0			91	16
GVB	11-Apr-18	35-21	1750	20	1.0					100	5.4
		21-16	2310	23	0.20	23	0.29			90	0.96
		16-0	3470	25	5.4					66	14
BR-13	14-Apr-18	95-87	1730	6.4	0.04					33	0.21
		87-30	3710	23	0.83	20	1.2			53	2.5
		30-0	3350	29	0.01	29	0.01			80	0.03
ML-02	14-Apr-18	167-159	1575	30	0.84	35	0.75			190	4.6
		159-105	3985	9.5	0.98	20	2.2	8.8	1.0	29	3.9
		105-56	3885	14	0.35					32	0.82
		56-0	4410	28	0.01	43	0.01			73	0.02
EB-02	15-Apr-18	105-100	2035	18	0.00					81	0.00
		100-49	3070	9.9	0.95					29	2.8
		49-0	3315	38	0.01	42	0.01	36	0.01	110	8.9
GVB	17-Apr-18	51-39	3055	27	0.89	21	0.60			71	2.2
		39-22	3910	10	2.4					23	5.5
		22-0	2130	200	5.4					850	23
HDF-10	18-Apr-18	166-160	2670	13	0.11					45	0.37
		160-110	3310	20	0.22					56	0.60
		110-53	4010	13	0.21					29	0.48
		53-0	3140	14	0.00	17	0.00			45	0.00
KV-08	19-Apr-18	173-169	2870	12	0.00					38	0.00
		169-105	2720	13	1.2					44	4.0
		105-47	2860	21	0.13					68	0.41
		47-0	3590	100	0.01	93	0.01			250	0.03

[+] *Calculated using the volume of the filtered sample and the total surface area of the filter, 9.079 cm², see calculations in section 2.2.3.*

Appendix B. Measured Elemental and Organic Carbon (continued)

Table B.4. Seasonal Flux Calculations for 2018 Snow Pits

Site	*Date*	*Layer Depth Top (cm)*	*Layer Depth Bottom (cm)*	*Density (g/cm^3)*	*SWE (g/cm^2)*	*[EC] (ng/g)*	*EC Flux (ng/cm^2)*	*[OC] (ng/g)*	*OC Flux (ng/cm^2)*
BR-13	14-Apr-18	95	87	0.232	1.9	0.21	0.39	33	62
		87	75	0.232	2.8	2.5	6.9	53	150
		75	55	0.368	7.4	2.5	18	53	390
		55	35	0.358	7.2	2.5	18	53	380
		35	30	0.505	2.5	2.5	6.3	53	130
		30	15	0.505	7.6	0.03	0.21	80	600
		15	0	0.253	3.8	0.03	0.10	80	300
					Total Seasonal Flux		***50***		***2000***
ML-02	14-Apr-18	167	159	0.158	1.3	4.6	5.8	187	230
		159	147	0.158	1.9	3.1	6.0	29	56
		147	105	0.305	13	3.1	40	29	380
		105	87	0.305	5.5	0.82	4.5	32	180
		87	56	0.453	14	0.82	11	32	450
		56	47	0.453	4.1	0.02	0.08	73	300
		47	27	0.400	8.0	0.02	0.16	73	580
		27	7	0.379	7.6	0.02	0.16	73	550
		7	0	0.391	2.7	0.02	0.06	73	200
					Total Seasonal Flux		***68***		***2900***
EB-02	15-Apr-18	105	100	0.253	1.3	0.00	0.00	81	100
		100	85	0.253	3.8	2.8	11	29	110
		85	65	0.284	5.7	2.8	16	29	170
		65	49	0.390	6.2	2.8	18	29	180
		49	45	0.390	1.6	0.03	0.04	107	170
		45	25	0.495	9.9	0.03	0.27	107	1100
		25	5	0.453	9.1	0.03	0.25	107	970
		5	0	0.505	2.5	0.03	0.07	107	270
					Total Seasonal Flux		***45***		***3000***
GVB	17-Apr-18	51	48	0.140	0.42	2.2	0.93	71	30
		48	47	0.700	0.70	2.2	1.5	71	50
		47	39	0.160	1.3	2.2	2.8	71	91
		39	30	0.290	2.6	5.5	14	23	61
		30	28	0.600	1.2	5.5	6.5	23	28
		28	22	0.200	1.2	5.5	6.5	23	28
		22	0	0.700	15	23	360	850	13000
					Total Seasonal Flux		***390***		***13000***

Appendix B. Measured Elemental and Organic Carbon (continued)

Table B.4. *Seasonal Flux Calculations for 2018 Snow Pits (continued)*

Site	*Date*	*Layer Depth Top (cm)*	*Layer Depth Bottom (cm)*	*Density (g/cm^3)*	*SWE (g/cm^2)*	*[EC] (ng/g)*	*EC Flux (ng/cm^2)*	*[OC] (ng/g)*	*OC Flux (ng/cm^2)*
HDF-10	18-Apr-18	166	160	0.379	2.3	0.37	0.85	45	100
		160	146	0.379	5.3	0.60	3.2	56	300
		146	126	0.484	9.7	0.60	5.8	56	540
		126	110	0.421	6.7	0.60	4.1	56	380
		110	106	0.421	1.7	0.48	0.80	29	49
		106	86	0.400	8.0	0.48	3.8	29	230
		86	66	0.411	8.2	0.48	3.9	29	240
		66	53	0.474	6.2	0.48	2.9	29	180
		53	46	0.474	3.3	0.00	0.00	45	150
		46	26	0.495	9.9	0.00	0.00	45	450
		26	6	0.400	8.0	0.00	0.00	45	360
		6	0	0.386	2.3	0.00	0.00	45	100
					Total Seasonal Flux		***25***		***3100***
KV-08	19-Apr-18	173	169	0.200	0.80	0.00	0.00	38	30
		169	153	0.200	3.2	4.0	13	44	140
		153	133	0.305	6.1	4.0	24	44	270
		133	113	0.358	7.2	4.0	28	44	310
		113	105	0.379	3.0	4.0	12	44	130
		105	93	0.379	4.5	0.41	1.9	68	300
		93	73	0.284	5.7	0.41	2.3	68	380
		73	53	0.390	7.8	0.41	3.2	68	530
		53	47	0.284	1.7	0.41	0.70	68	120
		47	33	0.284	4.0	0.03	0.10	249	990
		33	13	0.274	5.5	0.03	0.14	249	1400
		13	0	0.178	2.3	0.03	0.06	249	580
					Total Seasonal Flux		***86***		***5100***

Appendix C. Measured Levoglucosan Content

Table C.1. Measured Levoglucosan Concentrations in 2018 Surface Snow Samples (LOD: 25.3 pg/mL, MDL: 47.0 pg/mL)

Site	*Date*	***Levoglucosan (pg/mL)***
KV-02	5-Apr-18	212
KV-04	5-Apr-18	52.0
KV-06	5-Apr-18	*< MDL*
KV-09	5-Apr-18	*< MDL*
GVB	8-Apr-18	90.8
BR-06	8-Apr-18	216
BR-10	8-Apr-18	427
BR-13	8-Apr-18	305
KV-02	10-Apr-18	250
KV-04	10-Apr-18	209
KV-06	10-Apr-18	167
KV-09	10-Apr-18	99.1
GVB	10-Apr-18	276
GVB	11-Apr-18	184
GVB	13-Apr-18	271
EB-01	13-Apr-18	50.4
EB-02	13-Apr-18	61.8
BR-04	13-Apr-18	210
BR-13	13-Apr-18	167
ML-02	13-Apr-18	75.7
HDF-02	13-Apr-18	222
HDF-06	13-Apr-18	157
HDF-10	13-Apr-18	187
KV-02	13-Apr-18	92.3
KV-06	13-Apr-18	238
KV-09	13-Apr-18	103
BR-13	14-Apr-18	298
ML-02	14-Apr-18	134
EB-02	15-Apr-18	348
HDF-10	18-Apr-18	135
KV-02	19-Apr-18	115
KV-04	19-Apr-18	132
KV-06	19-Apr-18	*< MDL*
KV-08	19-Apr-18	*< MDL*
BR-13	21-Apr-18	339
GVB	21-Apr-18	306
GVB	23-Apr-18	56.9
GVB	1-May-18	48.8

Appendix D. Measured Trace Element Content

Table D.1. Measured Trace Element Concentrations in 2018 Surface Snow, all concentrations reported in ppb

Site	*Date*	*[Cd]*	*[Pb]*	*[Bi]*	*[Al]*	*[Ca]*	*[Mn]*	*[Fe]*	*[Co]*	*[Cu]*	*[Zn]*	*[Sr]*	*[K]*
KV-01[+]	5-Apr-18	0.0055	0.36	0.0064	280	1300	23	530	0.26	0.35	0.73	5.8	270
KV-02	5-Apr-18	0.0025	0.093	0.0077	9.2	140	1.4	13	0.013	<LOD	0.30	1.1	31
KV-04	5-Apr-18	0.0038	0.068	0.0037	4.8	74	0.64	9.6	0.0047	<LOD	0.26	0.59	12
KV-06	5-Apr-18	0.0040	0.072	0.0038	11	120	0.88	9.5	0.039	<LOD	0.55	0.79	15
KV-09	5-Apr-18	0.0039	0.090	0.0025	2.3	44	0.20	2.1	<LOD	<LOD	1.7	0.34	11
BR-06	8-Apr-18	0.0042	0.18	0.0044	12	120	0.53	6.3	0.0075	<LOD	5.2	1.00	81
BR-10	8-Apr-18	0.0044	0.18	0.0029	6.6	130	0.35	3.7	0.0059	<LOD	11	1.4	140
BR-13	8-Apr-18	0.0049	0.14	0.0026	7.5	100	0.25	3.2	0.010	0.45	4.4	0.72	64
GVB	8-Apr-18	0.0041	0.11	0.0039	8.3	120	0.65	12	0.0092	<LOD	0.77	1.2	52
KV-01[+]	10-Apr-18	0.010	0.51	0.012	300	980	29	610	0.38	0.60	3.0	5.5	270
KV-02	10-Apr-18	0.0080	0.29	0.0077	13	150	1.0	13	0.013	0.17	4.9	3.7	200
KV-04	10-Apr-18	0.0059	0.16	0.0049	4.0	140	0.52	4.9	0.0082	<LOD	6.4	1.7	75
KV-06	10-Apr-18	0.0045	0.17	0.0032	4.4	140	1.5	6.0	0.020	<LOD	6.2	1.6	85
KV-09	10-Apr-18	0.0034	0.095	0.0035	4.3	83	0.41	3.7	0.046	<LOD	4.0	0.79	39
GVB	10-Apr-18	0.0089	0.19	<LOD	4.7	87	0.53	3.2	0.0075	<LOD	1.9	1.7	91
GVB	11-Apr-18	0.045[++]	0.17	0.0037	13	100	0.67	5.5	0.019	0.20	11	0.68	160
HDF-02	13-Apr-18	0.0058	0.096	0.018	4.5	100	0.35	2.8	0.0066	0.55	8.6	1.1	140
HDF-06	13-Apr-18	0.0053	0.061	0.011	3.0	90	0.20	2.2	0.0069	1.2	16	0.74	130
HDF-10	13-Apr-18	0.0027	0.078	0.013	11	110	0.23	4.7	0.0054	<LOD	2.1	0.66	24
KV-02	13-Apr-18	0.0026	0.072	0.0021	4.2	140	0.73	5.2	0.0081	<LOD	1.6	0.96	35
KV-06	13-Apr-18	<LOD	0.048	<LOD	2.9	96	0.24	2.7	0.0032	<LOD	2.2	0.82	34
KV-09	13-Apr-18	<LOD	0.057	<LOD	4.1	73	0.18	3.9	<LOD	<LOD	4.4	0.54	27
EB-01	13-Apr-18	<LOD	0.067	<LOD	2.5	85	0.26	2.0	<LOD	<LOD	0.46	1.5	69
EB-02	13-Apr-18	0.0034	0.092	<LOD	3.4	82	0.24	3.4	0.0038	<LOD	0.58	0.88	34
MLB-02	13-Apr-18	0.0040	0.083	0.0044	3.8	100	0.29	3.6	0.0049	0.25	2.9	1.9	93
BR-04	13-Apr-18	0.0076	0.27	0.0029	6.0	98	0.65	15	0.0071	<LOD	0.71	1.8	91
BR-13	13-Apr-18	0.0056	0.15	0.0036	3.9	93	0.29	2.6	0.0041	<LOD	1.0	2.0	93
GVB	13-Apr-18	0.0050	0.14	0.0044	6.5	130	0.43	6.1	0.0062	0.17	4.7	1.6	100
BR-02	14-Apr-18	0.0029	0.080	0.011	7.3	200	0.34	5.1	0.0064	<LOD	17	3.4	190
MLB-02	14-Apr-18	0.0051	0.12	0.0036	7.7	120	0.41	11	0.0061	<LOD	8.3	2.3	120
EB-02	15-Apr-18	0.0042	0.12	0.0071	12	180	0.61	7.0	0.011	<LOD	15	1.8	150
HDF-10	18-Apr-18	0.0033	0.049	0.0069	4.0	110	0.31	4.9	0.0073	0.29	3.0	0.45	24
KV-01[+]	19-Apr-18	0.0082	0.14	0.0028	87	580	12	170	0.13	1.70	15	4.9	550
KV-02	19-Apr-18	0.0048	0.12	0.015	11	160	1.3	14	0.018	<LOD	3.7	2.1	89
KV-04	19-Apr-18	0.0028	0.079	0.0047	4.9	120	0.35	6.2	0.0046	<LOD	5.7	0.88	59
KV-06	19-Apr-18	0.0025	0.036	<LOD	4.9	110	0.50	4.7	0.0072	<LOD	4.0	2.0	78
KV-08	19-Apr-18	<LOD	0.047	<LOD	4.3	58	0.31	2.4	0.0041	<LOD	0.59	0.59	27
BR-02	21-Apr-18	0.0033	0.12	0.0076	23	150	0.36	7.7	0.0067	0.50	8.7	0.79	87
GVB	21-Apr-18	0.0065	0.19	0.0029	17	75	0.32	4.9	0.0062	<LOD	4.3	0.47	49
GVB	23-Apr-18	0.0038	0.16	<LOD	6.5	98	0.61	15	0.0083	<LOD	2.5	1.5	72
GVB	1-May-18	<LOD	0.10	<LOD	4.4	82	0.53	6.2	0.0094	<LOD	1.5	0.98	60
LOD		0.0024	0.0096	0.0018	0.46	2.1	0.034	0.14	0.0026	0.12	0.18	0.14	7.2

[+] *Snow samples from KV-01 sites contained high levels of sedimentary material and were not used in the spatial variance analysis*

[++] *Removed as an outlier*

Gabrielle Emma Kleber

Spatial Variability of Black Carbon Deposited on Snow in Ny-Ålesund, Svalbard: Impact of Anthropogenic Activities

NTNU
Norwegian University of
Science and Technology